Lateral Behaviour and Direct Displacement Based Design of a Novel Hybrid Structure: Cross Laminated Timber Infilled Steel Moment Resisting Frames

by

Matiyas Bezabeh

B.Sc., Addis Ababa University, 2011

A THESIS SUBMITTED IN PARTIAL FULFILLMENT OF THE REQUIREMENTS FOR THE DEGREE OF

MASTER OF APPLIED SCIENCE

in

THE COLLEGE OF GRADUATE STUDIES

(Civil Engineering)

THE UNIVERSITY OF BRITISH COLUMBIA

(Okanagan)

August 2014

Abstract

Recently, an innovative hybrid structure has been developed as an alternative lateral-load resisting system at The University of British Columbia. The hybrid structure incorporates Cross Laminated Timber (CLT) shear panels as an infill in steel moment resisting frames (SMRFs). In order to increase the applicability of the proposed system, in this thesis, a direct displacement based design methodology has been developed and analytically validated.

Initially, a nonlinear time history analysis (NLTHA) was carried out to study the lateral behaviour of the proposed hybrid structure. For this purpose, a total of 162 different hybrid buildings were modeled and analyzed in OpenSees by using twenty earthquake ground motions (2% probability exceedance in 50 years). Post-earthquake performance indicators (Maximum Interstory Drift (MISD) and Residual Interstory Drift (RISD)) were obtained from the analyses. To assist the post-seismic safety assessment of the hybrid buildings, surrogate models for MISD and RISD were developed using Response Surface Methodology and Artificial Neural Network (ANN). By using the ANN surrogate models as fitness functions for the Genetic Algorithm, optimal modeling parameters of the hybrid system were obtained.

Secondly, to represent the energy dissipative capacity of the hybrid system, an equivalent viscous damping (EVD) equation was developed. To formulate the EVD equation, 243 single-storey single-bay CLT infilled SMRF models were developed and subjected to monotonic static and semi-static cyclic analysis. The EVD of each model was calculated from the hysteretic responses based on Jacobsen's area based approach and later calibrated using NLTHA.

Finally, an iterative direct displacement based design method was developed for the proposed hybrid structure. A detailed description of the proposed methodology is presented with a numerical example. In order to verify the proposed method, hybrid buildings with 3-, 6-, and 9- storey heights were designed. A calibrated EVD-ductility relationship was used to obtain the energy dissipation of the equivalent SDOF system for all case study buildings. Nonlinear time history analysis using twenty ground motion records was used to validate the performance of the proposed design methodology. The results indicate that the proposed design method effectively controls the displacements resulting from the seismic excitation of the hybrid structure.

Preface

This research work is carried-out at The University of British Columbia under direct supervision of Dr. Solomon Tesfamariam and Professor Sigi F. Stiemer. All the literature review, simulations and mathematical calculations of this thesis are carried-out by the author. A list of my journal and conference publications at The University of British Columbia are listed as follows.

Journal Papers

1. Bezabeh, M. A., Tesfamariam, S., Stiemer, S.F. 2014. "Equivalent Viscous Damping for CLT Infilled Steel Moment Resisting Frames", *Journal of Structural Engineering,ASCE*, Prepared for submission (Version of Chapter 4).

2. Bezabeh, M. A., Tesfamariam, S., Stiemer, S.F. 2014. "Prediction of Maximum Interstorey Drift of Cross laminated Timber Infilled Steel Moment Frames from Post-Earthquake Residual Interstorey Drift: Response Surface Methodology", *Structures*, Prepared for submission (Version of Chapter 3).

3. Bezabeh, M. A., Tesfamariam, S., Stiemer, S.F. 2014. "Coupled Artificial Intelligence and Genetic Algorithm for the Multi-objective Optimization of CLT infilled Steel Moment Resisting Frames", *Journal of Computing in Civil Engineering, ASCE*, Prepared for submission (Version of Chapter 3).

4. Dickof, C., Stiemer, S. F., Bezabeh, M. A., and Tesfamariam, S. 2013. CLT-Steel Hybrid System: Ductility and Overstrength Values Based on Static Pushover Analysis. *Journal of Performance of Constructed Facilities, ASCE* [Accepted].

5. Bezabeh, M. A., Tesfamariam, S., Stiemer, S.F. 2014. "Direct Displacement Based Design of CLT Infilled Steel Moment Resisting Frames", *Canadian Journal of Civil Engineering*, Prepared for submission (Version of Chapter 5).

6. Tesfamariam, S., Stiemer, S. F., Dickof, C., and Bezabeh, M. A. 2013. Seismic Vulnerability Assessment of Hybrid Steel-Timber Structure: Steel Moment Resisting Frames with CLT Infill. *Journal of Earthquake Engineering* [Accepted].

Conference Papers

1. Bezabeh, M. A., Tesfamariam, S., Stiemer, S.F. 2014. "Equivalent Viscous Damping of CLT Infilled Steel Moment Frames", *World Conference on Timber Engineering (WCTE)*, August 10-14, Quebec City, Canada. (Accepted)(Version of Chapter 4).

2. Bezabeh, M. A., Tesfamariam, S., Stiemer, S.F. 2014. Residual Drift Demands of CLT Infilled Steel Moment Frames. *In the* 7^{th} *European Conference of Steel and Composite Structures (EUROSTEEL 2014)*, September 10-12, 2014, Naples, Italy. (Accepted)

3. Bezabeh, M. A., Tesfamariam, S., Stiemer, S.F. 2014. "Application of Soft Computing to Quantify the Optimal Modeling Parameters of Cross Laminated Timber Infilled Steel Moment Resisting Frames", *12th International Conference on Applications of Statistics and Probability in Civil Engineering*, ICASP 12, July 12-15, 2015, Vancouver, Canada. Submitted (Version of Chapter 3).

Table of Contents

List of Tables

List of Figures

Acknowledgments

First of all, I would like to express my deepest appreciation and thanks to my supervisors Dr. Solomon Tesfamariam and Professor Siegfried F. Stiemer, for offering me the MASc student position, their support, guidance, and unlimited hours of supervision required to complete this thesis. Their advice on both academic and non-academic matters have been priceless.

Besides, I would like to thank my friends in UBC Okanagan, for the interesting discussions, for the great Ping-Pong games, and for all of the fun we had in the last 18 months. Also I thank my roommate Dessalegn Amenu, for being with me in peaks and valleys of life during my days of MASc.

Finally, I wish to thank my parents especially my sisters Tsgae and Kalkidan. Without your love and blessings, as well as your moral support, this thesis would not have been possible.

Dedication

Dedicated to my mother for her endless love from the Heaven

1
Introduction

During the last decade, the use of hybrid structural systems has increased across North America. A hybrid system combines two or more materials and allows them to work jointly. Its main advantages are constructability, cost effectiveness, construction speed, and aesthetics. Considering the height limitation on timber as a structural material, feasibility studies have been carried out at The University of British Columbia (UBC) on hybridizing timber with steel to meet the current performance requirement [SDT12, STKP12, DST12, Dic13, DSBT14]. The proposed hybrid system incorporates Cross Laminated Timber (CLT) as an infill in steel moment resisting frames (SMRFs)(Figure 1.1). The proposed system proved to have higher seismic resistance and lower the seismic vulnerability [TSDB14]. Moreover, the proposed system can be applied to strengthen existing buildings after a seismic event. The CLT panels are characterized by high stiffness to weight ratio, which makes them appropriate material for the seismic design of buildings.

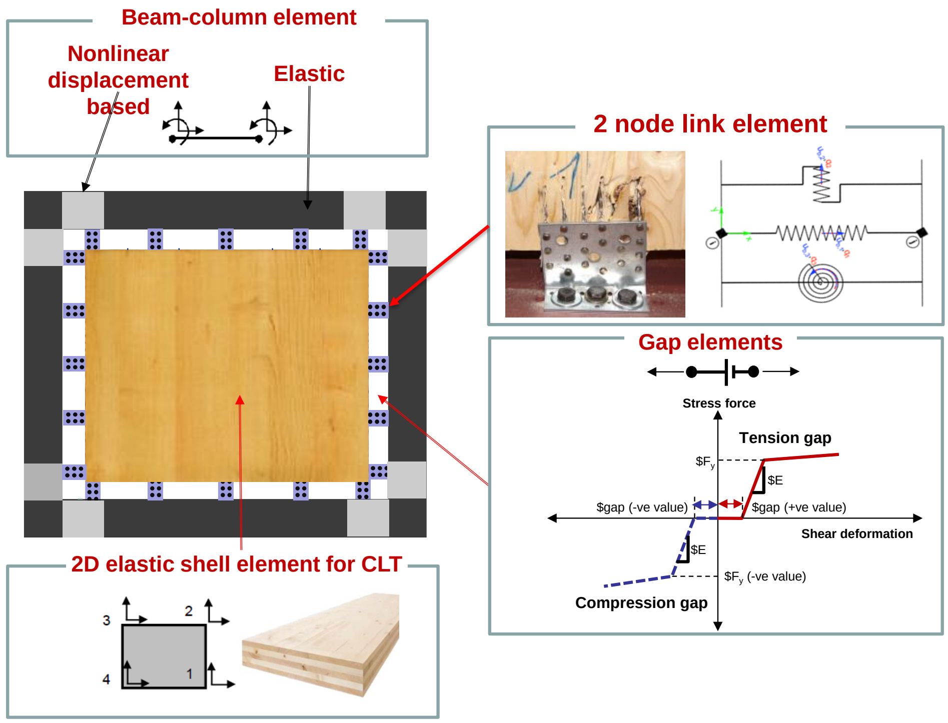

Figure 1.1: CLT infilled SMRF ([TSDB14] Adapted with permission from publisher)

The hybrid system under study is achieved by using L-shaped steel brackets as a connector between the CLT panel and steel frame. These connection brackets are bolted to the steel frame and nailed to the CLT panel. Thorough experimental studies have been carried out on the seismic behaviour of the bracket connections at UBC for the past four years [SKP+13]. These connections provided to ensure full confinement between the structural elements and prevent out of plane failure of the infill panels during a seismic event. The interface between the CLT infill wall and the steel frame is provided with a small gap to allow the connection brackets to deform under lateral load. This permits the frame and panel to act independently and influence each other under lateral loading, which makes the interaction complex.

1.1 Motivation

As discussed in previous paragraphs, the proposed hybrid system can be an alternative construction practice for medium- and high-rise buildings. In the literature, extensive researches have been carried out for masonry and concrete infilled steel frames [EDEH03, Mog04, MTM08, SR78, DSS89, ED02, CGA02]. However, using CLT as a structural infill panel is not thoroughly explored. The hybridization of timber with steel as shown in Figure 1.1 is promising to increase the height requirement on timber buildings. Moreover, the investigation on the composite action under extreme seismic events also creates a new research dimension.

In order to make this type of hybrid system ready for designers and builders, the first step is to make sure that the system is seismic resistant. Design guidelines and standards are needed for the proposed system. In compliance with the current design philosophy, force based design, the latest Canadian code does not have appropriate R_d and R_o factors to perform the design of the proposed hybrid system. Therefore, the objectives of the current study are to examine the lateral behaviour under seismic excitation and to develop a performance based design methodology for the hybrid system. This design method will be used as a baseline to develop the design guide rules that can be applied to prepare design standards. In addition, this type of construction method offers the following advantages:

(a) The hybrid building system elements are suitable for prefabrication. This can result rapid erection time and avoids on site construction errors.

(b) The proposed structural typology, CLT as an infill in SMRFs, can be used for the strengthening of existing buildings after a seismic event.

(c) This type of building system avoids the use of formworks and scaffoldings which yields quality construction and safe project area.

(d) Given the aim of maximizing the use of timber in buildings, among construction industry stakeholders hybrid tall buildings become prevalent.

The proposed hybrid system is an ideal candidate as a high seismic resistant tall building.

1.2 Research methodology

Initially, a thorough investigation is carried out to study the lateral behaviour of the proposed hybrid system and to identify the optimal modeling parameters that results in minimum damage on the building during the seismic event. For the purpose, a total of 162 different hybrid buildings are modeled in OpenSees [MMS$^+$06] by varying six decision variables: building storey [3-, 6- 9-], CLT infill configuration [one-bay infilled, two-bays infilled and three-bays infilled], CLT panel thickness [99, 169, 239 mm] and strength [17.5, 25, 37.5 MPa], and connection bracket spacing 800 and 1600 mm. Twenty earthquake ground motions (with 2% probability exceedance in 50 years) have been used as an input for the analysis. In order to identify the optimal modeling variables, prediction equations and black box functions are developed using Response Surface Methodology (RSM) and Artificial Intelligence, respectively. Multi-objective optimization procedures are applied to identify the optimal modeling parameters. The result highlights that the drift demands of the proposed hybrid systems are quite different from the bare SMRFs. Therefore, rather than considering the CLT infill as a non-structural element, it is of a great advantage to consider it during the design process. For this reason, a design philosophy that incorporates deformation as an input parameter during the design process is chosen. These procedures are called performance based design methods, specifically, Direct Displacement Based Design (DDBD) method. As a first step for the DDBD method, the energy dissipative capacity of the proposed system is quantified through equivalent viscous damping (EVD). This process leads to the development of EVD-ductility law that can be used in the design. Initially this law is developed using Jacobsen′s approach and then corrected using inelastic time history analysis. Subsequently, a new iterative direct displacement based design method for the proposed system has been developed and tested by designing 3-, 6-, and 9- storey hybrid buildings. Finally, the performance of the proposed design method is verified using nonlinear time history analysis.

1.3 Organization of the thesis

This thesis contains 6 chapters. The outline of this thesis is depicted in Figure 1.2. The introduction chapter includes, an overview to innovative hybrid system (CLT infilled SMRF), motivation, research methodology, and organization of thesis. Chapter 2 presents a thorough literature review including research development at UBC on the proposed hybrid system. In addition, it reviews some notable researches on DDBD of structural systems with additional lateral load resisting systems. Chapter 3 provides the prediction equation for the maximum interstorey drift (MISD) of the hybrid system from modeling parameters and residual interstorey drift (RISD). It applies RSM procedure with D-Optimal experimental design technique for the prediction equation development. Moreover, Chapter 3 presents the application of soft computing (Artificial Intelligence and Genetic Algorithm) for the multi-objective optimization of drift demands of the hybrid system. Chapter 4 provides an EVD-ductility law for the DDBD design of CLT-SMRF system. Initially, this law was developed using Jacobsen's area based approach and then corrected using inelastic time history analysis from a total of 8640 simulations. Chapter 5 presents the DDBD methodology that is developed for the proposed hybrid system. The developed design method is presented with a numerical example for a 3 storey hybrid building. In addition, this chapter includes design verification using nonlinear time history analysis. Finally, the conclusions and future research perspectives are presented in Chapter 6.

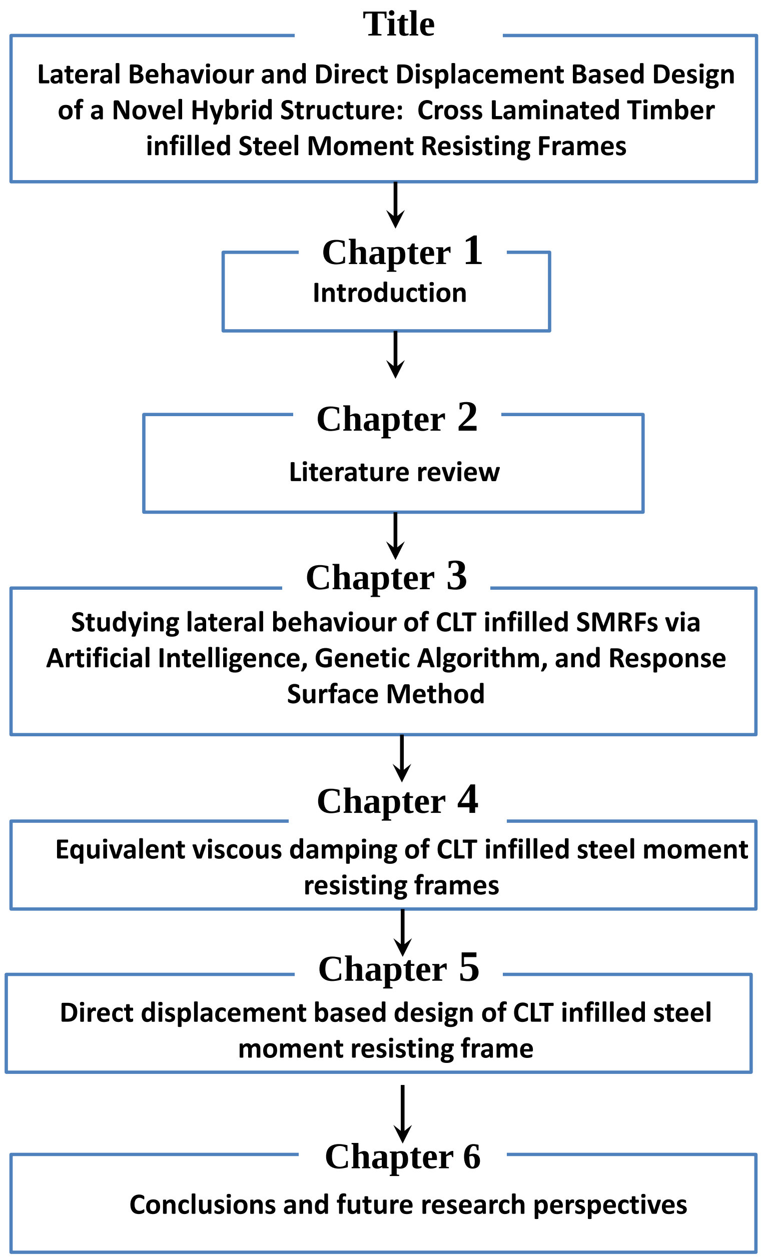

Figure 1.2: Outline of the thesis

2
Literature review

2.1 Cross Laminated Timber (CLT) walls

Cross Laminated Timber (CLT) panel is an engineered wood product with several cross layers of lumber arranged orthogonally that are glued together by adhesives or fasteners. The cross-section of CLT panel has odd numbers of layers in order to create symmetry at the central layer. Softwood lumber and adhesives are the main materials to produce CLT panels. Panel sizes may vary on the specification of the manufacturer; typically in British Columbia (BC), thickness range is 99-309 mm with maximum available panel size of 3 x 12.2 m. Figure 2.1 shows typical arrangement of CLT layers.

Figure 2.1: Five-layer Cross Laminated Timber (CLT) element ([SHE10] Adapted with permission from publisher)

Generally, several researches have been conducted in Canada and other parts of the world on the seismic behaviour of CLT structural systems. These systems include connections between CLT components, CLT walls, and entire CLT building tests. Review on some of notable researches is presented in subsequent sections.

Popovski et al. [PKC11] Seismic Performance of cross-laminated timber buildings

FP innovation conducted a series of quasi-static tests on CLT wall panels. The purpose of the study was to assess the seismic performance of CLT panel wall systems. Several tests, for various wall configurations and connection types, were carried out. Connections applied at the base of walls to connect walls with floors underneath. The test set-up used for the walls is indicated in Figure 2.2.

Figure 2.2: Test set-up used for the CLT walls tests
(© 2011, FPInnovation, by permission)

The CLT walls, during the tests, behaved as a rigid body with small shear deformation. Moreover, static tests revealed that much deformation occurred in the brackets while considerable deformation was observed on the fasteners for cyclic tests. This observation also varied the peak deformation and deformation as shown in Figure 2.3. Moreover, some observed connection failures of brackets with spiral nails and annular ring rails is depicted in Figure 2.4.

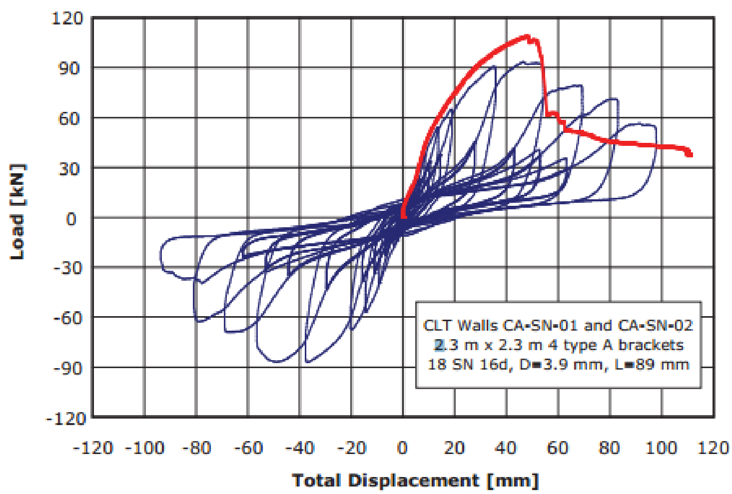

Figure 2.3: Test set-up used for the CLT walls tests
(© 2011, FPInnovation, by permission)

a) b)

Figure 2.4: Failure modes of the bracket connections at late stage of testing for a) wall with spiral nails; and b) wall 04 with annular ring nails
(© 2011, FPInnovation, by permission)

In general, results showed that adequate seismic performance was achieved when steel brackets used with nails or slender screws. The authors also estimated the seismic reduction factor (R) factors for the CLT systems in compliance with National Building Code of Canada (NBCC)[NRC05]. A conservative estimate of $R_d = 2$ and $R_o = 1.5$ is suggested. Furthermore, the authors briefly discuss the application of capacity design method for the CLT structures.

Ceccotti and Follesa [CF06] Seismic behavior of multi-storey XLam buildings

As a part of SOFIE (Fiemme house constructive system) project, a collaboration of Trees and Timber Institute of National Research Council of Italy (CNR-IVALSA), National Institute for Earth Science and Disaster Prevention In Japan (NIED), Shizouka University, and the Building Research Institute (BRI) in Japan leads to a shaking table tests on the 3- storey CLT building. The test was carried out in the laboratory of NIED in Japan. The dynamic test carried out for 3 different earthquakes at two levels of PGA. The simulated earthquakes applied in three different configurations (distinct opening layout) in order to capture the effect of wall length and torsional behaviour of the building system under seismic excitation. "The test house survived 15 destructive earthquakes without any severe damage, i.e. any damage that couldn′t allow for any further reparation of the building" [CF06].

Ceccotti et al. [CSY10] Seismic behaviour of multistory building cross-laminated timber buildings

As a continuation is the 3- storey CLT building test in the above section, another notable shaking table test was carried out in Japan on a 7- storey CLT building. The design of building was conducted by using a behaviour factor (q) value of 3 and importance factor of 1.5. A 100% of Kobe Earthquake (M = 7.2) record was applied in all orthogonal directions. From the dynamic test under, it is observed that the maximum interstorey drift of the system is less than the drift that cause the connections to fail.

2.2 Advancements on CLT infilled SMRFs at UBC

As a basic components of building system, timber and steel have been used independently. However, the height limitation on timber as a main structural element and the trend to build tall wood buildings makes hybridization a feasible solution. In general, hybridization offers an efficient use of the best engineering properties from each material it constitutes. This hybridization can be done in different scale: system level and building level. A novel hybrid structure that incorporates Cross Laminated Timber (CLT) as an infill panel in steel moment resisting frames (SMRFs) is developed at UBC [SDT12, STKP12, DST12, Dic13, DSBT14, TSDB14]. In this section, a brief summary of previous researches at UBC on the development of innovative hybrid system is presented. The review is started with the research made on the experimental investigation of steel bracket connection system between CLT and steel frame [SKP+13]. This followed by a review on the finite element validation of the experiments by [SST+13]. Review on the research that combined the above two studies to develop the CLT infilled SMRF hybrid system by [DSBT14] is also included. Finally a probabilistic assessment of the CLT- SMRF system by Tesfamariam et al. [TSDB14] is presented.

Schneider et al. [SKP+13] Damage assessment of connection used in cross laminated timber subject to cyclic loads

A total of 98 different CLT bracket connections are examined under vertical (parallel to the grain) and horizontal (perpendicular to the grain) directions. The authors focused on studying the damage indices and their correlation with the observed damages under monotonic and cyclic loading. In their work, the authors also calibrated the Kraetzig‘s energy based model by using the data from experiments. Moreover, a damage scale ranges from 1-5 was defined using 24 experimental tests. This damage scale was also verified using 37 cyclic loading tests. The test results revealed that the pullout failure of connectors was common type of observed failure mechanism for the tests in the parallel to the grain direction. However, wood crushing of the outer layer was predominant failure mode for tests in perpendicular to the grain direction. From the analysis, Bracket A with spiral nails and ring shank nails offers the largest ductility value. From the observed failure modes, the authors noticed the dependency of failure modes on the grain orientation of CLT element. In general, from their study, the authors concluded that the failure on most of the brackets are occurred when the average damage index reaches 0.8.

Shen et al. [SST+13] Hysteresis behaviour of bracket connection in cross laminated timber shear walls

Calibration of Pinching4 [LMA03] and Saw models [FF01] of Opensees [MMS+06] for the experimental tests performed by ([Sch09, SST+12] is the main goal of the research. The experimental test results of three types of connection systems, i.e., one bracket (Bracket A of [SKP+13]) and 3 fastener types were considered for the calibration purpose. Figure 2.5 shows the connection details that are considered in the study.

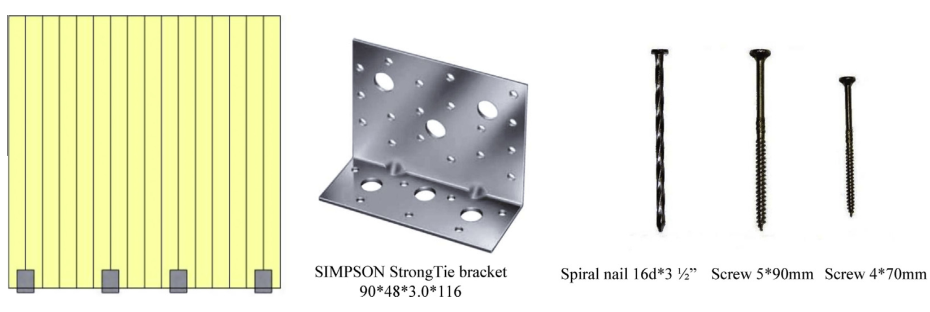

Figure 2.5: CLT wall and connection configuration. ([SST+13] Adapted with permission from publisher)

The results of calibration process using finite element (FE) study are discussed as follows. Comparison between results of the (FE) models and experimental tests are depicted in Figure 2.6a and b for monotonic tests in parallel and perpendicular direction, respectively. From the Figure 2.6a it can be inferred that the both analytical models predict very well for test in perpendicular to the grain direction. However, in Figure 2.6b the SAW model failed to capture failure point after degradation from the peak load.

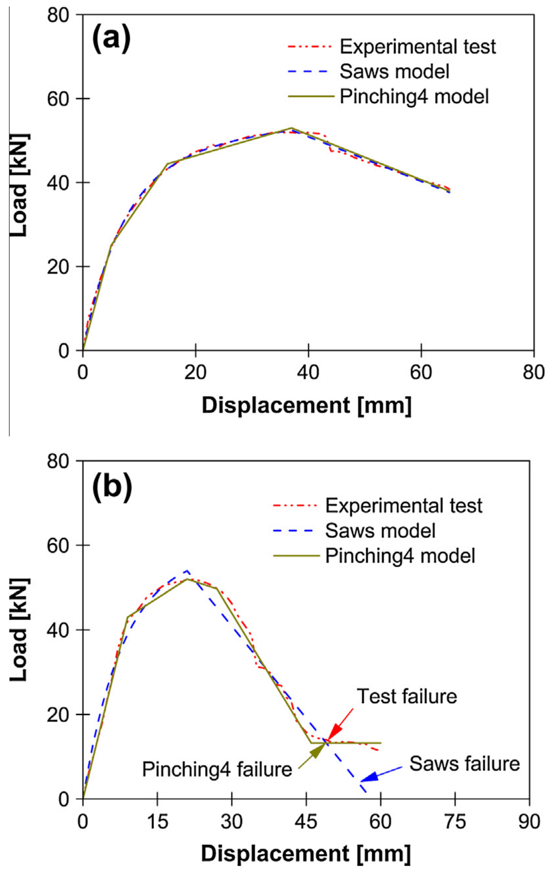

Figure 2.6: Monotonic envelope curves of connection tests, saws and pinching4: (a) perpendicular to grain for Connection A; and (b) longitudinal to grain for Connection A. ([SST+13] Adapted with permission from publisher)

Figure 2.7 shows the comparison of the analytical model responses and experimental tests for connections under cyclic loading. Considering reloading stiffness and degrading slope, the Pinching4 model is found to be the better analytical model.

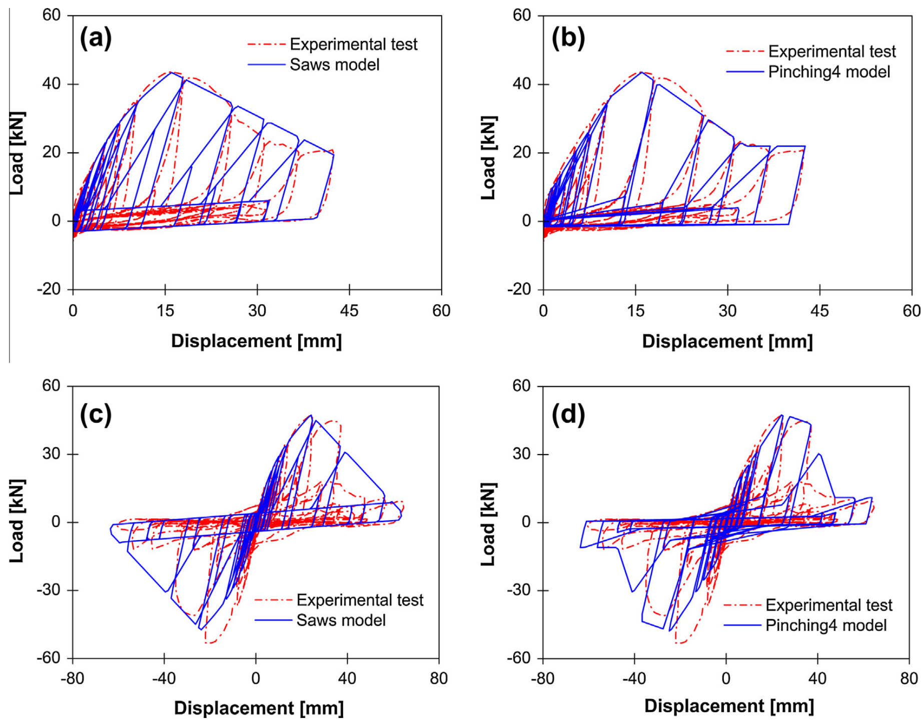

Figure 2.7: Hysteretic response of connection tests, Saws model and Pinching4 model for Connection C: (a) Test and Saws for longitudinal to grain; (b) Test and Pinching4 for longitudinal to grain; (c) Test and Saws for perpendicular to grain; and (d) Test and Pinching4 for perpendicular to grain. ([SST+13] Adapted with permission from publisher)

Furthermore, the authors implemented the analytical models of the connection in the CLT wall to compare FE results with experimental tests conducted by [Sch09]. From their study, it is found that Bracket-A with spiral nail 16×3(1/2) is an excellent connector of CLT system with steel members. From a computational point of view, the Pinching4 analytical model showed good result in simulating the behavior of CLT wall under both static and cyclic loads.

Dickof et al. [DSBT14] CLT-steel hybrid system: ductility and overstrength values based on static pushover analysis

In this paper, the authors extended the development of an innovative steel-timber hybrid structure from [SDT12, STKP12, DST12, Dic13]. The proposed system incorporates a CLT infill shear panels inside a steel moment resisting frame. Figure 2.8 shows the developed innovative hybrid structure.

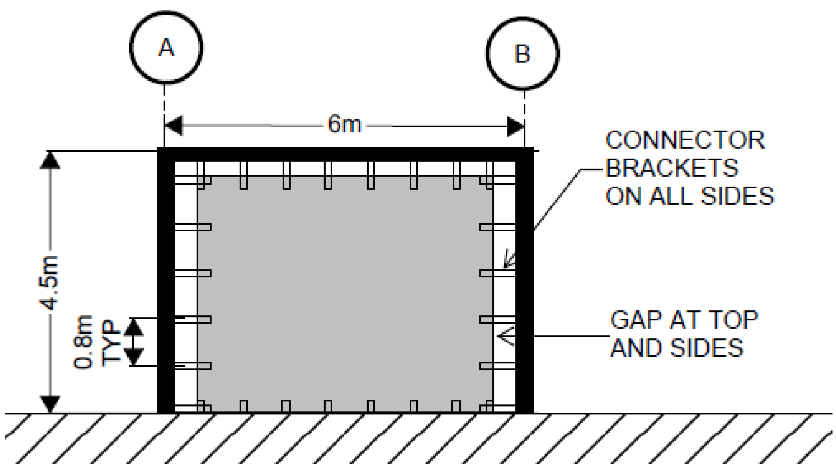

Figure 2.8: Single Bay, Single Storey, CLT Infilled Frame with Bracket Locations ([DSBT14] Adapted with permission from publisher)

The hybrid system is achieved by using steel bracket connections that were tested by [Sch09, $SST^{+}12$]. In order to study the effect of physical properties of CLT shear panels inside steel frames, the authors performed a thorough parametric study on the single bay single storey of the proposed system. From the analysis they found out that CLT thickness, crushing strength and gap between CLT and steel frame affect the ultimate strength, ultimate drift, and post peak behavior of the system. Subsequently, an analytical study has been carried out on the multi-degree-of-freedom (MDOF) of the proposed system. 3-, 6- and 9- storey frames with different infill topology (Figure 2.9) were considered.

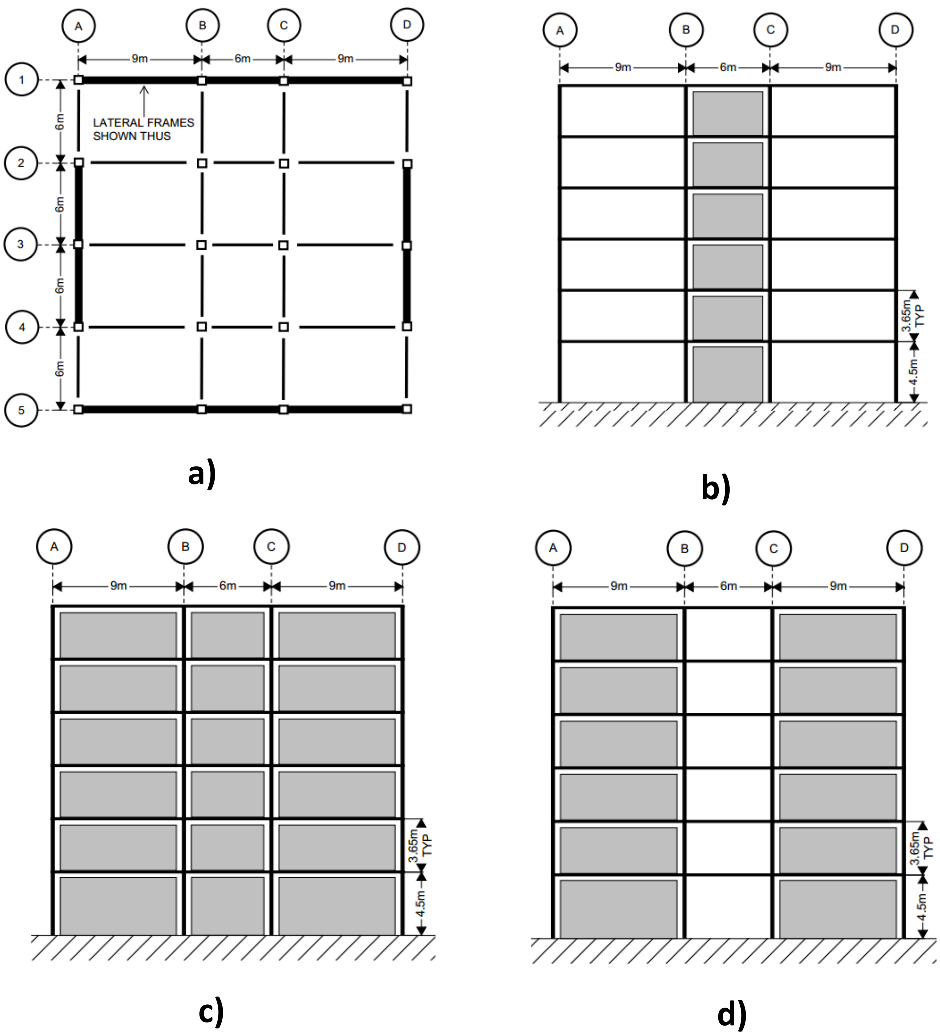

Figure 2.9: Details of the 6-storey frame, a) base building floor plan, b) one infilled bay configurations, b) two infilled bay configurations, and, b) three infilled bay configurations ([DSBT14] Adapted with permission from publisher)

Monotonic pushover analysis was performed to establish preliminary values of the over-strength and ductility factors. A thorough discussion is also included on the definition of first yielding point. It is indicated that bracket yielding occurs at an early stage of loading with very little influence on the initial stiffness of the system. In this case, calculating the system ductility with the bracket yielding deformation will create unrealistic ductility demand. Therefore, the authors chose to use a system yielding deformation. Finally, in order to perform a force based design of the proposed hybrid structure, the authors suggested a ductility and over-strength values of 2.5 and 1.25, respectively.

Tesfamariam et al. [TSDB14] Seismic vulnerability assessment of hybrid steel-timber structure:steel moment resisting frames with CLT infill

This paper performs a probabilistic seismic vulnerability assessment on the innovative hybrid system that was developed at UBC by [SDT12, STKP12, DST12, Dic13, DSBT14]. The study is conducted on the buildings designed for the earthquake hazard level of Vancouver, Canada. Three, six and nine storey buildings with three different infill configurations were considered. Moreover, in order to quantify the effect of ductility class of the steel frames, the study considers both Limited Ductile (LD) and Ductile (D) categories of NBCC 2010 [NRC10]. A global system response parameter, peak interstorey drift ratio (PISD), is adopted as a performance indicator. The spectral acceleration at 5% damping is chosen as an intensity measure (IM) to develop the fragility curves. In order to obtain PISD, a nonlinear time history analysis was carried out using 10 earthquake ground motions scaled to the hazard level of 2%, 5%, 10%, and 40% in 50 years return period. From the parametric studies, significant reduction in the fundamental period of structure was observed as the infill bays increased from bare to all bays infilled frame. For all bays infilled systems, the effect of ductility class on PISD was found to be minimal. From the fragility curves, it can be inferred that the incorporation of CLT shear panels decreases the vulnerability of the system. Generally, the study shows that the proposed hybrid system can be a substitute construction type in moderate and high seismic regions. Moreover, the authors recommended further research on the residual drift demand of the proposed system as it can be high with the stiffening behavior of the shear panels.

2.3 Force based design

Generally, most design codes use a force based design approach (FBD) for the seismic design of structures. This method calculates the elastic design base shear and reduces it by using a force reduction factor (R) to perform inelastic design that considers ductility and over-strength of structures. The National Building Code of Canada (NBCC)[NRC10] uses a combined ductility related (R_d) and over-strength related (R_o) reduction factors to reach to inelastic design. The details and necessary steps of FBD method can be found elsewhere [Dic13, PCK07b]. Medhekar and Kennedy [MK00b], Priestley [Pri00], and Priestley et al. [PCK07b], pointed out the limitations of current FBD method. The following list includes some issues that are related to the FBD method.

1. FBD method requires the fundamental period of the structure at the start of the design process. Building design codes suggest empirical equations to determine the fundamental period of structures. These equations are solely dependent on the type and geometry of a structure. Moreover, these equations are conservative and are not convenient for structures with irregularities [YA13].

2. The R factors that are used reduce the elastic base shear is formulated based on an equal displacement approach. Priestley [Pri00] and Priestley et al. [PCK07b] pointed out the problem associated with this approach for short and long period structures. Moreover, it is stated that the approach becomes questionable for the system having hysteretic behaviour different from elasto-plastic.

3. In FBD method displacements are only checked at the end of the design process. This may create large deformation when R factors greater than 1.0 are used for the design. This large displacement can result in poor performance of non-structural elements under earthquakes related to serviceability limit state. Moreover, this large displacement can result in structural instability at ultimate limit state.

As the proposed CLT infilled SMRFs achieved by L-shaped steel brackets to connect CLT panel with steel frame, the hysteresis behaviour of the system is quite different from elasto-plastic. Moreover, the hysteresis behaviour of the hybrid system is dependent on the gap between CLT and steel frame, panel thickness, panel strength, and connection bracket spacing. In addition, NBCC [NRC10] does not specify appropriate ductility and overstrength factors for the proposed hybrid structure. Due to these reasons, it is of a great advantage to develop the displacement based design approach for CLT infilled SMRFs that avoids the illogical assumptions of the FBD method.

2.4 Performance based design

Over the last 50 years, seismic design of structures shows considerable advancement. One of the key advancement during the last 20 years is the development and progress of performance based engineering. Performance based engineering provides guidelines to design, construct, and maintain all kinds of civil infrastructures to meet prefixed performance level for the given seismic hazard. Performance based seismic design (PBSD) is one component of performance based engineering where the design criteria are defined to achieve prescribed performance objectives when the structure is subjected to a certain level of seismic hazard [Gho01]. Four notable researches are considered as the corner stone of PBSD, i.e. [Com95, ATC96, UC97, Fed97]. SEAOC Vision 2000 [Com95] aimed at developing a framework to design a structure to meet multiple performance objectives. The document includes four performance levels, i.e. fully operational, operational, life safety, and near collapse. Moreover the document suggests elastic and inelastic design methods. Conventional force and strength, displacement based design, energy approaches and prescriptive design are among the suggested design methods [Com95]. ATC 40 (Applied Technological Council)[ATC96] document, provides a design and analysis methods for concrete buildings in California. The document uses performance based methodology for the evaluation and retrofit design of buildings by considering certain performance objectives. Development and application of capacity spectrum method for the performance assessment of existing buildings is presented in detail. The Federal Emergency Management Agency (FEMA) [UC97, Fed97] also defined performance levels and ranges to meet multiple objectives for a given ground motion intensity. The document proposes limits on drift values for various types of main structural and non-structural elements. Four different analytical procedures are discussed in detail, i.e. Linear Static, Linear Dynamic, Nonlinear Static, and Nonlinear Dynamic to be applied for systematic rehabilitation. Moreover in the document, stiffness, strength, and ductility characteristics of different structural elements are presented from thorough laboratory and analytical studies. Ghobarah [Gho01] grouped the performance levels and earthquake hazard from the above research documents as shown in Table 2.1 and Table 2.2, respectively.

Table 2.1: Performance levels, corrsponding damage state and drift limits ([Gho01] By permission from publisher)

Performance level	*Damage state*	*Drift*
Fully operational, Immediate occupancy	No damage	<0.2%
Operational, Damage control, Moderate	Repairable	<0.5%
Life safe-Damage state	Irreparable	<1.5%
Near collapse, Limited safety, Hazard reduced	Severe	<2.5%
Collapse		>2.5%

Table 2.2: Proposed earthquake hazard levels ([Gho01] By permission from publisher)

Earthquake frequency	*Return period in years*	*Probablity of exceedence*
Frequent	43	50%in 30 years
Occasional	72	50%in 50 years
Rare	475	10%in 50 years
Very rare	970	5%in 50 years or 10%in 100 years
Extremely rare	2475	2%in 50 years

2.5 Direct displacement based design (DDBD)

Direct Displacement Based Design (DDBD) is a subset of performance based seismic design wherein the performance objectives are defined based on the level of damage sustained in the structure. The sustained damage in structures is related to the displacement and drift values during the response under seismic excitation [GEAA00]. DDBD was first introduced by Priestly [Pri93], with the aim of designing structures for specific target displacement. The details of the DDBD of structures is presented in Chapter 5.

2.6 Review on DDBD of structures with lateral load resisting systems

Medhekar and Kennedy [MK00b] Displacement-based seismic design of buildings-theory

A thorough theoretical discussion on performing a displacement based design of SDOF and MDOF steel buildings is carried out in the paper. Clear limitations of spectral acceleration method of National Building Code of Canada (NBCC 1995) [NRC95] are also discussed. This is followed by the discussions on the displacement based design of a SDOF concentrically braced frame (CBF). The authors established the displacement based design for the MDOF system by assuming a harmonic response according to the initial displaced shape. The other notable assumption on the paper is the base shear due to earthquake excitation of the MDOF system and the substitute SDOF is equal. The design procedures suggested for MDOF systems is to first transform the MDOF system to an equivalent SDOF and then to design it using the procedure developed for SDOF systems. Moreover, suggestions are included to consider torsional effects in the process of building design. Accounting for the center of mass translation at the start of the design process and subsequent considerations of twisting displacements on iterative basis are suggested for building with asymmetry in plan. Finally, some issues regarding the application of the proposed method to design bridge structures (masses and stiffness are lumped in parallel) have been raised.

Medhekar and Kennedy [MK00a] Displacement-based seismic design of buildings-application

As a continuation of the theoretical study by Medhekar and Kennedy [MK00b], this research applied the displacement based design method for concentrically braced frames. Two and eight storey frames that are located in Vancouver (Canada) are presented as a case study to apply the proposed design method. Both elastic and inelastic designs are performed for the buildings. Subsequently, the performance of the designed buildings is checked by using nonlinear static and time history analysis. Moreover, the example case studies are extended to consider torsion due to asymmetric building layout, column shortening, and higher mode effects.

Wijesundara and Rajeev [WR] DDB seismic design of steel concentric braced frame structures

In this research much development on consideration of the appropriate level of equivalent viscous damping and yielding displacement of CBF structures is made. Contrary to the design approach by [MK00b], this paper used an equivalent viscous damping expression as a function of ductility and brace slenderness ratio that is developed by Wijesundara et al. [WNS11]. In the paper, the yielding displacement profile is derived by considering both brace yielding and axial column deformation. Considering sway mechanism that results the change in brace length with rigid body rotation of the storey that induces an column deformation as shown in Figure 2.10, the authors formulated the interstorey yielding displacement ($\Delta_{y,i}$) expression as follows.

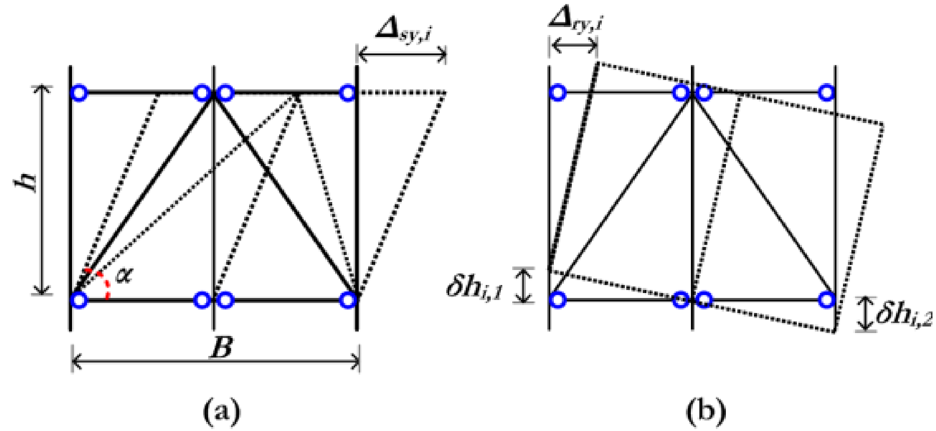

Figure 2.10: a) storey sway mechanism b) rigid body rotatio of i^{th} storey ([WR] Adapted with permission from publisher)

$$\Delta_{yi} = (\frac{\epsilon_y}{sin\alpha cos\alpha})h_i + (\beta\epsilon_{yc}h_i)tan\alpha \tag{2.1}$$

where, ϵ_y is yield strain of the brace steel, α is the brace angle in unreformed shape, h_i is the storey height, β is the ratio of the axial to yielding force of the column, β is the ratio of the design axial force to the yielding force of the column section at i^{th} storey, and ϵ_{yc} is yield strain of the column. A design displacement profile that is suggested for frame structures by Priestley et al. [PCK07b] is adopted with the conventional equations to transform MDOF CBF to a SDOF system. Figure 2.11 outlines the developed flowchart of the DDBD of steel CBF structures. By using the formal procedure of DDBD method, as a case study, the authors designed four and eight storey CBF MDOF frames. Moreover, the buildings were designed for a 1% target drift. In order to avoid conservative estimates of brace sizes, the material overstrength and strain hardening ratios were not considered. After obtaining the design base shear the braces were sized to resist the entire shear in each floor. Moreover, beams and columns of the system were designed to be elastic under gravity loads and lateral loads (specifically during nonlinear response of braces). Finally the performance of designed building are checked using nonlinear dynamic analyses (NDA) under seven earthquake ground motions. For all building heights and bracing types an agreement was obtained between the average NDA response and initial assumed shape.

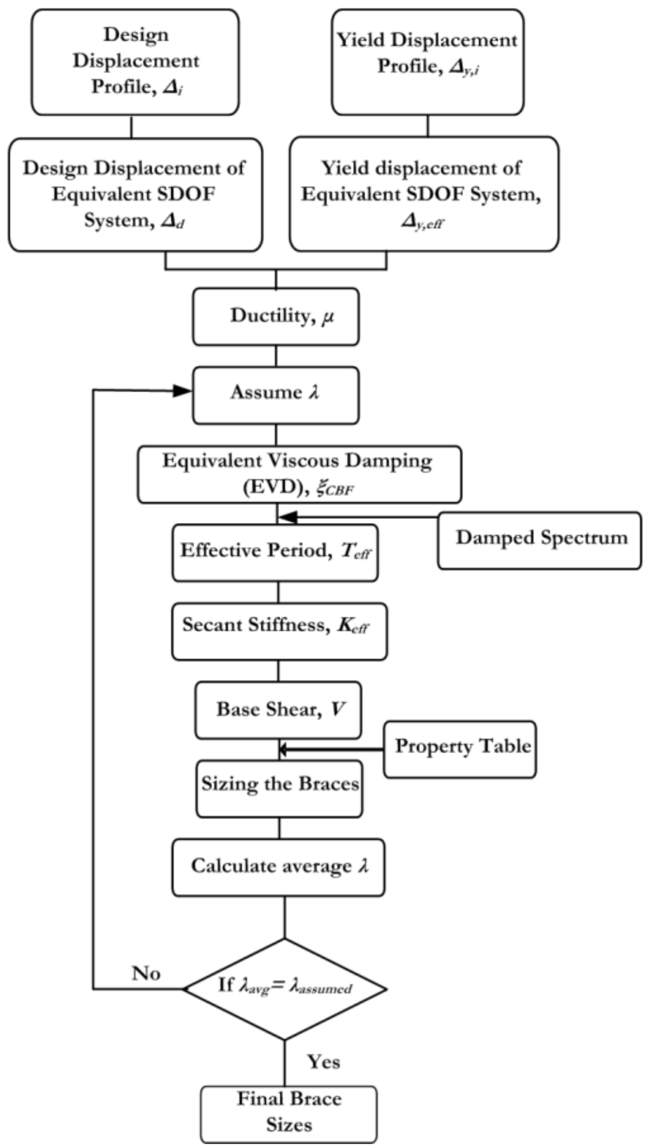

Figure 2.11: Flow chart on DDBD procedure of CBF structures ([WR] Adapted with permission from publisher)

Garcia et al. [GSC10] Development of a DBD method for steel frame-RC wall buildings

This research is a direct extension of the displacement based design procedure developed by Sullivan et al.[SPC06] for RC frame wall structure. In this paper, the applicability of the DDBD method is validated for steel frame-RC wall structures. This type of system is a typical steel-concrete hybrid system at a building level. The flow chart used to design this system which is adopted from Sullivan et al.[SPC06], is shown in Figure 2.13. Important steps of the flowchart are discussed in the following paragraphs.

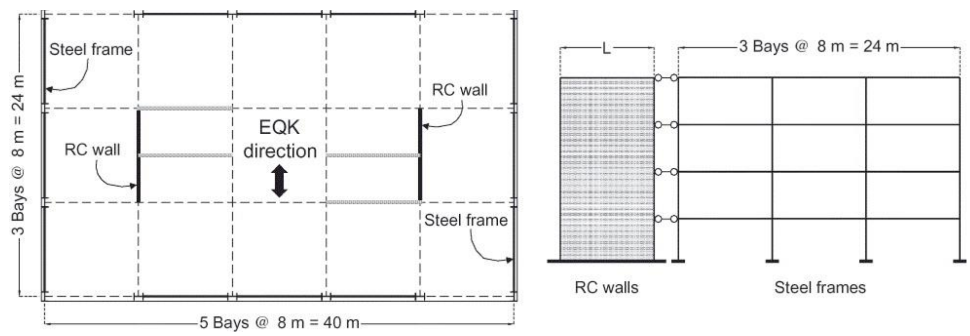

Figure 2.12: Geometry of frame-wall structures used in the evaluation ([GSC10] Adapted with permission from publisher)

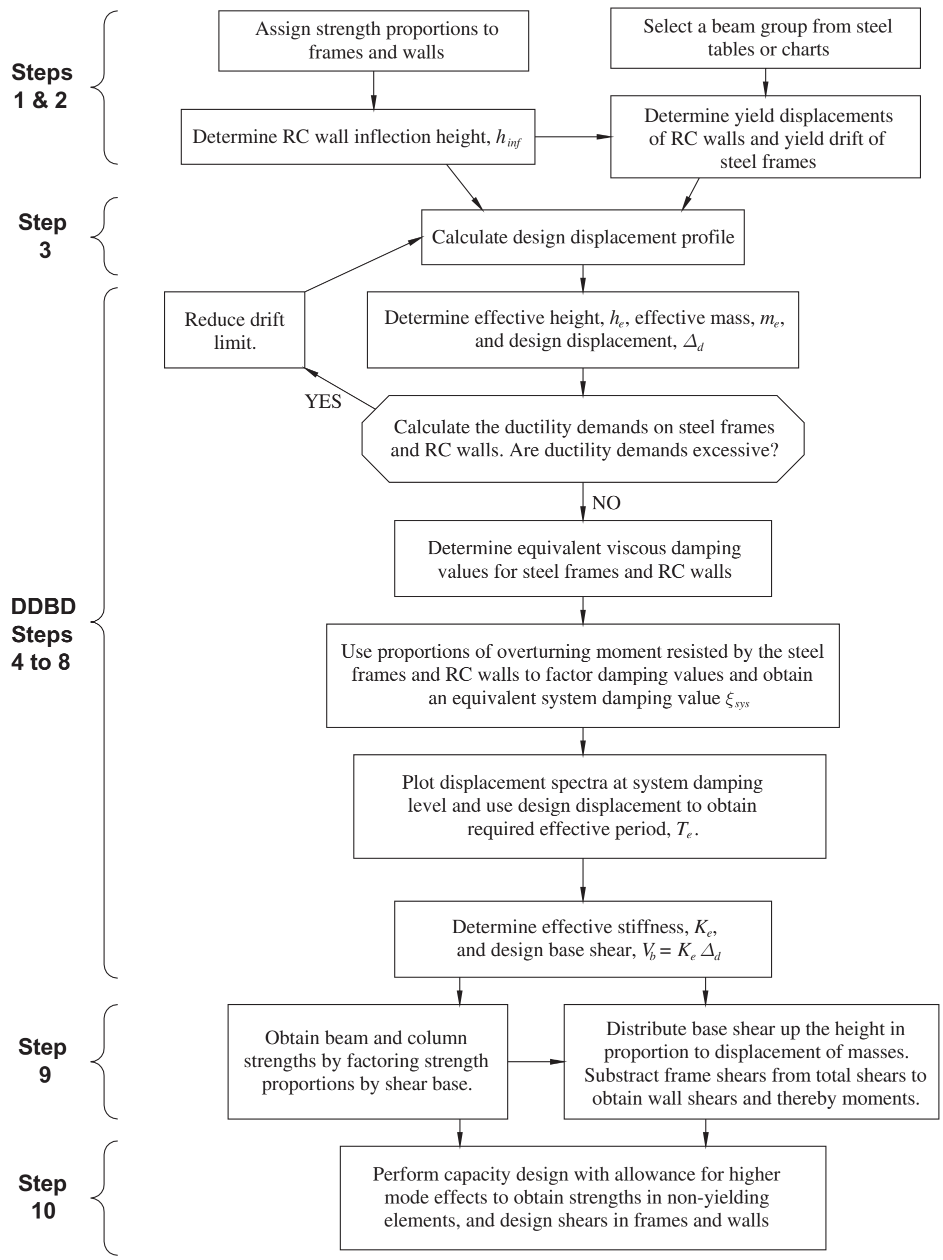

Figure 2.13: Flowchart of DBD for dual systems ([GSC10] Adapted with permission from publisher)

One of the critical advancements of this design methodology is its flexibility to assign strength proportion at the start of the design process. The strength assignment is carried out by allocating a portion of the total base shear for the frames and walls. The design displacement profile is then governed by the assigned strength proportions. By using the relative strength distribution of frame elements, the frame shear profile is calculated by using Equation 2.2.

$$V_{i,frame} = \frac{\sum M_{b,i} + \sum M_{b,i-1}}{2(h_i - hi - 1)} \tag{2.2}$$

where, $V_{i,frame}$ is the frame shear at level i, $M_{b,i}$, and $M_{b,i-1}$ are the beam strengths at i and *i-1* storeys, and h_i and h_{i-1} are the storey heights for level i and *i-1*. The total shear profile is estimated from Equation 2.3.

$$\frac{V_{i,total}}{V_b} = 1 - \frac{i(i-1)}{n(n+1)} \tag{2.3}$$

where, $V_{i,total}$ is the total shear at level i, n is the total number of storeys, and V_b is the design base shear. Then the base shear carried by the wall ($V_{i,wall}$) can be calculated by deducting the frame shear from the total shear.

From the shear profiles developed through the above equations, the moment diagram of the wall can be drawn to calculate the height of inflection. The height of inflection is then used to calculate the properties of equivalent SDOF system. Another contribution of this research is the expression of the equivalent viscous damping ξ_{hyst} which is a weighted average between the wall and frame based on their overturning moment capacity given below in Equation 2.4.

$$\xi_{sys} = \frac{M_{wall}\xi_{wall} + M_{frame}\xi_{frame}}{M_{wall} + M_{frame}} \tag{2.4}$$

where, ξ_{sys} is the system equivalent viscous damping and M_{wall}, ξ_{wall}, M_{frame}, ξ_{frame} are the wall overturning moment, equivalent viscous damping for wall, overturning moment of frames, and equivalent viscous damping for frame, respectively. Finally 4-, 8-, 12-, 16-, and 20- storey buildings were designed using the proposed method. Two dimensional time history analyses have been carried out to check the performance of buildings by comparing response displacement profiles with the initial target profile. For the case study buildings, the proposed method worked very well in controlling the deformations.

Malekpour et al. [MGD13] DDBD of steel braced reinforced concrete frames

This research work develops a direct displacement based design method for steel concrete hybrid system. The system consists of reinforced concrete frames with steel cross bracing. The authors applied the concept of initial strength proportion assignment for frames and bracing to obtain the design displacement profile based on the idea of Sullivan et al. [SPC06]. Simultaneous iterative calculations of equivalent viscous damping [Bla04] and design process were carried out until the trial effective period converged to the effective period from the displacement spectra corresponding to design displacement. Figure 2.14 shows the developed flowchart of the DDBD of RC steel braced frames (Figure 2.15).

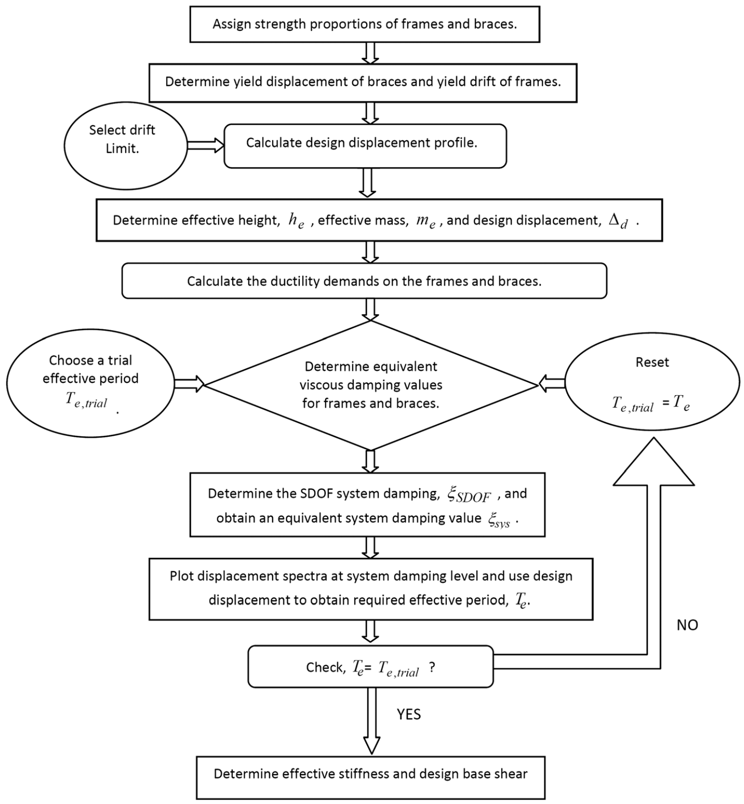

Figure 2.14: Flowchart of DDBD for steel braced reinforced concrete frames

The storey yield displacement of bracing is computed using Equation 2.5 by assuming the tension yielding of bracings ([GA07]).

$$\triangle_{yi} = \frac{F_y L_{bri}}{E cos\theta_i} \tag{2.5}$$

where F_y is the yield strength of the brace, L_{bri} is the length of bracing, E is the modulus of elasticity of the steel, and θ_i is the angle of bracing with horizontal. The design displacement profile is calculated by using Equation 2.6 that considers the design drift. The design drift (θ_d) is reduced as given in Equation 2.7 to account for higher mode effects ([SPC06]).

$$\triangle_i = \triangle_{iy} + (\theta_d)(h_i) \tag{2.6}$$

$$\theta_d = \theta_{d,limit}\left[1 - \frac{N-5}{100}\left(\frac{M_{OT,frame}}{M_{OT,total}} + 0.25\right)\right] \leq \theta_{d,limit} \tag{2.7}$$

In order to calculate the equivalent viscous damping, the initial effective ($T_{e,trial}$) period is computed as:

$$T_{e,trial} = \frac{N}{6}\sqrt{\mu_{sys}} \tag{2.8}$$

where N is the number of storeys of the building under consideration and μ_{sys} is the system ductility. Once the equivalent viscous damping is developed the usual procedure of DDBD method was followed to calculate the design base shear.

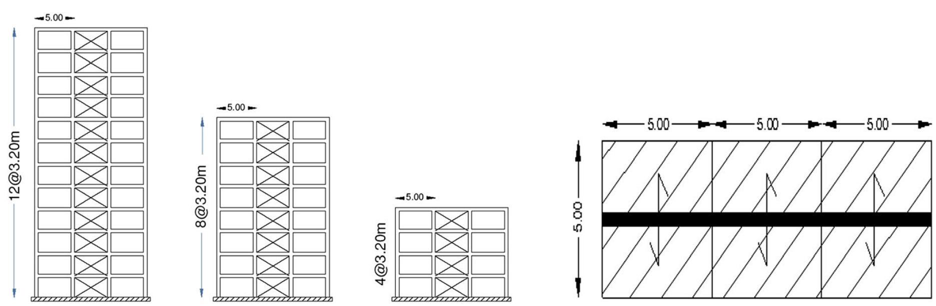

Figure 2.15: Geometry of steel braced reinforced concrete frames used in the evaluation ([MGD13] Adapted with permission from publisher)

Finally the performance of the designed buildings were investigated using nonlinear time history analysis. From the responses, it is found that the interstorey drift of four and eight storey buildings is lower than the initial target value. However, due to buckling of the braces at the lower stories the interstory drift for the 12 storey building is greater than 2.5%.

Sullivan [Sul09] DDBD of a RC wall-steel EBF dual system with added dampers

A direct displacement based design method is developed and verified for an eight- storey hybrid RC wall-steel eccentrically braced frame (EBF) with visco-elastic dampers. The structural system and the developed design method are shown in Figures 2.16 and 2.17, respectively.

2009.pdf

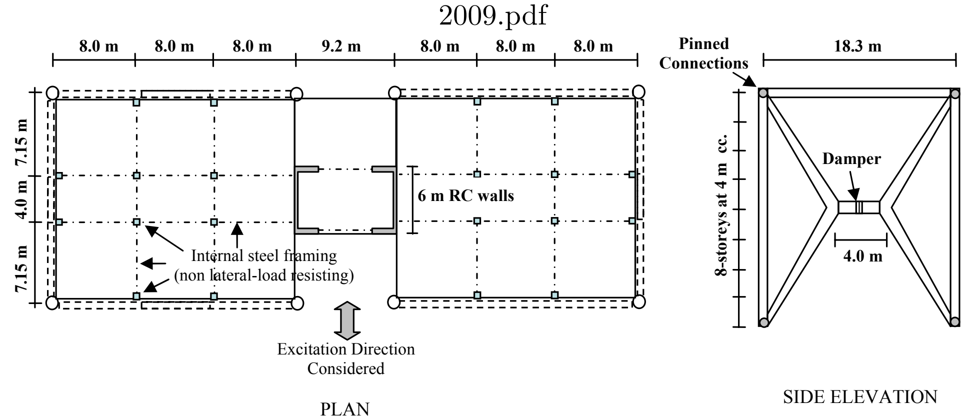

Figure 2.16: Plan and elevation of the 8-storey dual-system case-study building ([Sul09] Adapted with permission from publisher)

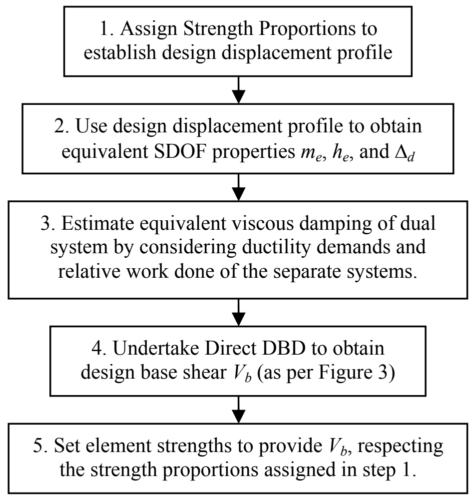

Figure 2.17: Flowchart of DDBD for RC wall-steel EBF dual system with added dampers

The design method is started by assuming strength proportions to the EBF and RC wall to develop the contra-flexure height and the corresponding design displacement shape. The displaced shape at the peak displacement is calculated using Equations 2.9-2.11.

$$\Delta_i = \Delta_{iy} + \left(\theta_d - \frac{\phi_{yWall} h_{cf}}{2}\right) h_i \tag{2.9}$$

where Δ_i is the design displacement for level i

θ_d is the design storey drift limit

ϕ_{ywall} is the wall yield curvature

h_i is the height to the level i

h_{cf} is the contra-flexure height in the walls

Δ_{iy} is given in Equations 2.10 and 2.11

$$\Delta_{iy} = \frac{\phi_{ywall} h_{cf} h_i}{2} - \frac{\phi_{ywall} h_{cf}^2}{6} \qquad for \quad h_i > h_{cf} \tag{2.10}$$

$$\Delta_{iy} = \frac{\phi_{ywall} h_i^2}{2} - \frac{\phi_{ywall} h_i^3}{6h_{cf}} \qquad for \quad h_i \leq h_{cf} \tag{2.11}$$

In this paper, the equivalent viscous damping is calculated by superposing the dissipated energy of different structural elements. The system equivalent viscous damping (ξ_{sys}) is calculated based on the amount of base shear (V_b) and damping force (F_{damper}) of the hybrid system. The equation used to calculate the system equivalent viscous damping is given in Equation 2.12.

$$\xi_{sys} = \frac{2V_{wall}\xi_{wall} + 2V_{EBF}\xi_{EBF} + F_{damper}}{2V_b} \tag{2.12}$$

where V_{wall},V_{EBF}, ξ_{wall}, ξ_{EBF} are wall shear, EBF shear, equivalent viscous damping for wall, and equivalent viscous damping for EBF, respectively. After this step, the procedure of DDBD Priestley et al. [PCK07b] is followed to calculate the design base shear. 85% of the total overturning moment is used to design the flexural reinforcement for the RC walls. EBF members were designed by considering both maximum displacement and velocity conditions. Moreover, the required damping stiffness is computed that can be used to manufacture a visco-elastic damper. From the validation using time history analysis, the displaced profile of the system is matched with the initial design profile. The author of this thesis believes that the method of establishing equivalent viscous damping without requiring extensive dynamic analysis on the assumed hysteretic behaviour is a novel contribution.

Christopoulos [CPP04] Seismic design and response of buildings including Residual Drift

This paper contributes a novel approach to account the residual deformation in the initial stage of the DDBD process of frame structures. The paper initially discusses the residual deformation damage index and suggests the use of combined residual and maximum drift performance matrix for assessing structures. Subsequently, a procedure to evaluate the global damage of the MDOF system based on a combined performance matrix is presented. The global performance level is defined by aggregating the contribution of individual storey levels with appropriate weighting factors. In order to incorporate residual drift in to the design process, the authors developed inelastic residual drift spectra using 20 ground motion records for ductility values of 2, 3, 4, and 5. The developed inelastic residual drift spectra were aimed at extending the extensive research on residual deformation of SDOF system by Kawashima et al. [KMHN98]. Two types of hysteretic rules i.e., Takeda degrading stiffness (TK) and bilinear elasto-plastic (EP) were considered. Plots of maximum and residual displacement response with elastic period and effective period are produced from the analyses. A relationship is provided to derive the residual drift of MDOF (RD_{MDOF}) systems from the residual drift of SDOF (RD_{SDOF}) systems using amplification factors given in Equation 2.13. The factors f_{MDOF} and $f_{p-\triangle}$ are incorporated to account for higher modes and P-$\triangle$ effects, respectively.

$$RD_{MDOF} = RD_{SDOF} . f_{MDOF} . f_{P-\triangle} \tag{2.13}$$

Having the residual displacement response spectra using SDOF oscillator with an expression to generate the equivalent residual drift of MDOF system, the authors proposed a DDBD procedure that incorporates residual drift at the initial stage of DDBD. The proposed method introduces one more step on the conventional DDBD procedure of Priestley et al. [PCK07b]. After obtaining an equivalent SDOF system using conventional DDBD method [PCK07b], a check for residual deformation is added before calculating the design base shear. From the target displacement and effective period of equivalent SDOF, the residual displacement can be obtained from the residual displacement spectra. By using Equation 2.13, the residual drift of MDOF system can be calculated using the appropriate amplification factors. If the obtained RD_{MDOF} is within the acceptable limit then the process can proceed to calculate the design base shear. However, if the residual drift has exceeded the limit, the properties of equivalent SDOF should be modified and all the steps will be repeated. Finally, the paper presents recommendations to control the residual drift of MDOF frame structures.

Alaee [MASR] Towards a DDBD procedure for cold-formed steel frame / wood panel shear walls

Two important inputs of direct displacement based design method, equivalent viscous damping (EVD) and design displacement profile, are formulated for cold-formed steel frame / wood-panel (CFSFWP) systems. For this purpose, several nonlinear time history analyses are carried out to develop the EVD as a function of ductility for different effective periods of a given hysteretic law. Moreover, for low rise systems, verification is included to use a linear displacement profile for DDBD. The EVD ξ_e expression is developed for thin and fat hysteretic models in terms of ductility (μ) and is given in Equation 2.14.

$$\xi_e = 0.05 + 0.478\left(\frac{\mu - 1}{\mu\pi}\right) \tag{2.14}$$

In addition, for the DDBD procedures the authors suggested the following expression for equivalent viscous damping (Equation 2.15) that needs small trial and error.

$$\xi_e = \begin{cases} 0.095\mu - 0.045 & if 1 \leq \mu \leq 2 \\ 0.145 & if \mu > 2 \end{cases} \tag{2.15}$$

As part of recommendation to use linear displacement profile, a plot of mean interstorey drift with the assumed profile is given that shows the applicability of the assumption for 3 storey CFSFWP structures.

3

Studying lateral behaviour of CLT infilled SMRFs via artificial intelligence, Genetic Algorithm, and Response Surface Method

3.1 Predicting MISD of CLT infilled SMRFs: Response Surface Method

The 1995 Hyogo-ken Nanbu (Kobe, Japan), the 1985 Michoacan earthquake (Mexico City, Mexico) and the 1994 Northridge earthquake (California, US) caused significant damage to the infrastructure. Generally, the damage sustained in the buildings can be related to the structural deformation [KMA03, EY04, MK05, GAEB99, KC04]. Also, several reinforced concrete buildings damaged by the 1985 Michoacan earthquake were demolished due to large permanent (residual) drift [RM86]. Recent studies are highlighting the importance of residual drift in the post-earthquake performance assessment of new and existing structures [CPP03, PCP03, CP04, LBC04, BCMM04, YD08]. Gupta and Krawinkler [GK99] reported the residual drift demands SMRF frames and highlighted the increase in uncertainty along with the intensity of ground motions. In order to satisfy a reparability limit state, Iwata et al. [ISK06] suggested that the maximum residual inter-storey drift angle for steel moment-resisting frames (SMRFs) buildings should be limited to 1/90. McCormick et al. [MAIN08] proposed residual drifts of 0.5% as permissible value on the study conducted in Japan.

Wu et al. [WLYL04] showed the combination of maximum and residual deformation is effective to evaluate structural performance under seismic excitation. Pampanin et al. [PCP03] developed performance matrix using interstorey and residual drift as a framework for an alternative performance assessment. Erochko et al. [ECTC10] developed an equation to express the residual drifts as function of peak drifts and damage concentration factor. More recently, Christidis et al. [CDHB13] proposed a simple method to evaluate the maximum seismic roof displacement of steel framed structures from their residual drifts. These studies prompted the need to develop an equation for rapid and direct evaluation of the post-earthquake performance of steel-timber hybrid structures. Recently, [SDT12, STKP12, DST12, Dic13, DSBT14] investigated the potential use of Cross Laminated Timber (CLT) as an infill in steel moment resisting frames to couple the light and stiff behaviour of timber with a strong and ductile steel frame. In addition, Tesfamariam et al.[TSDB14] studied the seismic vulnerability of this hybrid system with consideration of MISD.

The primary objective of this section is to develop an equation to predict MISD from post-earthquake residual interstory drift (RISD) and modeling parameters of CLT infilled SMRFs. For this purpose, two-dimensional (2D) dynamic analysis of the proposed hybrid system was performed for various modeling parameters, i.e. building height, infill pattern, CLT panel thickness and strength, and connection bracket spacing. The analyses were carried out by using OpenSees [MMS$^+$06] FE software for twenty maximum considered earthquake (MCE) ground motions (2% in 50 years). Response surface methodology (RSM) with D-Optimal experimental design technique was adopted for the development of prediction equation. Finally, the proposed equation is statistically validated to check its capability of prediction for data points other than the model training data set.

3.1.1 Building design and modeling

Design of Buildings

A typical 3-, 6- and 9- storey steel frame office building, with regular geometric shape, was considered. The plan view is shown in Figure 3.1. The buildings were designed for the seismic events of the magnitude possibly occurring in Vancouver, Canada. The buildings were modeled as two-dimensional structure and, due to its symmetry in plan, accidental torsion was neglected both in design and analysis phase. For the seismic load, the equivalent static load (ESL) procedure as suggested by NBCC 2010 [NRC10] was used. The buildings were designed to meet the requirement of moderate ductility (with $R_d = 3.5$, and $R_o = 1.5$) as specified in CSA S16 [CSA09]. Only building frames along the north-south directions were considered for the design and analysis. All steel sections used in design were based on CSA G40.21-04 [CSA09] specification and the section details are presented in Table 3.1 and 3.2.

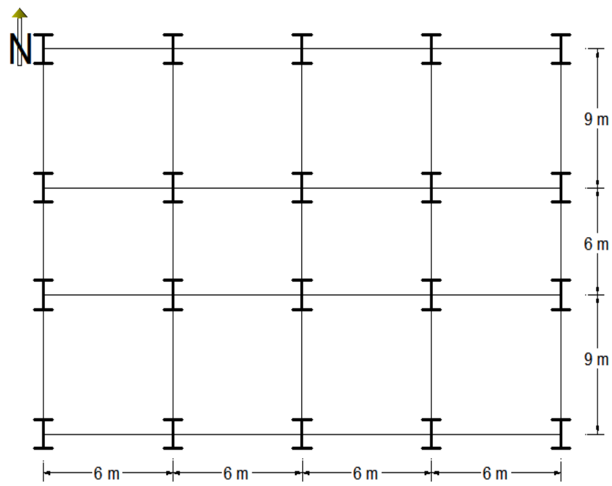

Figure 3.1: Typical building plan

Table 3.1: beam design details

Building storey	*Storey number*	*External*	*Internal*
3	1−2	W310×60	W310×60
	3	W310×52	W310×52
6	1−3	W310×79	W310×79
	4−5	W310×74	W310×74
	6	W310×60	W310×60
9	1−6	W310×86	W310×86
	4−5	W310×74	W310×74
	6	W310×60	W310×60

Table 3.2: column design details

Building storey	*Storey number*	*External*	*Internal*
3	1−3	W310×67	W310×86
6	1−3	W310×107	W310×107
9	1×6	W310×107	W310×118
	4−6	W310×67	W310×86
	7−9	W310×67	W310×67

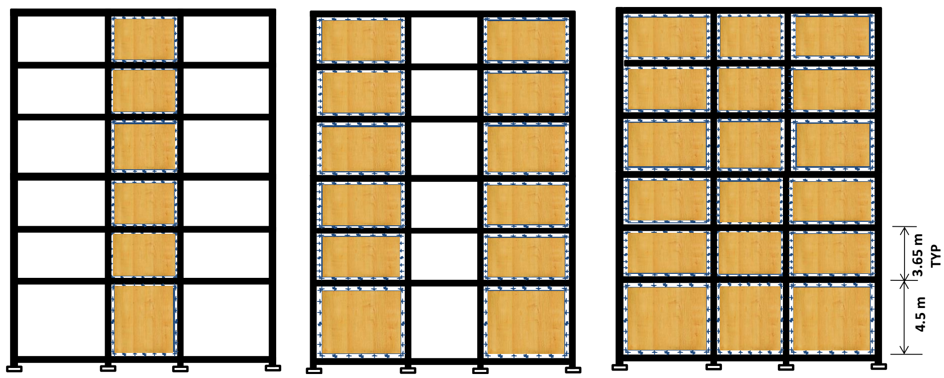

Figure 3.2: CLT infill distributions of 6-storey typical building, a) Frame with infill only in the middle bay (0-1-0); b) Frame with infill in two exterior bays (1-0-1), and c) Frame with infill in all bays (1-1-1)

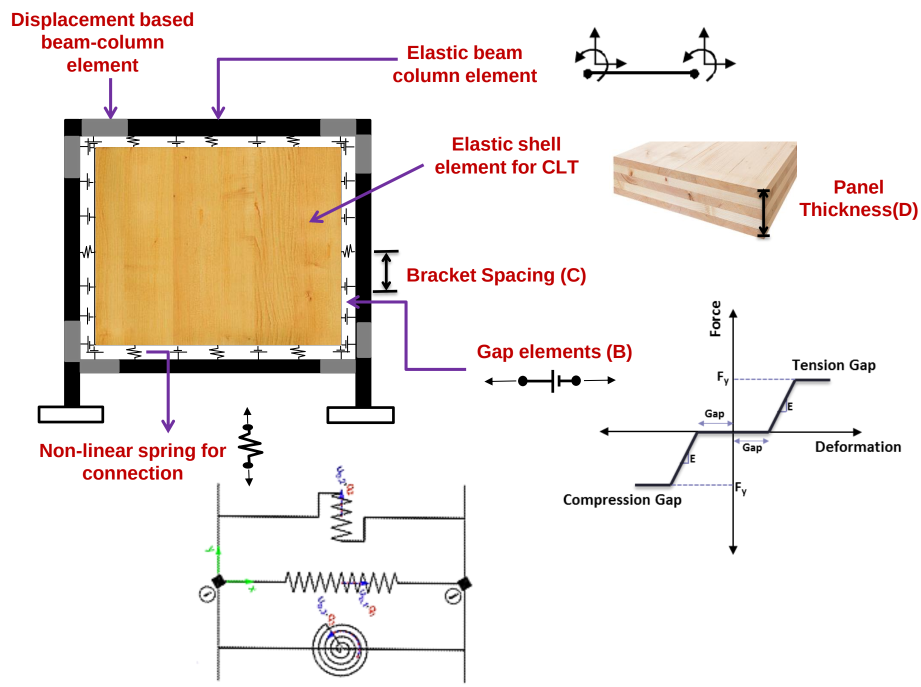

Figure 3.3: Details of connection, Gap and CLT infill panels

Modeling of building structures

Detailed modeling of both structural members and CLT infill panels were performed using OpenSees FE software [MMS+06]. The details are provided in the subsequent paragraphs.

Modeling of structural frames elements: spread plasticity principle

The structural frame elements have been modeled using combination of linear and nonlinear elements. Linear elastic and non-linear displacement based beam-column elements used for the center and end of the frame member respectively are shown in Figure 3.3. Modified Ibarra Krawinkler Deterioration model [LK10] used with a bilinear material property based on moment-curvature relationships are given in the ASCE 41 [C+07] for nonlinear parts of the frame elements.

Modeling of CLT panels

CLT panels were modeled as a linear elastic shell element as shown in Figure 3.3. For simplicity, the section of CLT panel was modeled as single layer with linear elastic- isotropic wood material property of *Quad* elements of OpenSees. The material model used for these quad elements was the *ndMaterial-ElasticIsotropic*. The CLT mechanical properties used for modeling can be found elsewhere [Dic13, DSBT14, TSDB14].

Modeling of connection between CLT panels and steel frames

The connection between the steel frames and CLT walls was achieved by using steel brackets; which were bolted with steel and nailed to CLT panels. Non-linear spring model was used to represent the behaviour of the bracket that connects CLT with steel frame. A more realistic characterization of the CLT to frame connection could be accomplished with the so-called *Pinching4* material model of OpenSees [SST+13]. Figure 2.7 shows a good agreement between experimental test data and Pinching4 analytical model. Therefore, the calibrated *Pinching4* model was used to model the non-linearity of the bracket connection. The OpenSees *twoNodeLink* and Elastic Perfectly Plastic Gap (EPPG) elements were used to model connection and gap respectively. The bracket behaviour was assigned both in the shear and axial direction. Additionally, the EPPG gap property was modeled in parallel formulation with the axial behaviour of bracket.

3.1.2 Seismic input

Twenty ground motions records were obtained from the Pacific Earthquake Engineering Center [PEE05] database by comparing the ratio of seismic motion (A/V) to Vancouvers A/V. The A/V (A in g and V in m/s) of Vancouver is close to 1.0 and an average of 0.97 was obtained from selected ground motions. All GMRs were obtained from stations on soil class C of NBCC, 2010 [NRC10]. The events had moment magnitudes in range of 5.42 - 7.36 with in epicentral distance of (14.4-76 km). Table 3.3 summarizes the selected GMRs for this paper.

Table 3.3: Ground Motion properties

No.	*Earthquake*	*Station*	*Mw*	*PGA/PGV*	*D(Km)*	*tD(Sec)*	*AI(m/s)*
1	San Fernando, 1971	CDMG 24303 LA - Hollywood Storage FF	6.4	1.11	39.49	9.26	0.76
2	San Fernando,1971	CDMG 24271 Lake Hughes	6.61	0.81	26.1	7.93	0.83
3	Parkfield,1966	CDMG 1016 Cholame-Shandon Array 12	6.19	0.98	6.18	25.81	0.83
4	Northridge,1994	CDMG 24461 Alhambra - Fremont School	6.69	1.02	40.15	7.45	0.74
5	Northridge,1994	CDMG 24283 Moorpark - Fire Sta	6.69	1.03	31.45	6.98	0.86
6	Livermore,1980	CDMG 57064 Fremont - Mission San Jose	5.8	1.2	37.28	5.41	0.36
7	Coaglina,1983	CDMG 46175 Slack Canyon	6.36	1.016	33.52	7.53	0.6
8	Morgan Hill,1984	CDMG 57064 Fremont - Mission San Jose	6.19	0.91	31.83	30.28	0.53
9	Morgan Hill,1984	CDMG 57383 Gilroy Array 6	6.19	1.196	36.34	23.94	1.09
10	Loma Prieta, 1989	CDMG 57383 Gilroy Array 6	6.93	1.092	34.47	15.89	0.93
11	Gazli USSR, 1976	9201 Karakyr	6.8	1.047	12.82	14.9	5.9
12	Northridge, 1994	USC 90015 LA - Chalon Rd	6.69	0.929	14.92	9.01	0.85
13	Northridge, 1994	USC 90020 LA- W 15th St	6.69	1.04	29.59	19	0.76
14	Northridge, 1994	UCSB 78 Stone Canyon	6.69	1.107	14.41	8.31	1.17
15	Imperial Valley, 1979	UNAMUCSD 6621 Chihuahua	6.53	0.923	18.8	23.97	1.35
16	Iprina Italy, 1980	ENEL 99999 Rionero In Vulture	6.2	0.92	29.83	27.35	1.23
17	Iprina Italy, 1980	ENEL 99999 Calitri	6.9	0.83	15.04	31.36	1.35
18	Kern Country, 1952	USGS 1095 Taft Lincoln School	7.36	1.132	43.49	29.88	1.45
19	Hecotr Mine, 1999	SCSN 99999 Hector	7.13	0.895	26.53	11.26	1.08
20	Hector Mine, 1999	CDMG 12647 Joshua Tree N.M	7.13	1.15	75.38	11.9	0.89

Two additional characteristics of the selected records are found in the Table 2; significant duration (t_D) and Arias Intensity (AI). Significant duration (t_D) is estimated as suggested by [TB75], which is a time interval at which 5% and 95% of the Arias Intensity (AI) accumulates. Although it is believed that strong motion duration does not have any significant effect on the response structure [SCBC98, BC94], some recent studies [MP97, Cha05, DM01] show that there is indirect relationship between strong ground motion duration and seismic response. Therefore, in this work seismicity was characterized by significant duration (t_D), calculated using SeismoSignal V 5.1.0 software. Figure 3.4 shows the definition of the t_D for Imperial Valley, 1979 record.

The selected GMRs were scaled to match with the response spectra of Vancouver at specified period range. Matching was done with in the period range of (0.2T $-$ 1.5T); 0.138 sec - 4 sec, where T is the fundamental period of the building. The ground motion matching was accomplished by matching the spectrum for a probability of exceedance of 2% in 50 years of NBCC 2010 [NRC10]. Figure 3.5 shows the scaled spectra with the mean and target spectrum for considered hazard value.

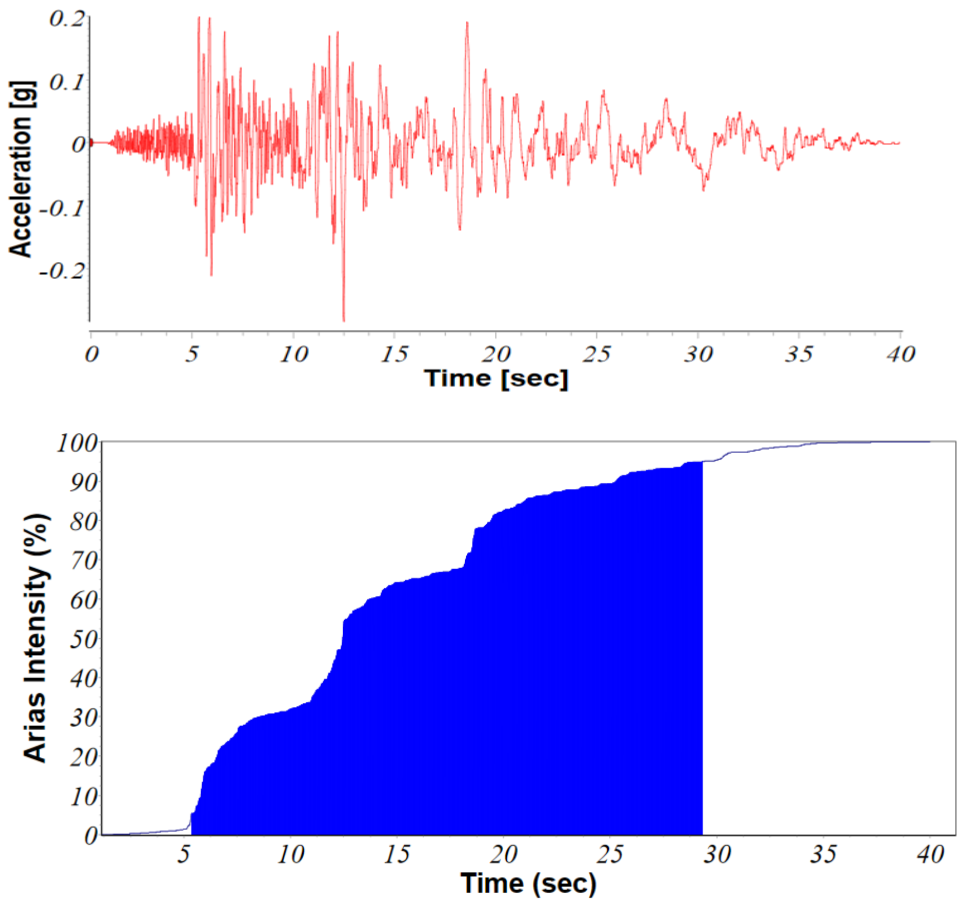

Figure 3.4: Significant duration definition according to ([TB75]) for Imperial Valley, 1979 earthquake

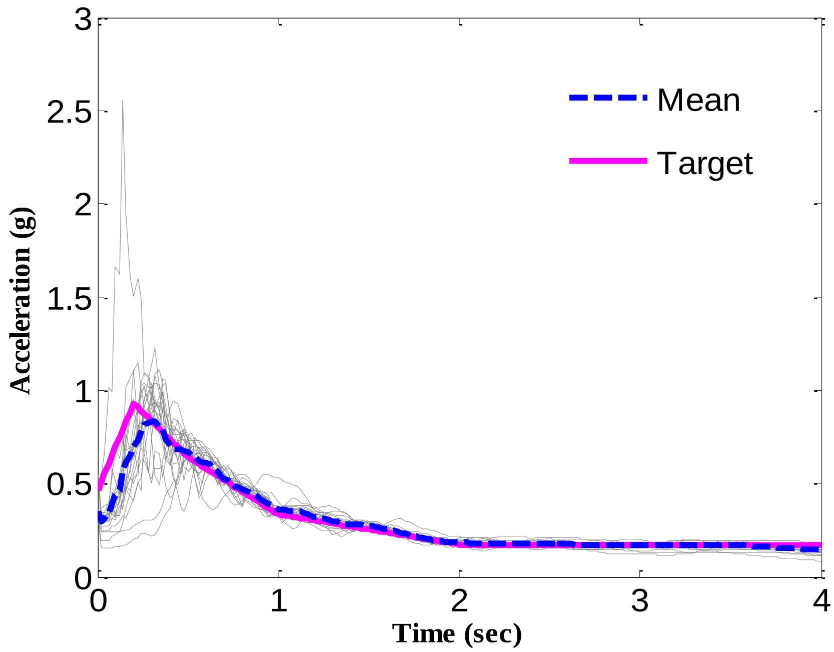

Figure 3.5: Comparison of mean and target response spectra for probability of exceedance of 2 % in 50 years

3.1.3 Maximum and residual interstorey drift results

Two dimensional nonlinear time history analysis was carried out to calculate MISD and RISD to develop the prediction equation. The factors and treatment levels that were used for dynamic analysis were chosen by considering market availability and simulation running time. Three, six , and nine storey frames were considered with with one (0-1-0), two (1-0-1) and three (1-1-1) bays infill, as shown in Figure 3.2. Bracket spacing of 0.8m and 1.6m were chosen by considering computational simplicity. A panel thickness of (99 mm, 169 mm, and 239 mm) and panel strength of (17.5 MPa, 25 MPa and 37.5 MPa) were selected by considering market availability. Analyses were carried out for each combination of factors considered and treatment levels. The results of dynamic analyses are presented in the form of performance matrix of MISD and RISD as shown in Figure 3.6. This plot was developed from 3240 scatter data points for only the storey in each building that has the largest drift for each seismic excitation. The higher drift scatter is for less infill patterns (0-1-0), large bracket spacing and 9-storey building. Some overlapped observations are depicted in the performance matrix, which indicates that there are some factors in the dynamic analysis that have a minimal effect on both MISD and RISD. This conclusion will be verified in subsequent sections using sensitivity analysis of input factors.

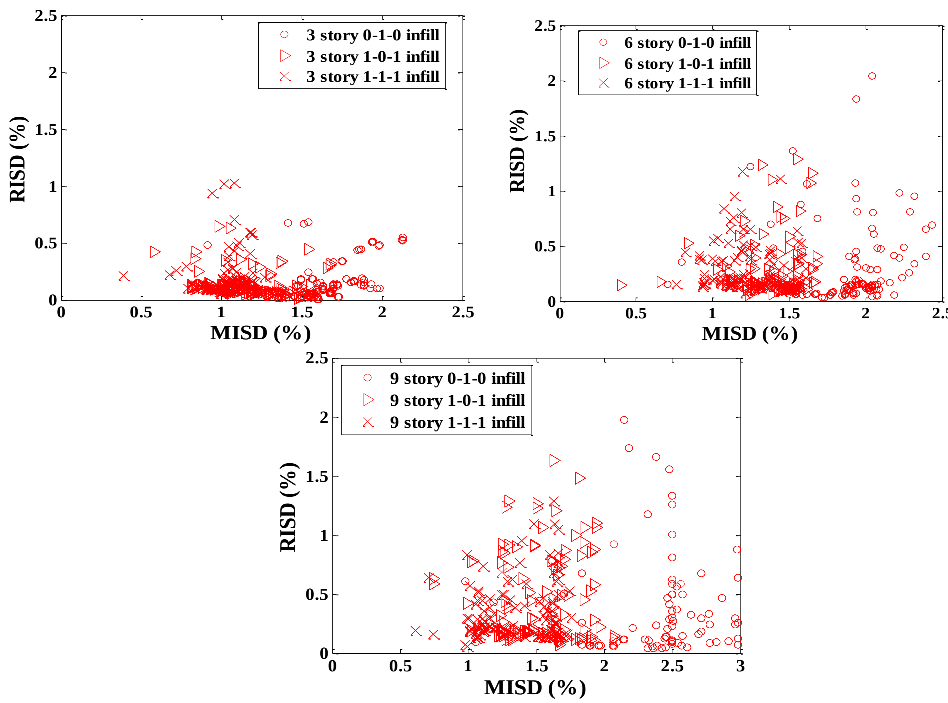

Figure 3.6: Performance matrix for residual and maximum interstorey drift

More specifically, Figure 3.7 depicts the time history of the top horizontal displacement for 3-story bare and CLT infilled frames. These plots are for bracket spacing, panel thickness and panel strength of 0.8m, 99mm and 25 MPa, respectively. As expected, the residual displacement (Uresidual) is decreases when the infill number increases. Significant reduction was observed at the maximum roof displacement (Umax) for 1-0-1 and 1-1-1 infill patterns.

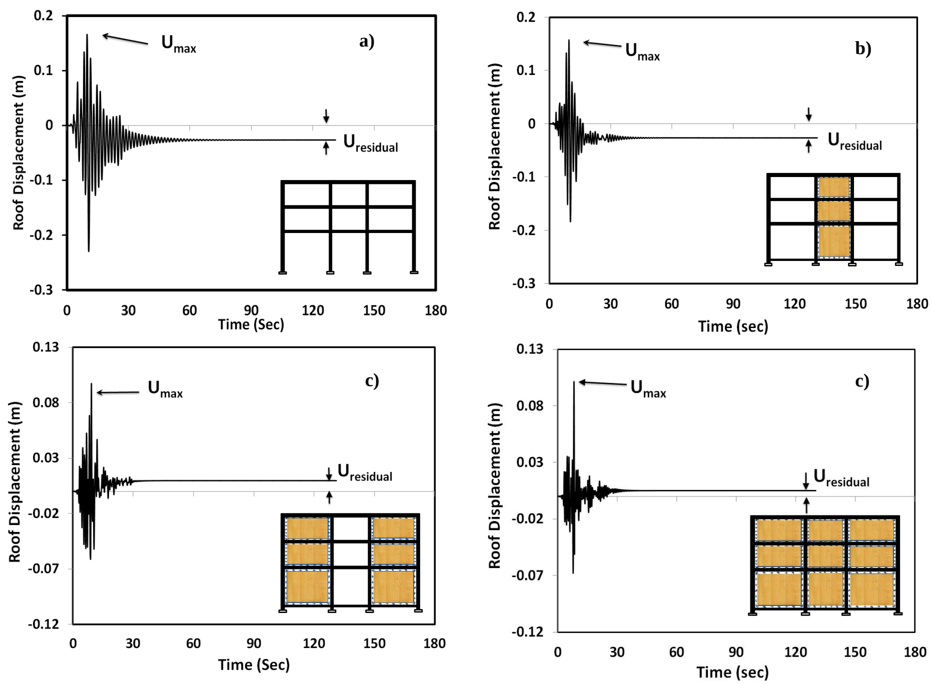

Figure 3.7: Displacement time histories of a typical 3 storey building, a) Bare frame; b) Frame with infill in the middle (0-1-0); c) Frame with infill in two exterior bays (1-0-1), and d) Frame with infill in all bays (1-1-1)

3.1.4 Surrogate Model for MISD

Sensitivity Analysis

A screening process using sensitivity analysis was needed to improve the efficiency of RSM for equation development. The process was used to identify input variables that have larger influence on the output. Figure 3.8 shows the effect plots of MISD with each indicated variable by keeping the other variables at their median value.

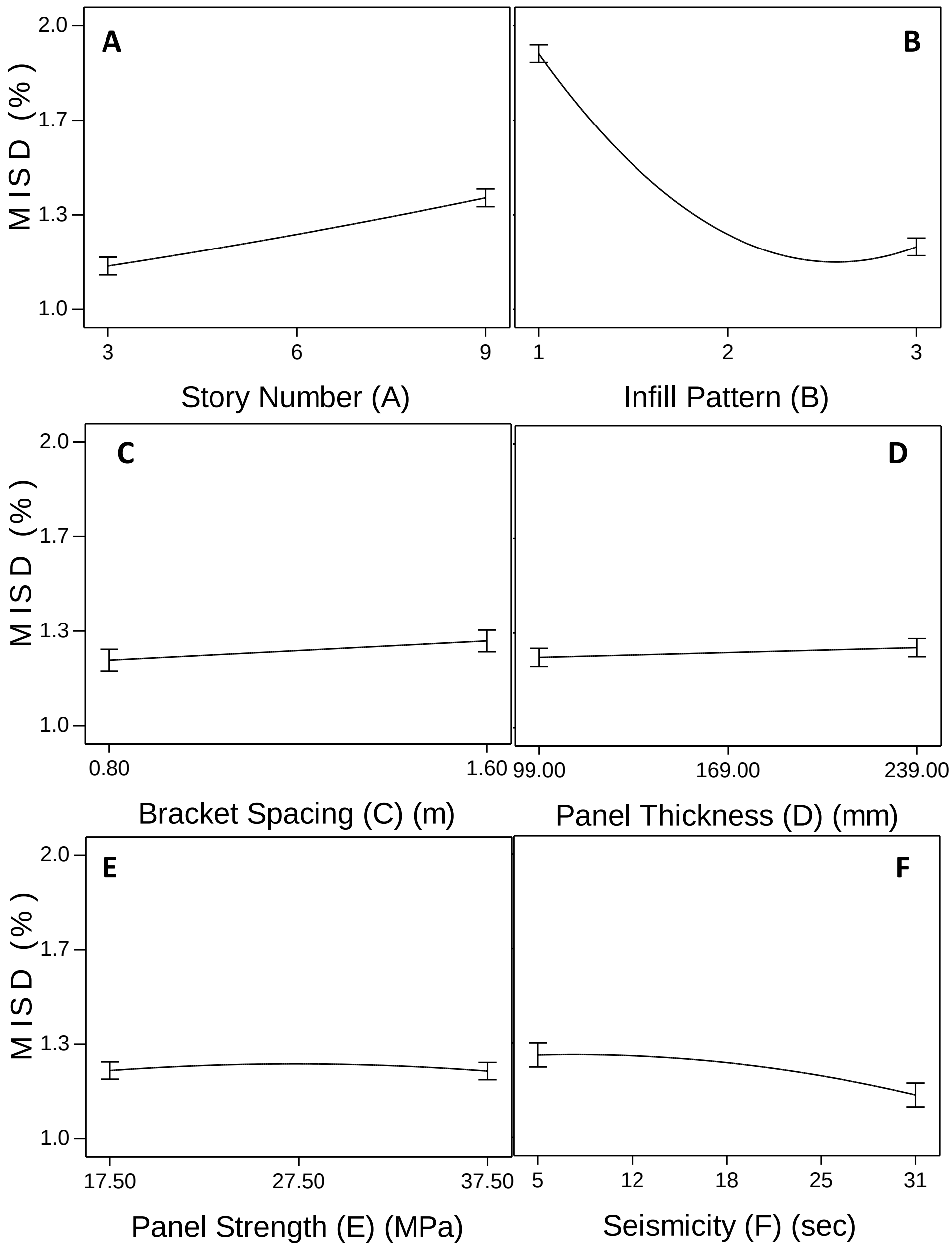

Figure 3.8: Effect plots of modeling parameters

The effect plots of bracket spacing, panel thickness and panel crushing strength revealed that their extent of influence is small. There is no strong evidence to reject these variables from further predictive equation development. However, MISD has been found to be sensitive to the significant duration (t_D), infill pattern, and number of storey.

Predictive equation using response surface methodology

Response surface methodology (RSM) consisted of a group of techniques used in the empirical study of the relationship between the response y and number of input variables x_1, x_2, ...,x_k [Mon97]. This relationship can be estimated with models from certain experimental data points. In this work, a D-Optimal deterministic experimental design technique was used for efficient sampling of design points of the dynamic analysis result. This type of design minimizes the overall variance of the estimated regression coefficients [KM10]. Moreover, this method is suitable for deterministic computer models and for simulations with an irregular experimental region [Mon97]. The factors and treatment levels that were used as input for experimental design with their upper and lower bound values are shown in Table 3.4. In this table RISD (output from dynamic analysis) is included as one input factor with 3240 levels.

Table 3.4: Definition of input variables

Factor	*Name*	*Units*	*Type*	*Subtype*	*levels*	*Minimum*	*Maximum*
A	Storey Number	-	Numeric	Discrete	3	3	9
B	Infill pattern	-	Numeric	Discrete	3	1	3
C	Bracket Spacing	m	Numeric	Discrete	2	0.8	1.6
D	Panel Thickness	mm	Numeric	Discrete	3	99	239
E	Panel Strength	MPa	Numeric	Discrete	3	17.5	37.5
F	Seismicity (t_D)	sec	Numeric	Discrete	20	5.41	31.36
G	RISD	%	Numeric	Discrete	2160	0.25	2.68

A second degree polynomial of the form shown in Equation 4.13 was used to set up relationship between y and x_1, x_2, ...,x_k; and used to predict MISD for the given settings of the modeling variables and RISD.

$$y = \beta_0 + \sum_{i=1}^{k} \beta_i x_i + \sum_{i=1}^{k} \beta_i x_i^2 + \sum \sum_{i<j} \beta_{ij} x_i x_j \tag{3.1}$$

In Equation 4.13, y is a regression function, and β_0, β_i and β_{ij} are the regression coefficients. In order to obtain the coefficients for the above second degree model, 87% of the data points from dynamic analyses were used for the model training, while the rest was kept aside for statistical validation. Analysis of Variance (ANOVA) test for significance level ($\alpha = 0.05$) was performed in Design Expert V8 [SE10] software to identify factors and their interactions that influence the response (MISD). Table 3.5 shows a standard ANOVA result with a corresponding degree of freedom, mean square and F-value for each factor and their interactions. Table 3.5 shows the only factors and interactions influencing the response, which possesses a P-value of less than 0.05.

Table 3.5: ANOVA table

Source	*Sum of square*	*df*	*Mean Square*	*F Value*	*P value*
Model	676.38	20	33.82	374.84	0.0001
A-Storey No	22.95	1	22.95	254.33	0.0001
B-Infill pattern	142.04	1	142.04	1574.28	0.0001
C-Bracket Spacing	0.22	1	0.22	2.46	0.1166
D-Panel Thickness	0.36	1	0.36	4.04	0.0444
E-Panel Strength	0.00293	1	0.00293	0.032	0.857
F-Seismicity (tD)	1.02	1	1.02	11.28	0.0008
G-RISD	0.089	1	0.089	0.99	0.3204
AB	47.71	1	47.71	528.75	0.0001
AC	3.73	1	3.73	41.36	0.0001
AD	0.26	1	0.26	2.92	0.0875
AE	0.2	1	0.2	2.2	0.1381
BC	1.61	1	1.61	17.87	0.0001
BD	0.51	1	0.51	5.63	0.0177
CG	0.81	1	0.81	9.01	0.0027
DE	0.27	1	0.27	2.95	0.0861
FG	0.57	1	0.57	6.3	0.0121
A^2	0.99	1	0.99	10.96	0.0009
B^2	60.1	1	60.1	666.09	0.0001
F^2	0.36	1	0.36	3.97	0.0463
G^2	0.42	1	0.42	4.69	0.0304

The model adequacy was checked for the ANOVA assumptions of normality and constant variance, during which nothing unusual was found. After this, regression analysis was performed based on the significant factors and interactions in order to estimate the coefficients of the proposed equation. Table 3.6 summarizes the coefficients for the proposed polynomial equation based on both normalized and actual factors.

Table 3.6: Equation coefficients

Source	*Normalized Coefficients*	*Actual Coefficients*
Intercept	1.22	2.304
A	0.12	0.055836
B	-0.34	-1.42639
C	0.029	-0.029398
D	0.017	1.19E-03
E	-1.51E-03	2.14E-03
F	-0.074	7.77E-03
G	-0.04	0.43916
AB	-0.097	-0.032272
AC	0.023	0.019398
AD	7.17E-03	3.42E-05
AE	6.13E-03	2.04E-04
BC	0.03	0.073855
BD	-0.02	-2.89E-04
CG	-0.065	-0.15923
DE	-0.015	-2.08E-05
FG	-0.071	-5.41E-03
A^2	1.00E-02	1.14E-03
B^2	0.31	0.31086
F^2	-0.037	-2.17E-04
G^2	-0.095	-0.091808

The effect of interactions was described using response surface plot in Figure 3.9 and 3.10 . These plots were constructed for the indicated axis labels while keeping the other parameters at their median value.

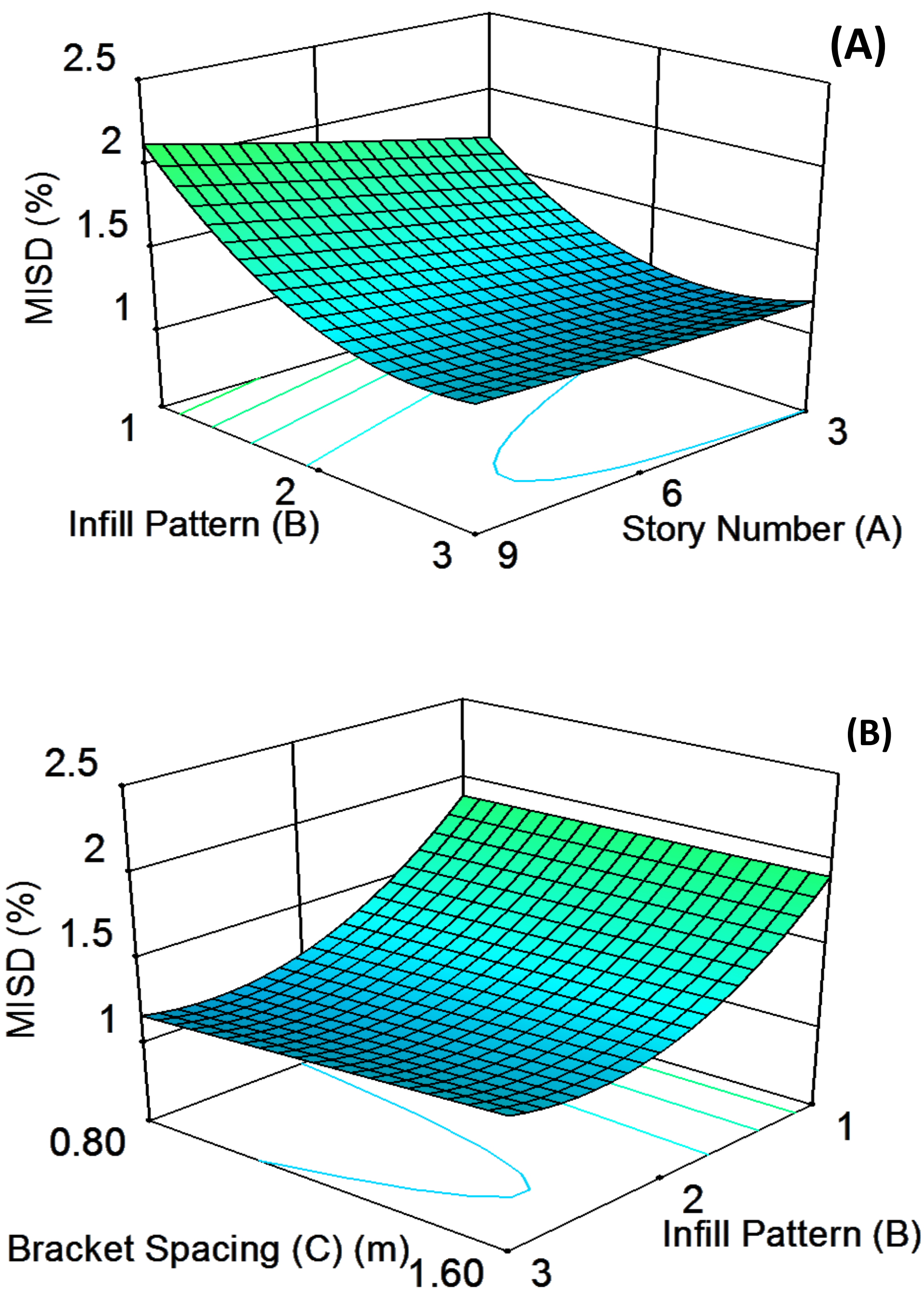

Figure 3.9: Response surface plot for interactions between; a) infill Pattern and storey Number and b) infill pattern and bracket spacing

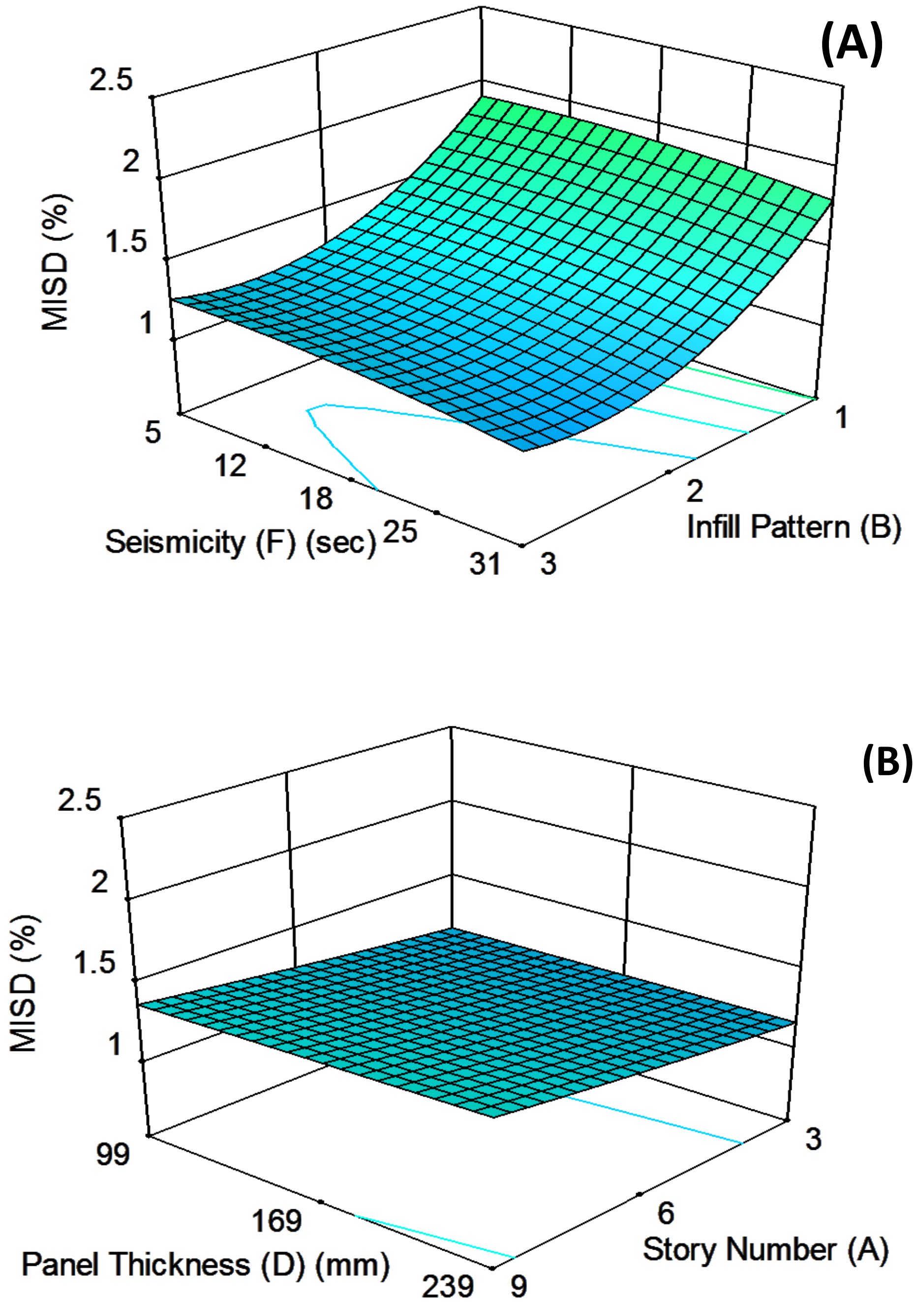

Figure 3.10: Response surface plot for interactions between; a) seismicity and infill pattern and b) panel thickness and storey Number

The lower infill patterns and nine storey building resulted in larger MISD as shown in Figure 3.9a. This observation is better supported by the larger absolute values of the normalized coefficients in the prediction equation of Table 3.6. It is also clear from Figure 3.9b that, MISD is heavily influenced by the infill pattern rather than the bracket spacing. This observation is reversed for a heavily infilled frame (1-1-1). From the above response surface plots it can be inferred that the addition of infilled bays decreases MISD significantly, which is strongly correlated with the increasing number of panels. Also, in Figure 3.10a the infill pattern is more dominant factor than the significant duration of the ground motions. Nine storey frames with 0-1-0 infill pattern experienced more storey drift than the other models. Focusing on the Panel thickness, Figure 3.10b indicates their minimal effect on MISD, which was consistent throughout effect plots and ANOVA test results of these two parameters.

3.1.5 Statistical validation of the proposed equation

Statistical tests such as F-test and R^2 test are widely used to validate regression models. However, due to the absence of random error they are incompatible with the current problem. Therefore, two alternate validations techniques [SPKA97] using the original and additional data points were applied. The former method uses validation using the adjusted R^2 (model sum of squares divided by total sum of squares) on the training data set. The latter one adopts statistical error measuring indexes such as average absolute error (%AvgErr) and root mean square error (%RMSE) of additional validation data points. For the second method, 432 randomly selected MISD values used from the results of dynamic analysis. Equations 3.2 and 3.3 show formulas that used to calculate the defined indexes.

$$AvgErr = 100 \times \frac{\frac{1}{N}\sum_{i=1}^{N} y_i - y_j}{\frac{1}{N}\sum_{i=1}^{N} y_i} \tag{3.2}$$

$$RMSE = 100 \times \frac{\sqrt{\frac{1}{N}\sum_{i=1}^{N}(y_i - y_j)^2}}{\frac{1}{N}\sum_{i=1}^{N} y_i} \tag{3.3}$$

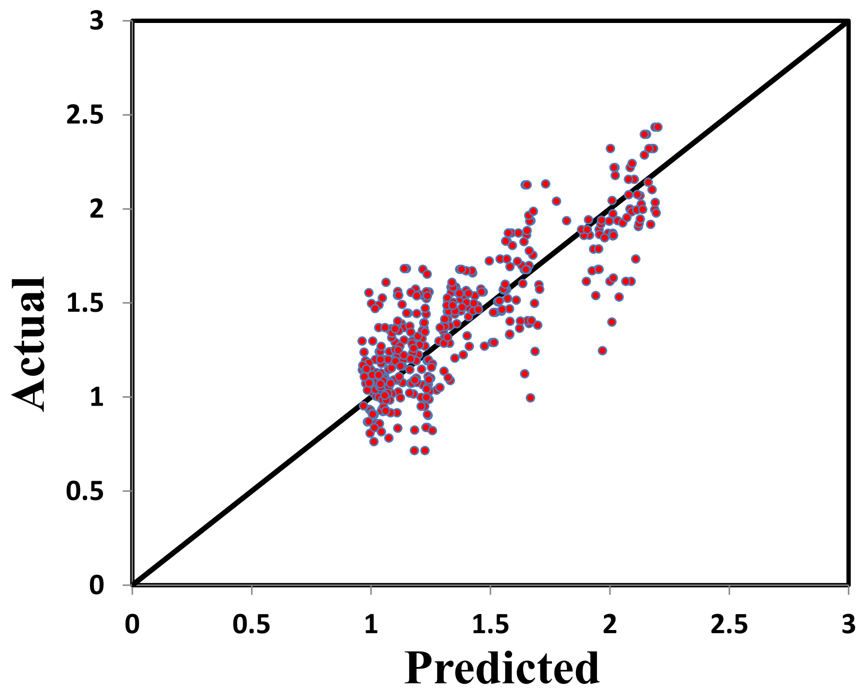

Figure 3.11: Validation plot; Predicted vs. Actual (red dots

Adjusted R^2 value of 0.73 was obtained from the first method, which shows how good the model fits with the original experimental data points. The statistical error measuring indexes (%AvgErr) and (%RMSE) values are 2.6% and 18.04%, respectively. The plot of predicted vs. actual values is shown in Figure 3.11. This plot possesses an R^2 value of 0.63 which confirms that the prediction equation approximates well the value of MISD.

3.2 Multi-objective optimization of drift demands of CLT infilled SMRFs

The primary objective of this section is to identify optimized modeling parameters of CLT infilled SMRFs by considering MISD and RISD as an objective functions. Responses surface plots are developed for MISD and RISD independently to study the effect of modeling parameters on the drift demands. For this purpose, 3 story building results of section 3.1 are used. Figures 3.12 and 3.13 show these two drift demands are conflicting each other as the number of infill bays is increased. Also as discussed in section 3.1.4, the infill pattern (which is directly related to the CLT wall length in the system) is the main factor that affect the drift demands of the hybrid system. This reason prompted the need to optimize the modeling parameters for the given conflicting objectives, i.e. MISD and RISD. To develop a more accurate models of objective functions, a concept of artificial intelligence is applied to all the dynamic results of section 3.1. Artificial Neural Network (ANN) model is trained and validated to predict MISD and RISD for further optimization. Finally, optimized modeling parameters were identified using Genetic Algorithm's multi-objective optimization capability that simultaneously minimizes MISD and RISD by defining the non-dominated Pareto front of design solutions.

3.2.1 Methodology

A framework that used to optimize the modeling parameters of the proposed hybrid system is depicted in Figure 3.14. The first step in the framework is to perform parametric study on the modeling variables using nonlinear time history analysis. The Modeling variables for the problem are determined by considering market availability and simulation running time. Three, six, and nine storey frames with regular geometry were used for this study. The first modeling variable (x_1) building height and the second variable (X_2) is infill pattern. One (0-1-0), two (1-0-1) and three (1-1-1) bays infill were considered, as shown in modeling section of Figure 1. Bracket

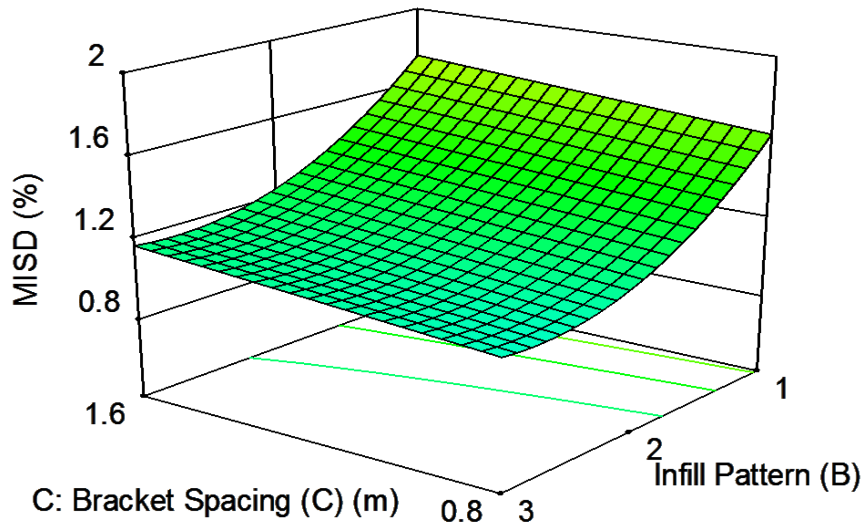

Figure 3.12: Response surface plot for MISD with infill pattern and bracket spacing

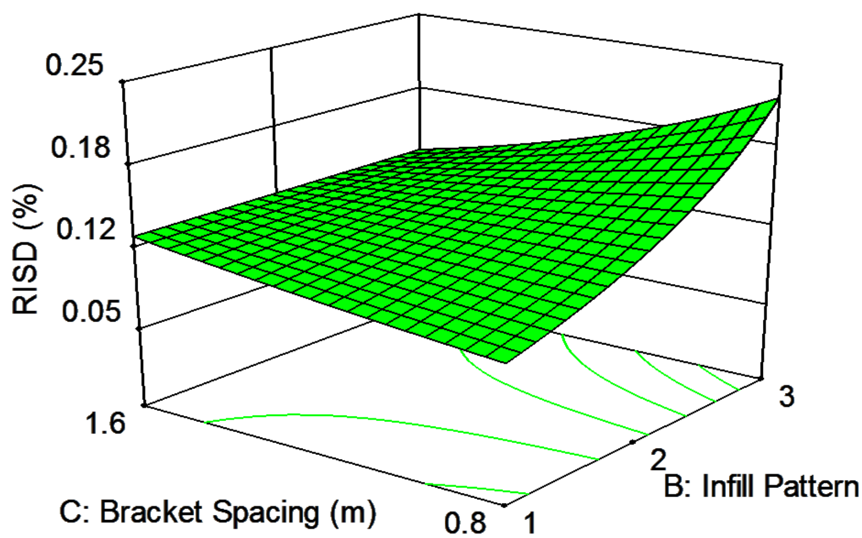

Figure 3.13: Response surface plot for RISD with infill pattern and bracket spacing

spacing (X_3) of 0.8m and 1.6m were chosen considering computational simplicity. A panel thickness (X_4) of (99 mm, 169 mm, and 23 9mm) and panel strength (X_5) of (17.5 MPa, 25 MPa and 37.5 MPa) were selected by considering market availability. Seismicity is represented by significant duration (X_6) obtained from the seismic hazard of Vancouver, Canada. The objective functions (RISD and MISD) are found from the result of time history analysis and depicted in Figure 3.14 as performance matrix plot. The details of this step are well discussed in subsequent sections. From this step for each combination of time history analyses the surrogate network function for RISD and MISD were obtained using ANN training method. Finally, multi-objective optimization using Genetic Algorithm (GA) is carried out to optimize the modeling parameters.

3.2.2 Surrogate Model using artificial intelligence

Artificial Neural Network

Artificial Neural Network (ANN) is a subset of Artificial Intelligence that simulates the behaviour of human brain that helps machines and computers to learn. ANN is a system that has a capability to simulate, learn and store knowledge for future usage [ASAH11]. ANN has been applied for various aspects of structural capacity predictions and yields accurate results when compared to experimental results and code justified formulations [Sel12, DAGT09, BBS07, CKS03, MDLZ04, CNS06]. In order to obtain a more accurate predictions of MISD and RISD, in this thesis, ANN is trained and validated using results from nonlinear time history analysis. The Multilayer preceptors (MLP) are the most widely used feed-forward networks consisting of input layer, hidden layer and output as shown in Figure 3.15. As shown in Figure 3.15, the input layer comprised of building height, bracket spacing, infill pattern, CLT panel thickness and strength, and seismicity (t_D). The output layer is representing MISD and RISD. The details of training and validation of the surrogate models are given in Appendix A.

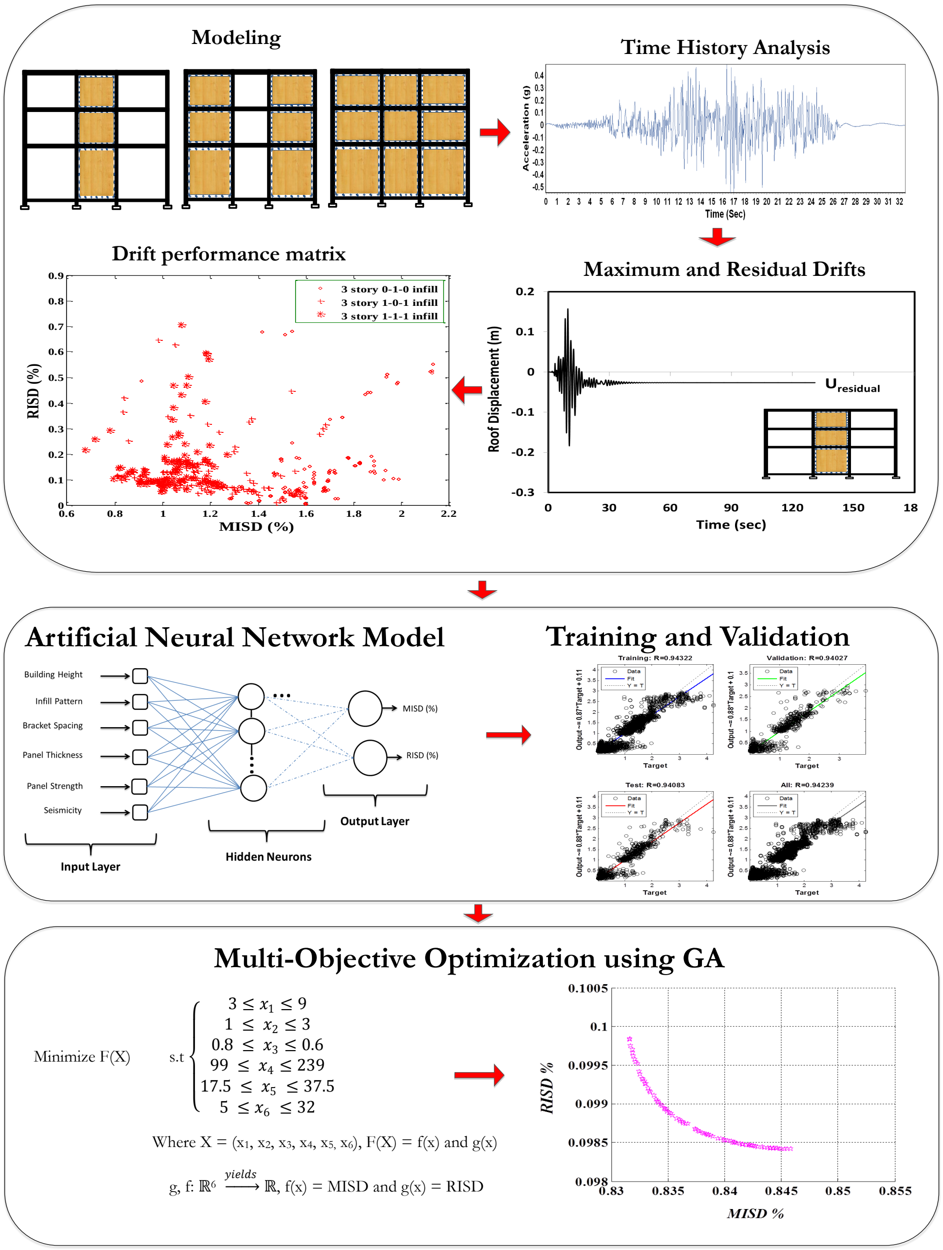

Figure 3.14: Outline of the methodology

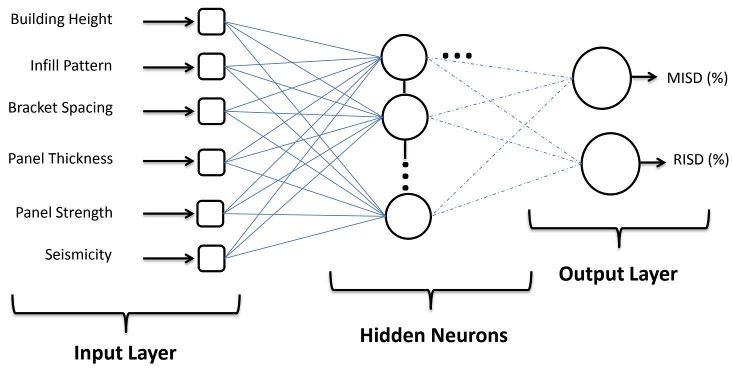

Figure 3.15: ANN model for prediction of objective function

3.2.3 Multi-objective optimization using Genetic Algorithm

Recently, Tesfamariam et al. [TBS14] optimized the modeling parameters of CLT infilled steel moment frames using the objective functions that are developed using response surface method. From their research they concluded that RISD and MISD are conflictive drift objectives with respect to the infill topology in the frame. Their conclusion gives imputes to perform multi-objective optimization of modeling parameters using black box functions developed using ANN analysis of previous section.

Genetic algorithm (GA) is a stochastic method to search the optimal point using population solution for multi-objective optimization problems [Deb01]. The optimization problem defined for the case understudy is given by:

$$
\begin{aligned}
&\underset{x}{\text{minimize}} && F(X) \\
&\text{subject to} = && \begin{cases} 3 \leq x_1 \leq 9 \\ 1 \leq x_2 \leq 3 \\ 0.8 \leq x_3 \leq 1.6 \\ 99 \leq x_4 \leq 239 \\ 17.5 \leq x_5 \leq 37.5 \\ 5 \leq x_6 \leq 32 \end{cases}
\end{aligned}
$$

where X = (x_1, x_2, x_3, x_4, x_5, x_6), F(X) = f(x) and g(x) and g, f: $R^6 \rightarrow$ R, f(x) = MISD and g(x) = RISD

The network is simulated and the outputs are assigned as fitness function for GA for the optimization process. A MATLAB tool box [MAT13] is used for the current problem with a population size of 250 for each of the iterations. Constraint dependent and intermediate functions were assigned for mutation and crossover, respectively. The generated Pareto-optimal solutions are presented in Figure 3.16.

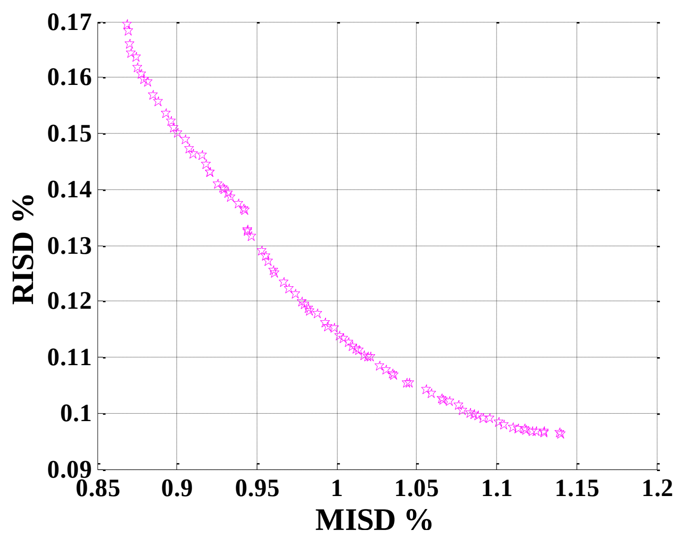

Figure 3.16: Pareto-optimal solutions

Results and Discussion

This section presents the results of the optimization and corresponding variables of Pareto-front curve shown in Figure 3.16. 3-story building appears to be optimal building height. The variables corresponding to Pareto-front curve of Figure 3.16 are depicted by using a higher-dimension matrix scatter in Figure 3.17. The matrix scatter plot shows the relationship between each optimal variable with respect to the height of the building. For the current optimization problem infill pattern in two bays (1-0-1) is always optimal. Bracket spacing in the range of [0.8 - 0.845 m], panel thickness [110

- 130 mm], and panel strength [17.5 - 35 MPa] are other optimal modeling parameters.

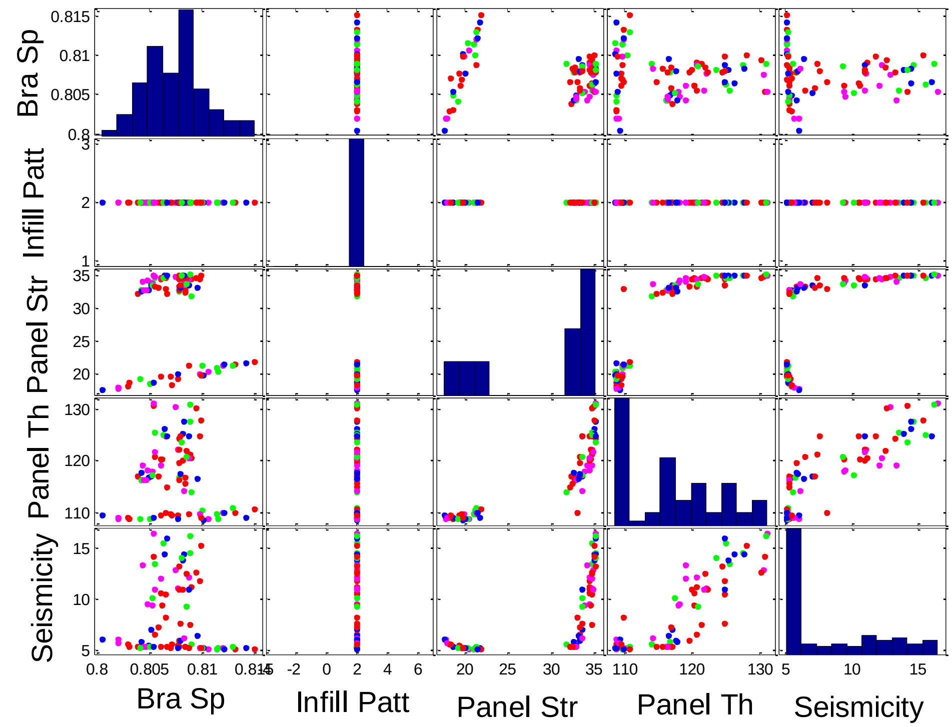

Figure 3.17: Higher order plot for variables corresponding to Pareto curve that trained using trainlm

3.3 Summary

This chapter proposed surrogate models for MISD and RISD of the CLT infilled SMRFs to identify optimum modeling parameters. For this purpose, two-dimensional (2D) time history analyses of the 162 hybrid buildings were performed utilizing 20 earthquake ground motions. Building height, infill pattern, CLT panel thickness and strength, and connection bracket spacing were selected as input decision variables for the analyses. In the first section, Response surface methodology with D-Optimal computer experimental design technique was adopted for the development of prediction equation of

MISD from modeling parameters and RISD. The developed second order polynomial equation was validated by statistical techniques with original and additional data sets. In the second section, more accurate surrogate models of MISD and RISD were developed using Artificial Neural Network. Subsequently, optimum modeling variables for the proposed hybrid system were identified. The optimization process adopts ANN based objective functions that are trained using Levenberg-Marquardt algorithm. This study adopted multi-objective optimization approach using Genetic Algorithm for conflicting objective functions. The obtained optimal modeling variables will be used as a starting point for the direct displacement based design of CLT infilled SMRFs in Chapter 5.

4

Equivalent viscous damping of CLT infilled steel moment resisting frames

4.1 Background

Generally, displacements due to seismic excitations are related to damage sustained in structures and associated failure [KMA03, EY04, MK05, GAEB99, KC04]. In performance based seismic design, the major advancement is to consider structural deformations as a main input for the deign process [PCK07b]. These methods are specifically known as direct displacement based seismic design. Direct Displacement Based Design (DDBD) utilizes a virtual representation of the nonlinear structures with an equivalent linear system through secant stiffness (K_e) and equivalent viscous damping (ξ_{eq}) at peak displacement ($\triangle_d$) as illustrated in Figure 5.1. This method uses equivalent viscous damping (EVD) to represent the energy dissipative capacity of the structural system. As shown in Figure 5.1d, the target displacement is used to obtain an effective period of the structure for the given level of EVD. From this step, the design base shear can be calculated from the effective mass (m_{eff}), secant stiffness (K_e), effective period (T_{eff}), and target displacement ($\triangle_d$)[PCK07b]. In this chapter, the motivation is to develop an EVD coefficient for a new steel-timber hybrid system [SDT12, STKP12, DST12, Dic13, DSBT14].

The EVD concept was introduced by Jacobsen [Jac60], which is based on the idea that nonlinear systems and equivalent linear system under sinusoidal excitation dissipate an equal amount of energy per cycle of response (Figure 4.1). The approach proposed by Jacobsen is called the area based approach and is shown in Equation 4.1.

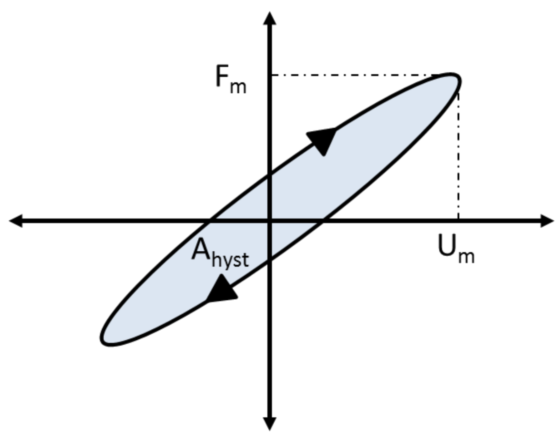

Figure 4.1: Hysteretic response area of one cycle

$$\xi_{hyst} = \frac{1}{2\pi}\frac{A_{hyst}}{F_m U_m} \tag{4.1}$$

$$\xi_{eq} = \xi_o + \xi_{hyst} \tag{4.2}$$

where A_{hyst} is the value of dissipated energy; F_m and U_m are the maximum force and displacement for the loop, respectively (Figure 4.1). The equivalent viscous damping ξ_{eq} in Equation 4.2 is the summation of elastic damping ξ_o and hysteretic component of damping ξ_{hyst} ([PCK07a]). Rosenblueth and Herrera [EI64] developed the EVD expression based on secant stiffness. Priestley [Pri93] adopted this for the DDBD method of structures. Miranda and Garcia [MRG02] validated Jacobsen′s approach with secant stiffness to determine the inelastic displacement demand of a Single Degree of Freedom System (SDOF) system. A comprehensive investigation of the accuracy of Jacobsen′s approach was performed by [DK04] for the Takeda hysteresis model using 100 earthquake records. Kowalsky and Ayers [KA02] found that the equivalent linear system based on Jacobsen′s approach, using effective period at maximum response, yields a good result for the assessment of a non-linear response for majority of considered cases. Blandon and Priestley [BP05] compared the EVD based on Jacobsen′s approach and EVD from the iterative time history analyses for six different hysteretic models. They concluded that Jacobson′s approach overestimate EVD values and proposed the corrected equations for DDBD method. Recently, the EVD was investigated for different types of structural systems [DKN07, WNS11, GJT12, LS06]. Dwairi et al. [DKN07] proposed a hyperbolic damping ductility law based on nonlinear ductility at peak displacement as follows:

$$\xi_{hyst} = C\left(\frac{\mu - 1}{\mu\pi}\right) \tag{4.3}$$

where C is a constant and μ is a ductility ratio. The authors have proposed values of C for unbonded post tensioned concrete systems, reinforced concrete beams, reinforced concrete walls and steel members in terms of the effective period. Wijesundara et al. [WNS11] derived the EVD expression for a concentrically braced frame based on Jacobsen′s method and calibrated the expressions using iterative time history analyses. They have also highlighted that pinching significantly affects the EVD. Ghaffarzadeh et al. [GJT12] proposed new EVD equations for the reinforced concrete (RC) moment resisting frames and RC concentrically braced frames. Lu and Silva [LS06] estimated EVD for seismic and blast loads for individual and multiple RC members. However, the EVD expression is not yet developed for the steel-timber hybrid system.

Since there is no definite hysteresis law to characterize the response of the proposed hybrid system, 243 single storey-single bay hybrid systems are analytically investigated to compute the EVD based on Jacobson′s area based approach and corresponding ductility. Different parameters are varied: gap between CLT panel and steel frame, bracket (connection) spacing, CLT panel thickness and strength, and post stiffness yield ratio of steel members. A least square regression method is used to calculate the value of C (Equation 4.3) for each system. An expression for the coefficient C as a function of different modeling parameters is developed using Response Surface Method (RSM). Subsequently, an expression is proposed to compute EVD from ductility and modeling parameters. Finally, an iterative nonlinear time history analyses is conducted using 20 spectrum compatible earthquake ground motions to calibrate EVD from Jacobsen′s area based approach.

4.2 Methodology

The method followed to formulate the EVD for the hybrid system is outlined below. A conceptual representation of the hybrid system is shown in Figure 3.3. Single-storey single-bay frame with the following model variables are considered:

- Three levels of bracket spacing were considered (A): 0.4 m, 0.8 m, and 1.6 m.
- Gap magnitude between steel frame and CLT infill (B) of 20, 50, and 80 mm, panel thickness (Ct) of (99, 169, 239 mm), panel strength (D) of (17.5, 25, and 37.5 MPa), and post stiffness yield ratio (E) of (1, 3, and 5 %) were selected.

Once the analytical models are developed, the procedure depicted in Figure 4.2 is followed to establish the EVD-ductility law. Monotonic static pushover and semi-static cyclic loading analysis are carried out for all considered models. The parameters considered in this study are summarized in Table 4.1. The total combination of all parameters constitutes the 243 models considered.

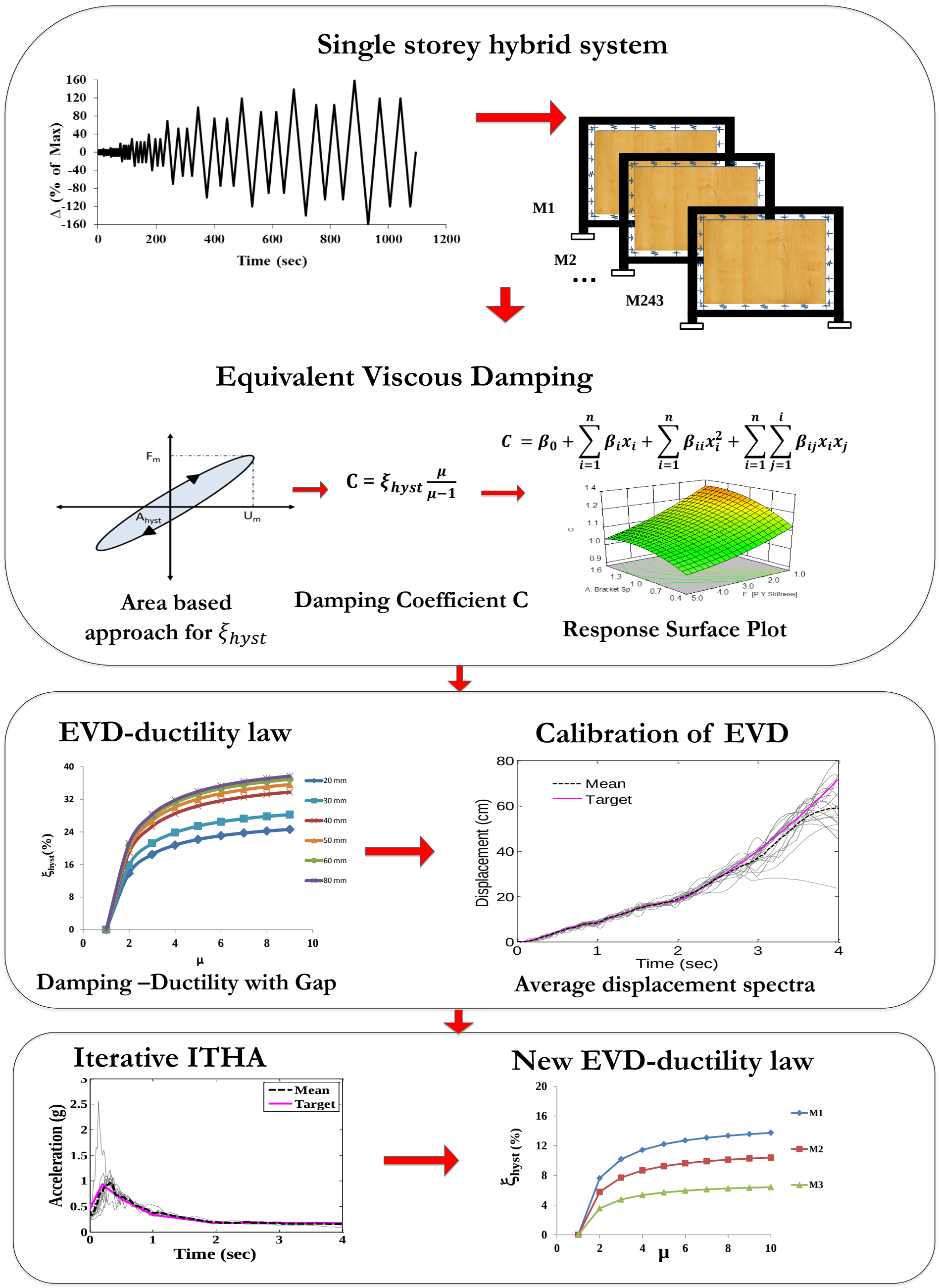

Figure 4.2: Framework for formulation

Table 4.1: Modeling variables

A:Bracket-Spacing(m)	**B:Gap(mm)**	**C_t: Panel Thickness (mm)**	**D: Panel Strength (MPa)**	**E: Post Yield Stiffness (%)**
0.4	20	99	17.5	1
0.8	50	169	25	3
1.6	80	239	37.5	5

The results of the pushover analysis are used to calculate the yielding and ultimate displacement of each hybrid system. Subsequently, the EVD and ductility of each system are computed from the hysteretic responses. Design of computer experiments and response surface methodology were applied to formulate the damping-ductility law. Finally, calibrations of sample models are carried out using nonlinear time history analysis (NLTH).

4.3 Formulation for yielding point

In order to establish the yielding point of the proposed hybrid system, a preliminary finite element analysis was carried out under monotonic pushover loading. Figure 4.3 shows the stress distribution of the CLT infill panel. As is shown in Figure 4.3, the compression strut response is formed under the lateral load that is accompanied with high compression stress at the corner of the panels. The panel crushing is indicated as an effective way of to dissipate energy and is simpler for maintenance purposes [Dic13, DSBT14, TSDB14]. The yielding point is obtained as discussed below and taken as the smaller of steel yielding or panel crushing values in connection brackets for all predetermined models. The steel yielding points are determined from the outputs of the finite element analysis. An expression is developed to calculate the panel crushing displacement using a simple mechanistic approach. The proposed single story hybrid system (Figure 3.3) is simplified to Figure 4.4 by representing the panels with compression and tension struts. Only the corner spring connection was considered to simulate the extreme case of crushing of panels. At this point it is to be noted that the tensile load (F_t) on steel members due to connection brackets is ignored for simplicity. Within the simplified free body diagram, F_s represents the crushing strength of the panel in the brackets and can be mathematically expressed as shown below.

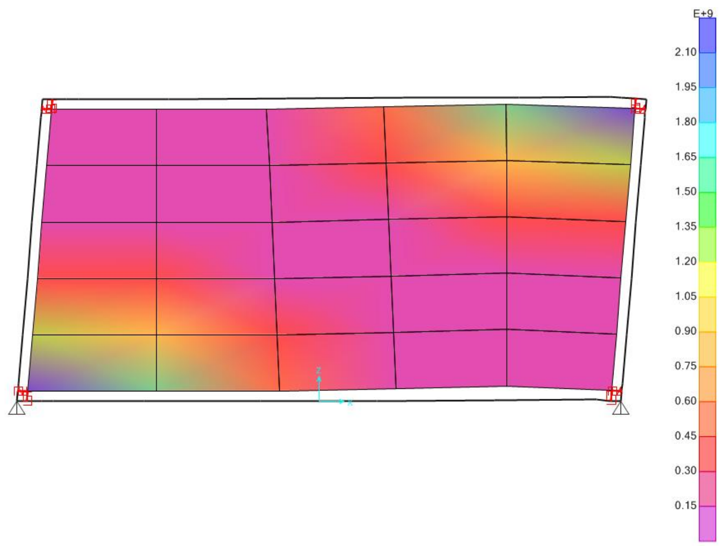

Figure 4.3: Compression strut action for the hybrid system

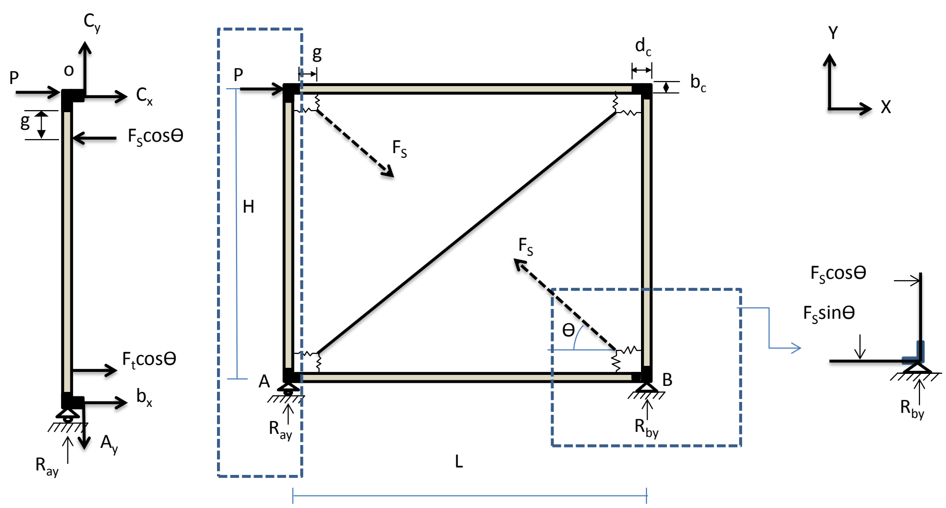

Figure 4.4: Compression strut action for the hybrid system

Considering the system equilibrium of forces in x direction and moment at point o of Figure 4.4 will give:

$$-F_s cos\theta + C_x + b_x + P = 0 \tag{4.4}$$

$$F_s cos\theta\left(\frac{b_c}{2} + g\right) - P\left(\frac{H}{L}\right)\left(\frac{d_c}{2}\right) - b_x H = 0 \tag{4.5}$$

Substituting Equation 4 in to Equation 5 gives:

$$P = \frac{F_s cos\theta L}{H}\left(\frac{b_c + 2g - H}{d_c - H}\right) \tag{4.6}$$

The compression resistance of the CLT wall (F_s) at a point of yielding can be calculated by the composite K theory as follows: For CLT the crushing strength is given by [GP11]

$$f_{c,90,eff} = f_{c,0} k_4 \tag{4.7}$$

where $f_{c,0}$ is the crushing strength and k_4 is given by:

$$k_4 = \frac{E_{90}}{E_0} + \left(1 - \frac{E_{90}}{E_0}\right)\left(\frac{a_{(m-2)} - a_{(m-1)} + ... \pm a_1}{a_m}\right) \tag{4.8}$$

where E_{90} and E_0 are the modulus of elasticity in bending in perpendicular and parallel to the major strength direction, respectively. The parameters a_m and a_{m-i} are shown in Figure 4.5.

Figure 4.5: Five layer CLT

The stiffness of cross layers for CLT is:

$$E_{90} = \frac{E_0}{30} \tag{4.9}$$

The crushing strength (F_s) is calculated by multiplying the perpendicular crushing strength $f_{(c,90,eff)}$ with the area of contact. The area of contact is calculated based on the macro modeling concept for masonry infill using the single strut approach as shown in Figure 4.6.

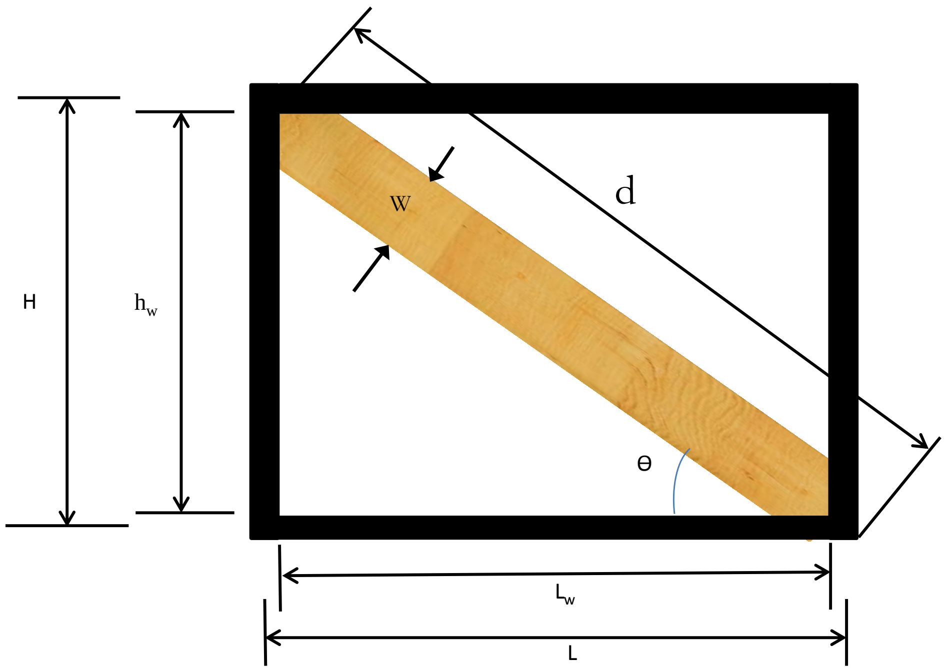

Figure 4.6: single strut representation of the hybrid system

$$F_s = f_{c,90,eff} wt \tag{4.10}$$

where t is the thickness of CLT panel and w can be calculated as follows [Sta67]:

$$w = 0.175d\left(h\sqrt[4]{\frac{E_w t_w sin2\theta}{4EIh_w}}\right) \tag{4.11}$$

Finally, substituting Equations 4.10 and 4.11 in to Equation 4.6, the applied force that crushes the CLT element is:

$$P = \frac{f_{c,90,eff} cos\theta.L.w.t}{H} \left(\frac{b_c + 2g - H}{d_c - H} \right) \tag{4.12}$$

The displacement that corresponds to the value of P (Equation 4.12) obtained from the pushover analysis is defined as the yield point for panel crushing in connection brackets.

4.4 Parametric study

4.4.1 Monotonic pushover analysis

Static monotonic pushover analysis was carried out for the 243 models. Results of the pushover analysis are used to calculate the yield and ultimate displacement of the system (Figure 4.7). The displacement corresponding to the point where 20% decrease in lateral capacity is defined to be the ultimate displacement of the hybrid system. The yield point of the hybrid system is established based on the displacement corresponding to the smaller of the crushing of panel and yielding of steel. Samples from the results of monotonic pushover analysis are depicted in Figure 4.7. As shown in the Figure 4.7, models having thicker and stronger CLT panels with larger post yield stiffness ratio possess larger load carrying capacity.

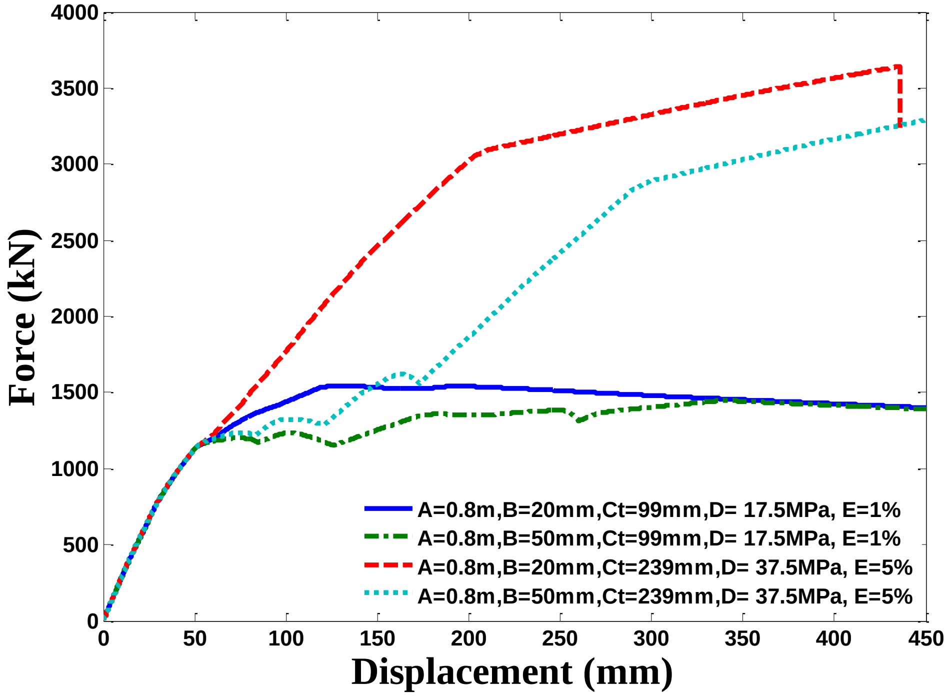

Figure 4.7: Sample monotonic pushover analysis results

4.4.2 Semi-static cyclic analysis

A hysteretic response of base shear with lateral displacement is obtained by applying a cyclic displacement history at the top node of each model. The cyclic loading test is conducted according to the CUREE-Caltech Wood frame project protocol [KPI$^+$01] (Figure 4.8). The ultimate displacement obtained from the monotonic pushover analysis is used for cyclic test with a correction factor of 0.4 to account for the difference in deformation capacity between monotonic test and cyclic test [KPI$^+$01].

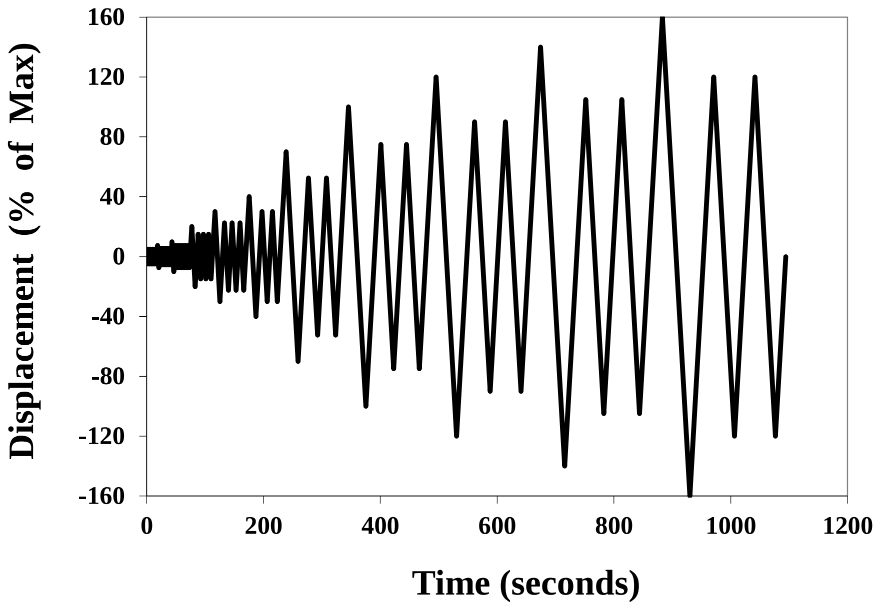

Figure 4.8: CUREE cyclic loading protocol

Samples from the results of semi-static cyclic analysis are depicted in Figure 4.9. The responses shown in Figure 4.9a and b are characterized by fat hysteresis loops with large energy dissipation. Also from Figure 11a and b, it is clear that the thinner (C_t = 99 mm) and weaker panels (D = 17.5 MPa) show less pinching behaviour. However, in Figure 4.9c and d, models with thicker (C_t = 239 mm) and stronger panels (D = 37.5 MPa) with higher post yield stiffness ratio (5%) are characterized by a higher degree of pinching. This pinching causes significant reduction in energy dissipation, which creates thinner hysteretic loops.

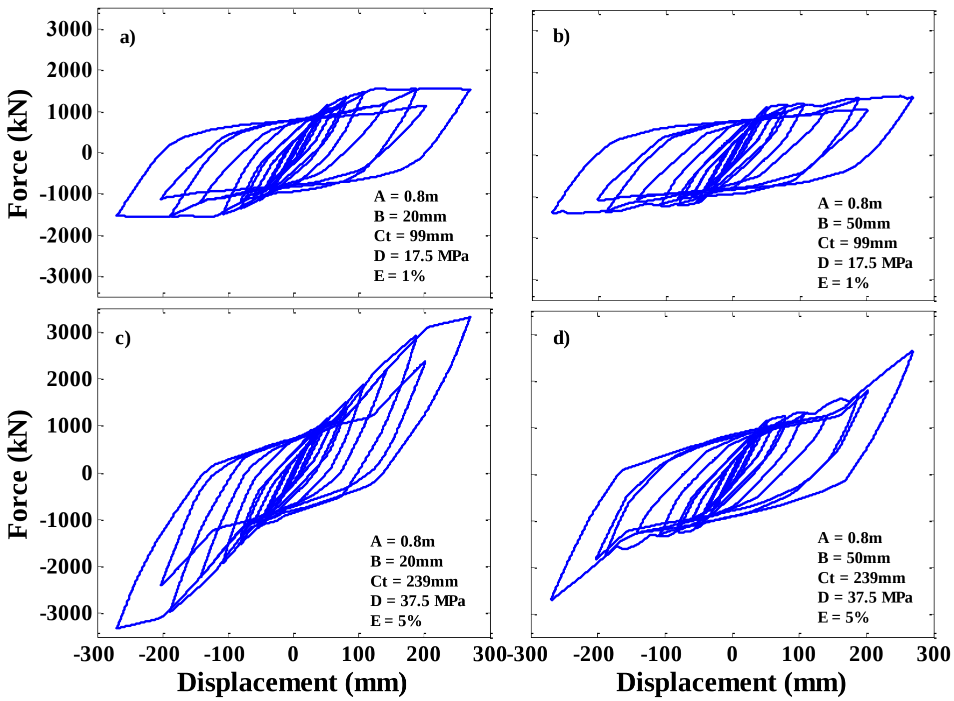

Figure 4.9: Sample semi-static cyclic analysis results

4.5 Equivalent viscous damping

The hysteretic damping corresponding to the cyclic response is calculated for each model based on Equation 1. Then a least square regression was applied to calculate the value of C for Equation 4.3 from hysteretic damping (ξ_{hyst}) and ductility values. All the variables in the RSM analysis are continuous. Response surface methodology (RSM) with the D-Optimal computer experimental design technique was used to develop an expression for C using the results from least square regression analysis. A second degree polynomial of the form shown in Equation **??** was used to set up relationship between C and the modeling variables (A, B, C_t, D, and E); In Equation 13, C is a regression function, and β_0, β_i and β_{ij} are the regression coefficients.

$$y = \beta_0 + \sum_{i=1}^{k} \beta_i x_i + \sum_{i=1}^{k} \beta_i x_i^2 + \sum \sum_{i<j} \beta_{ij} x_i x_j \tag{4.13}$$

In order to develop the desired relationship, data points are selected on the basis of optimality criteria, which are based on the proximity of the predicted response C to the mean response. In order to obtain the coefficients for the proposed second degree equation, 80% of the data points from the least square regression analysis were used for the model training, while the rest were kept aside for statistical validation.

After obtaining significant factors and interactions from RSM, the final expression for C, given in Equation 4.14, is developed using modeling parameters of Table 4.1.

$$\begin{aligned} C = \Big(& 0.43 + 0.5A + 0.015B + (1.27E - 03C_t) + (3.75E - 04D) \\ & - 0.054E - (2.74E - 04A.C_t) - (1.01E - 03A.D) \\ & - (0.019AE) + (2.62E - 05BD) - (3.2E - 04C_t.D) - 0.135A^2 \\ & - (1.045E - 04B^2) - (1.98E - 06C_t^2) + (5.9E - 03E^2) \Big) \end{aligned} \tag{4.14}$$

It can be inferred from the Equation 4.14 that the value of C is dependent on the complex interaction between the gap, panel properties and post yielding stiffness ratio of steel frames. The effect of variable interactions is illustrated using response surface plot in Figure 4.10,4.11,4.12, and 4.13. Figure 4.10 shows a decrease in the value of C with an increase in the post the yield stiffness ratio. As discussed earlier, the higher degree of pinching for systems with a large post yield stiffness ratio prohibits the formation of fat hysteresis loops that in turn decreases the value of C. Moreover, in Figure 4.10, for the hybrid systems with larger bracket spacing, the value of C showed an increase in a linear fashion. It is also clear from Figure 4.11 that the value C is heavily influenced by increasing the magnitude of the gap between CLT panel and steel frame. Originally, the gap was provided to accommodate construction tolerances and to develop the hysteretic behaviour. The increase in the gap allows the connection to deform and dissipate energy that increases the value of C. Equation 14 is statically validated for 43 data points outside of the training data set. R^2 value of 0.97 was obtained for the plot of actual vs. predicted values of C, as shown in Figure 4.14.

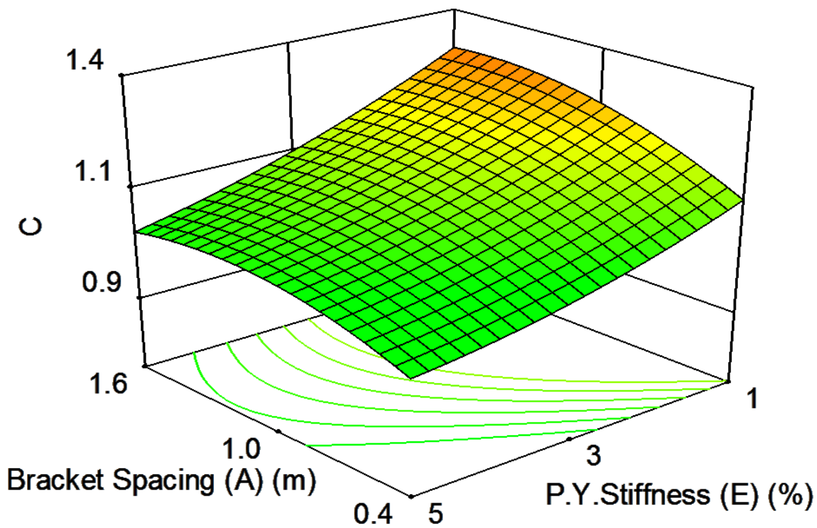

Figure 4.10: Response surface plot for the effect of interactions between bracket spacing (A) and post yielding stiffness ratio (E)

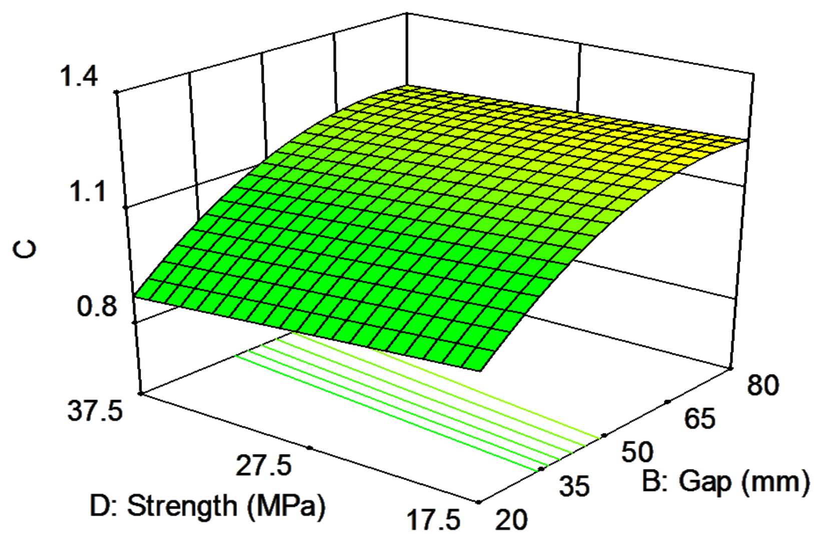

Figure 4.11: Response surface plot for the effect of interactions between Panel strength (D) and Gap (B)

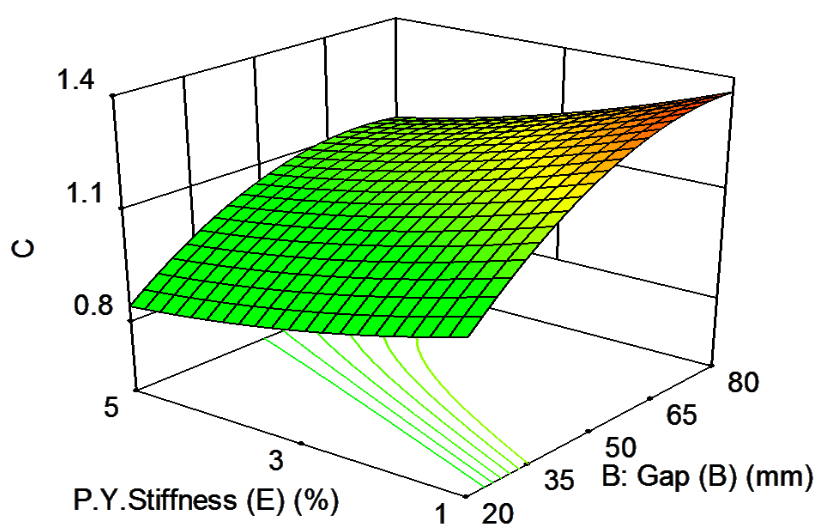

Figure 4.12: Response surface plot for the effect of interactions between post stiffness yield ratio (E) and Gap (B)

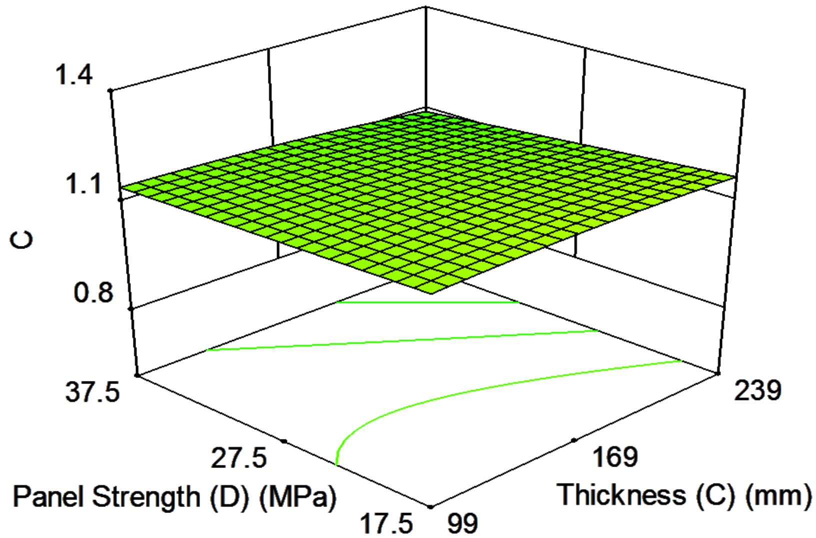

Figure 4.13: Response surface plot for the effect of interactions between Panel strength (D) and Panel thickness (C_t)

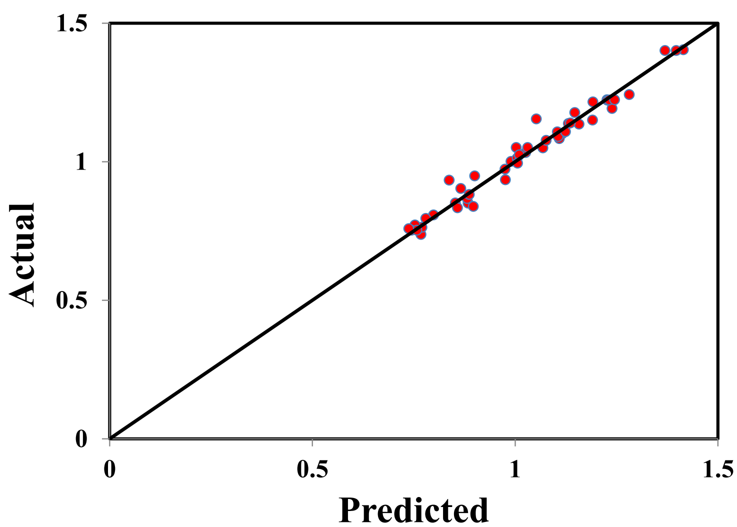

Figure 4.14: Validation plot; Predicted vs. Actual

The variation of the hysteretic damping (ξ_{hyst}) of the hybrid system under study with different modeling variables is given in Figure 4.15. Figure

4.15 shows the effect of modeling variables on the ξ_{hyst} by keeping the other variables at their median value. Figure 4.15a shows the variation of ξ_{hyst} and ductility μ for different levels of gap between the CLT wall and steel frame. As discussed in previous sections, the larger gap provided allows the connection brackets to deform and to dissipate energy. Figure 4.15(a) confirms this concept because the hysteretic damping is increasing with increase in the gap magnitude. However, the effect of increasing the gap magnitude will diminish for the gaps that are more than 40 mm. Bracket spacing and panel strength shows minimal effect on the hysteretic damping as shown in Figure 4.15b and c. Even though it is small, the hysteretic damping will increase for the models with larger bracket spacing. As can be seen from Figure 4.15d the value of hysteretic damping is heavily influenced by the magnitude of post yielding stiffness ratio of steel frame members. The higher degree of pinching for systems with large post yielding stiffness ratio prohibits the formation of fat hysteresis loops that in turn decreases the ξ_{hyst}. However, the sensitivity of ξ_{hyst} is smaller for models with post yield stiffness ratio more than 3%.

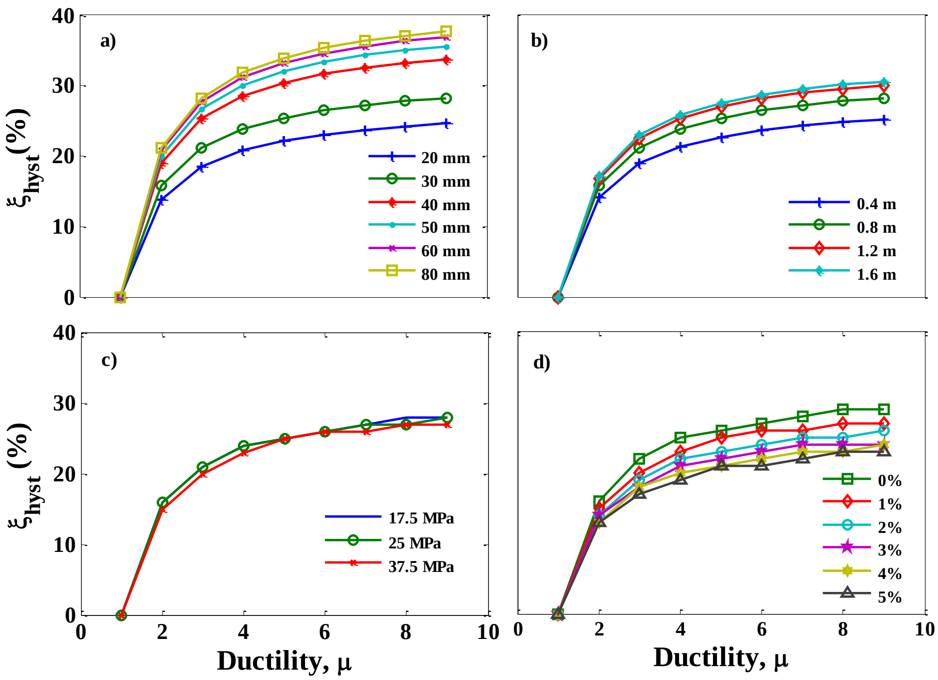

Figure 4.15: Damping ductility law for various modeling parameters

Figure 4.16 compares the results obtained using the new expression of C (Equations 4.3 and 4.14) with the results obtained from other notable studies. In general, the current study obtained the maximum value of ξ_{hyst} in the range of 18%-37% for a ductility value of 10. Referring to Figure 15, results of the proposed equation are between the damping ductility law given by [Pri03] for bare steel frame and [GJT12, WNS11] for the concentrically braced steel frames and concentrically braced reinforced concrete. The damping ductility law given by [DK04], for a steel member, is larger than the EVD of the current study. The damping ductility law suggested by [LDT] for reinforced concrete frames with masonry infill is similar to the highly pinched models of the proposed hybrid system. In general, the proposed equation proved to be in agreement with laws developed for frames with infill wall and bracings.

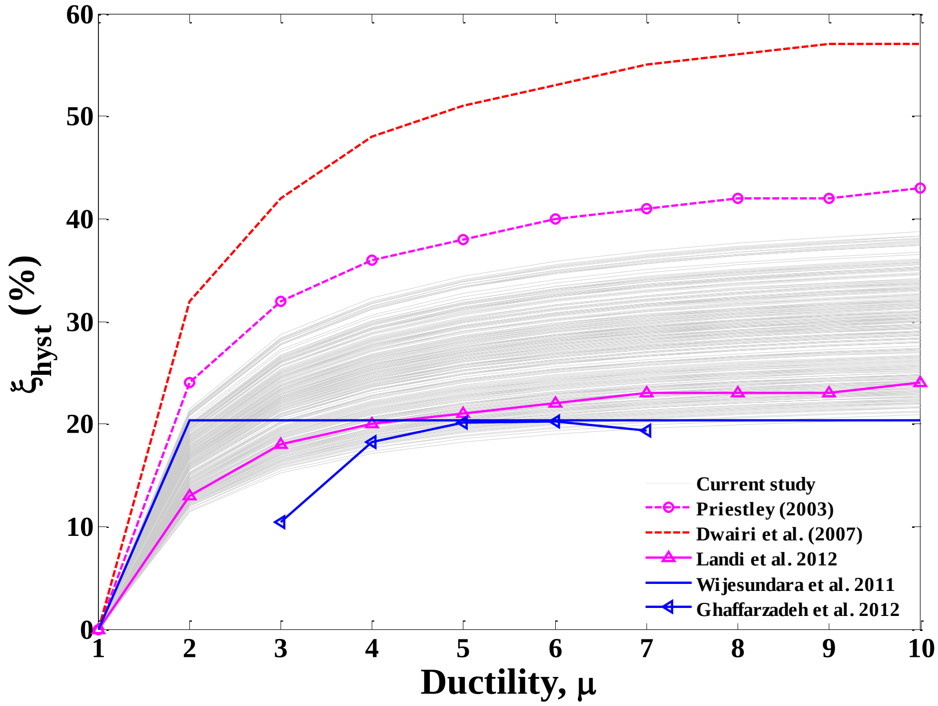

Figure 4.16: Comparison of EVD expressions with different researches

4.6 EVD calibration using nonlinear time history analysis

The methodology used to calibrate an EVD was computed based on Jacobsens area based approach in earlier sections is presented here. The purpose of calibration is to improve the agreement between the area-based approach and the time history analysis for the substitute structure. Only nine models with the gap magnitude of 20 mm are considered for the calibration purpose. Models with 20 mm gaps are shown to have stable hysteretic behaviour with less strength and stiffness degradation [DSBT14, Dic13]. Moreover, panel thickness and strength are shown to have minimal effect on EVD; therefore, for the calibration process here, they are fixed to be 99 mm and 17.5 MPa, respectively. Nonlinear time history analysis (NLTHA) using 20 spectrum compatible earthquakes are used for the calibration process. An iterative NLTHA analysis is applied for each model until the top displacement of the hybrid system from NLTHA matches the initial considered displacement from the semi-static cyclic analysis ([WNS11]). The steps followed are outline below with an example. Figure 4.17 shows the iterative steps used to calibrate EVD.

Step 1: Selection of models to be calibrated

The nine models considered for the current calibration process are given in Table 4.2. The models were selected based on their design implication for the DDBD of the hybrid system.

Table 4.2: Modeling variables

Models	A:Bracket-Spacing(m)	B:Gap(mm)	C_t: Panel Thickness (mm)	D: Panel Strength (MPa)	E: Post Yield Stiffness (%)
M1	0.4	20	99	17.5	1
M2	0.4	20	99	17.5	3
M3	0.4	20	99	17.5	5
M1	0.8	20	99	17.5	1
M1	0.8	20	99	17.5	3
M1	0.8	20	99	17.5	5
M1	1.6	20	99	17.5	1
M1	1.6	20	99	17.5	3
M1	1.6	20	99	17.5	5

Step 2: Force and displacement of considered hysteretic loop from semi-static cyclic loading analysis

The top node displacement ($\triangle_j$) and corresponding force (F_j) for each loop (j) of each model are obtained from the semi-static cyclic loading analysis. A total of 24 loops were obtained for each model, and subsequently, 24 force (F_j) and displacement ($\triangle_j$) values for the model under consideration are obtained.

Step 3: Calculate the ξ_{hyst} and μ for each loop (j)

The hysteretic damping (ξ_{hyst}) was calculated by using area based approach (Equation 4.1) and the ductility (μ) is obtained by dividing $\triangle_j$ of

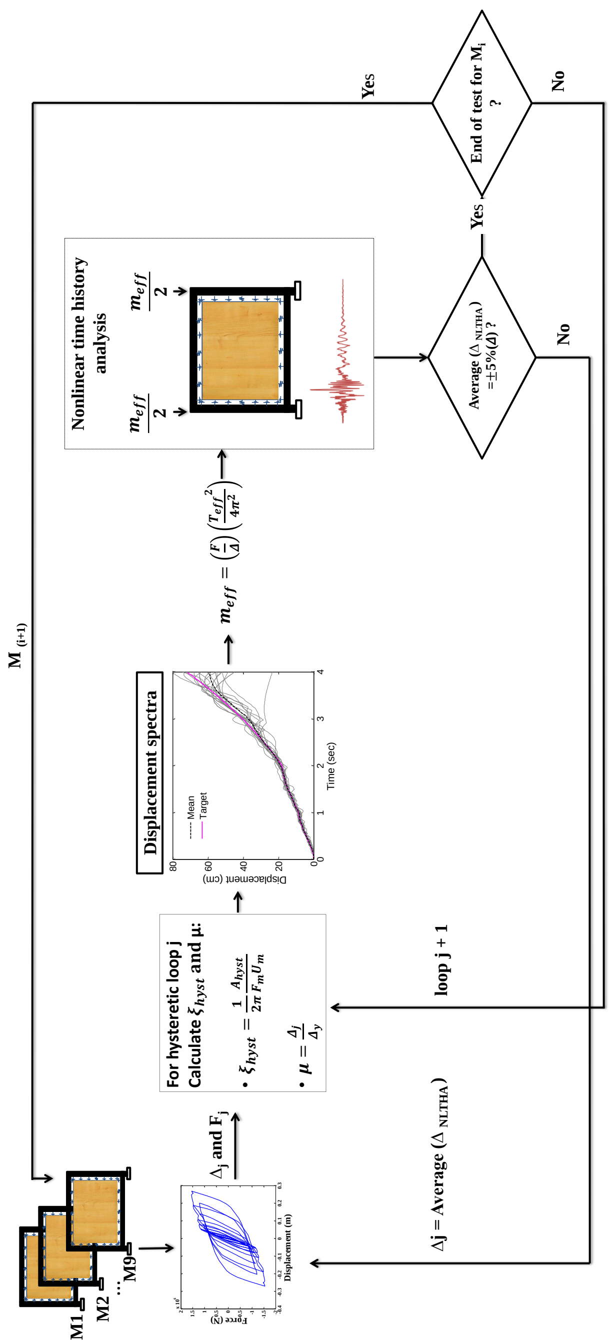

Figure 4.17: Calibration process for EVD

each loop by the yielding displacement ($\triangle_y$).

Step 4: Effective period (T_{eff})

The effective period (T_{eff}) can be obtained from the scaled average damped displacement spectra of Figure 4.19 with appropriate factor (Equation 4.16) corresponding to each $\triangle_j$. The details of development and scaling of the average displacement spectra will be discussed in step 6.

Step 5: Effective mass (m_{eff})

The effective mass (m_{eff}) is calculated by using Equation 4.15 as follows:

$$m_{eff} = \left(\frac{F_j}{\triangle_j}\right)\left(\frac{T_{eff}^2}{4\pi^2}\right) \tag{4.15}$$

Step 6: Nonlinear time history analysis (NLTHA)

NLTHA is conducted by lumping half of m_{eff} on each of the two top nodes of the model in the gravity direction. Opensees [MMS+06] finite element software tool with a tangent stiffness based 3% Rayleigh damping is used for the analysis. Twenty spectrum compatible earthquake ground motions of section 3.1.2 scaled to Vancouver′s design spectrum NBCC 2010 [NRC10] were used for the analysis (Figure 4.18). The ground motion records were obtained from the Pacific Earthquake Engineering Center [PEE05] database by comparing the ratio of seismic motion (A/V) to Vancouver′s A/V. The average 5% damped displacement spectrum from all the ground motions considered is compared with Vancouver′s design spectrum as shown in Figure 4.19. As it can be inferred from Figure 4.19, the mean and the target 5% damped displacement spectrum are in good agreement.

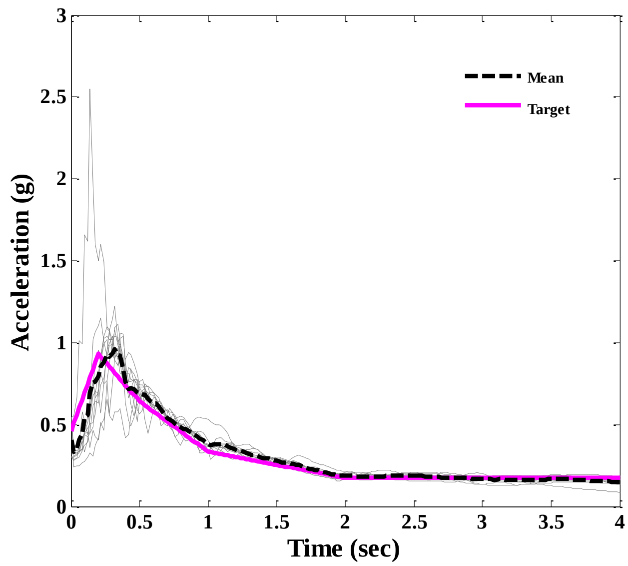

Figure 4.18: Comparison between mean and target spectrum for selected ground motion

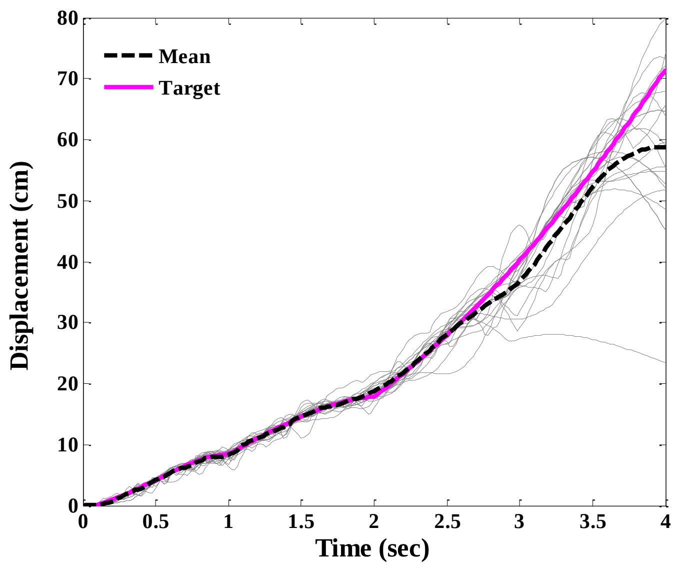

Figure 4.19: Displacement spectra at 5% damping level from the scaled ground motion

A scaling factor obtained from Equation 4.16 EC8 [dN98] is used to obtain the highly damped displacement spectrum corresponding to ξ_{hyst} for the hysteretic loop under consideration. By using the new spectrum, the T_{eff} corresponding to each $\triangle_j$ was obtained.

$$R_\xi = \sqrt{\frac{7}{2+\xi}} \qquad \geq 0.55 \tag{4.16}$$

Step 7: Outputs from the analysis and check for convergence

The average of maximum top displacement ($\triangle_{NLTHA}$) that is obtained from step 6 is compared with the initial considered displacement ($\triangle_j$). If the difference is within 5% error, the corresponding ξ_{hyst} and μ are considered as the true hysteretic damping and ductility values and the analysis will continue for the next loop (j+1). If the difference is significant, another ξ_{hyst} and μ value will be calculated based on the new $\triangle_{NLTHA}$ and all the procedures starting from step 2, will be repeated until convergence is obtained.

Step 8: Analysis for other models

Steps 1-7 were repeated for all 9 models considered.

A detailed numerical example is presented in order to clearly show the steps followed for the calibration process. The hysteretic loop details obtained from semi-static cyclic analysis for model M4 are given in Table 4.3. The yielding (panel crushing) displacement ($\triangle_y$) for this model is obtained from Equation 12 and the monotonic pushover analysis is 28.3 mm.

Table 4.3: Results of the semi-static cyclic analysis on model M4

No of Cycle	F_j (kN)	$\triangle_j$ (m)	A_{hyst}	ξ_{hyst}
1	378184	0.0135	76.18	0.002
2	547052	0.02025	1561.037	0.022
3	463256	0.01512	1411.148	0.03
4	463258	0.01512	1227.049	0.027
5	463258	0.01512	1227.05	0.027
6	463258	0.01512	1227.05	0.027
7	463258	0.01512	1227.05	0.027
8	711921	0.027	4431.471	0.036
9	571507	0.02025	1983.32	0.027
10	571519	0.02025	1672.793	0.023
11	571519	0.02025	1672.797	0.023
12	571519	0.02025	1672.799	0.023
13	571519	0.02025	1672.799	0.023
14	1158190	0.054	32446.2	0.082
15	909964	0.0405	17769.8	0.076
16	907065	0.0405	17710.76	0.076
17	1349150	0.081	106901	0.155
18	1060970	0.06075	55594.1	0.137
19	1060960	0.06075	48881.85	0.12
20	1478120	0.108	201085.7	0.2
21	1203500	0.081	111006.8	0.181
22	1557650	0.189	536739.4	0.29
23	1200120	0.14175	270829	0.253
24	1558390	0.27	786884.7	0.297

For simplicity, lets consider loop 14 with $F_j = 1158.1$ kN and $\triangle_j = 54$ mm. The corresponding ξ_{hyst} and μ are 8.2 % and 1.9, respectively. From step 4, the damped displacement spectrum corresponding to $\xi_{hyst} = 8.2$ % is obtained from Figure 4.20. The scaling factor associated with equivalent damping level is obtained using Equation 16. As suggested by [BP05], the influence of initial damping in the elastic range was not included in the process of time history calibration process. From Figure 17, the effective period (T_{eff}) associated with $\triangle_j = 54$ mm and $\xi_{hyst} = 8.2\%$ is 0.72 sec. By using Equation 15 of step 5, the effective mass (m_{eff}) is 281.923 ton. The NLTHA is carried out by lumping half of the effective mass calculated on each top node in the gravity direction.

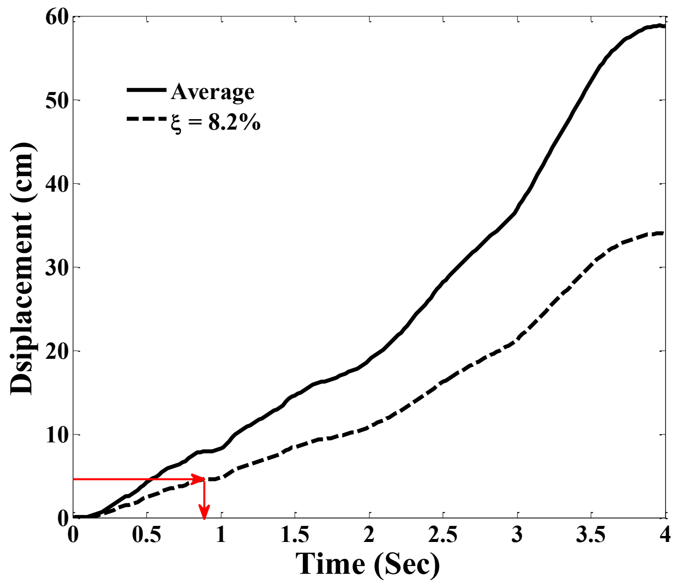

Figure 4.20: 8.2% damped average displacement spectrum

4.6.1 Results of calibration

The final calibrated EVD-ductility laws for the hybrid system under study are given in Figure 18. Figure 4.21a, b, and c shows the variation of the corrected EVD-ductility law for various post yield stiffness ratios of the steel members with bracket spacing of 0.4m, 0.8m, and 1.6m, respectively. As can be inferred from Figures 4.21a, b, and c, irrespective of the bracket connection spacing, models with higher post yield stiffness ratio dissipate less amount of energy.

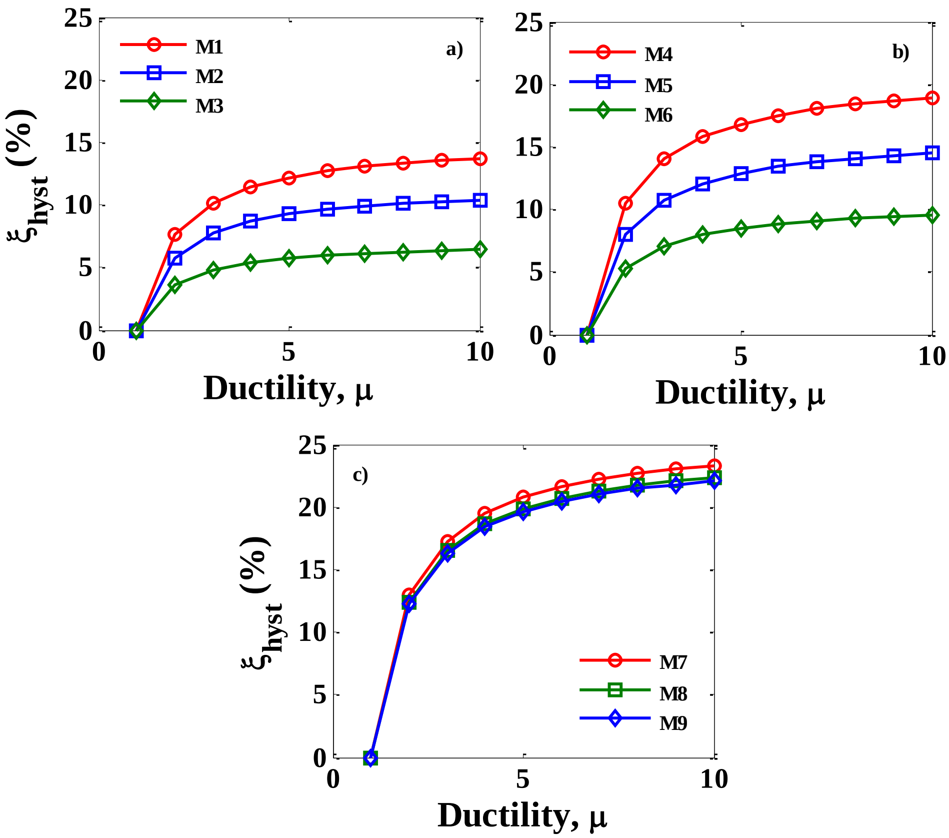

Figure 4.21: Calibrated hysteretic damping vs. ductility for bracket spacing of (a) 0.4 m ; b) 0.8 m; c) 1.6 m

4.7 Summary

This chapter proposes an equivalent viscous damping-ductility law for CLT infilled SMRFs. For this purpose, an analytical investigation was carried out for 243 predetermined single-storey single-bay CLT infilled SMRFs by varying the modeling parameters that affect the hysteretic behaviour of the system. The equivalent viscous damping and ductility of each model were obtained from the hysteretic responses of semi-static cyclic analysis. Then an expression is developed for equivalent viscous damping as a function of ductility and various modeling parameters. Finally, an iterative

NLTHA is conducted using 20 spectrum compatible earthquake ground motions to calibrate EVD from Jacobsen′s area based approach. The calibrated EVD-ductility law will be used in direct displacement based design (Chapter 5) of CLT infilled SMRFs to represent the energy dissipation of the hybrid system.

5

Direct displacement based design of CLT infilled steel moment resisting frames

5.1 Background

Direct Displacement Based Design (DDBD) is a performance based seismic design, where the performance objectives are defined by the designer based on the desired level of damage sustained in the structures [GAEB99]. The damage sustained is associated with the displacement and interstorey drift values during seismic excitation [KMA03, EY04, MK05, GAEB99, KC04]. In this chapter, the motivation is to develop a DDBD method for a new steel-timber hybrid system introduced by [SDT12, STKP12, DST12, Dic13, DSBT14].

The idea of incorporating displacements in the design process of structures through a concept of substitute-structure was first implemented by Shibata and Sozen [SS74]. Gulkan and Sozen [GS74] developed a method to estimate the design base shear of structures by considering their inelastic response. Moehle [Moe92] established a displacement-oriented approach for the design of reinforced concrete structures. Moreover, the author shows the simplicity and effectiveness of a displacement based method over the conventional ductility based approach. A true displacement based design philosophy is introduced by Priestley [Pri93] as an alternative over the spectral based design method.

Kowlasky et al. [KPM95] examines the applicability of DDBD method of Priestley [Pri93] on single-degree-of-freedom (SDOF) bridge columns. The applied method provides additional flexibility for the designers that satisfies the initial target displacement with an acceptable margin of error. Calvi and Kingsly [CK95] showed the application of the DDBD method to design multi-degree-of-freedom (MDOF) bridge structures. The authors applied the concept of transforming the MDOF system to an equivalent SDOF system to calculate the required secant stiffness. The proposed procedure was effective for relatively symmetrical bridges. However, the authors pointed out the deficiency of the method related to bridges with multiple dominant modes of vibration. A more interesting application of inelastic design spectra to the direct displacement based design is presented by Chopra and Goel [CG01]. In this research, the authors showed the deficiencies associated with the application of elastic design spectra in estimating ductility and displacement demands. Priestley and Kowalsky [PK00] applied the DDBD method to design MDOF reinforced concrete frames and wall buildings based on an initially estimated displacement profile.

Recently, the applicability of the DDBD procedure has been examined for different types of structures and hysteretic systems [MK00a, MK00a, SPC06, WR, MGD13, MASR, RHA13, GSC10, Sul09, CPP04, PR09, PR07, PvdLP12, FF02, vdLRPP12].

Medhekar and Kennedy [MK00a, MK00a] formulated the DDBD method and applied it to the design of two and eight storey concentrically braced steel frames. For both building types, the authors used 5% elastic damping as an effective damping. Recommendations are forwarded to include the hysteric component of damping to represent the total energy dissipative capacity of the structures. A more comprehensive DDBD of concentrically braced steel frames is presented by Wijesundara and Rajeev [WR]. In this research, the authors used calibrated equivalent viscous damping with a yield displacement profile. Sullivan et al. [SPC06] proposed a novel DDBD approach to design reinforced concrete frame-wall structures. The developed methodology was applied to 4, 8, 12, and 16 storeys frame-wall structures by considering different configurations of both frames and walls. In their paper, strength proportions between walls and frames are assigned initially to calculate the characteristics of an equivalent SDOF system. Malekpour et al. [MGD13] applied Sullivan's [SPC06] concept of initial strength proportion assignment to design steel concentrically braced reinforced concrete frames. As a step towards a DDBD approach for cold-formed steel frame wood panel shear walls, [MASR] derived an expression to calculate EVD and the design displacement profile. A work by Christopoulos [CPP04] modified the DDBD procedure of Priestley [Pri99] to incorporate residual deformation into the design process through the residual/maximum displacement spectra.

Even though wood structures have been effective with regards to collapse prevention and life safety in recent earthquakes (Loma Prieta 1999 and Northridge in 1994), the economic losses associated with these structures was enormous [PR09]. This reason prompted the need for a design method that satisfies both life safety and damage limit state. To address this concern, recently a DDBD approach was applied to wood frame structures [PR09, PR07, FF02, vdLRPP12]. Pang and Rosowski [PR09] applied the DDBD approach to design mid-rise regular wood-framed buildings. This procedure is intended to satisfy both the damage and safety limit states. In their research, a normalized modal analysis is used to develop the interstorey drift spectra. Moreover, the authors showed the applicability of the method by designing both commercial and residential type buildings. Filiatrault and Floz [FF02] and van de Lindt et al. [vdLRPP12] also outlined a DDBD procedure for wood frame buildings. Although the above researches have adopted the DDBD procedure for reinforced concrete, steel , and wood based structures, the procedure is not yet developed for the steel-timber hybrid system that incorporates CLT as an infill panel in SMRFs.

In this chapter, an iterative direct displacement based design method is developed for a CLT infilled steel moment resisting frame structure. The iterative design procedure is started by assuming the following initial modeling variables: gap between CLT panel and steel frame, bracket (connection) spacing, CLT panel thickness and strength, and post yield stiffness ratio of steel members. Subsequently, the design displacement profile is developed by assigning an initial relative strength between the CLT wall and frame elements. This profile is used to obtain the characteristics of an equivalent single degree of freedom (SDOF) system. A system ductility value is established based on the proportions of the overturning moment resistance of the CLT wall and steel moment frame. A calibrated EVD-ductility relationship is used to obtain the energy dissipation of the equivalent SDOF system. Effective period and secant stiffness of the system are calculated to obtain the final design base shear. Hybrid systems of three bays, 3-, 6-, and 9-storeys height buildings with an infilled middle bay are designed using the proposed method. Nonlinear time history analysis using twenty earthquake ground motion records is used to validate the performance of the proposed design methodology. The results indicate that the developed method effectively controls the displacements due to seismic excitation of the hybrid system.

5.2 Basics of Direct displacement based design (DDBD)

A through discussion on the fundamentals of the DDBD method for different types of structures is given in [PCK07b]. In this section, the basic steps and key equations of DDBD method are discussed. Figure 5.1 shows how DDBD utilizes a virtual representation of the nonlinear structures with an equivalent Single Degree of Freedom (SDOF) system through secant stiffness K_e and equivalent viscous damping ξ_{eq} at peak displacement Δ_d.

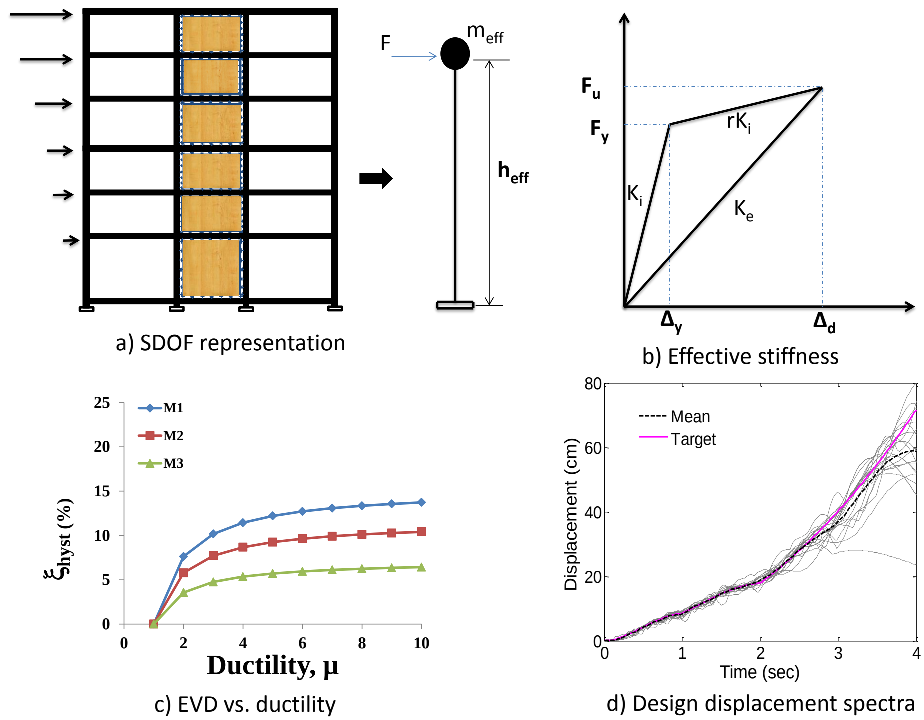

Figure 5.1: Basics of DDBD approach (adopted from Priestley et al. 2007)

One of the critical steps in the process of DDBD is the transformation of MDOF system in to an equivalent SDOF system. The equivalent SDOF system is represented by secant stiffness (K_e) at the maximum response. For this transformation process, a design displacement profile is needed. For frame type building, the design displacement is depends on the drift limits of lower stories [PCK07a]. The displacement profile suggested for frame structures in [PCK07a] is given by Equation 5.1.

$$\Delta_i = \delta_i \left(\frac{\Delta_c}{\delta_c} \right) \tag{5.1}$$

where δ_i is the inelastic mode shape as given by Equation 5.2, Δ_c is the design displacement at the first floor (level c), and δ_c is the value of mode shape at level c.

$$\text{for building frames} \begin{cases} for\ n \leq 4 & \delta_i = \frac{H_i}{H_n} \\ for\ n > 4 & \delta_i = \frac{4}{3}(\frac{H_i}{H_n})(1 - \frac{H_i}{4H_n}) \end{cases} \tag{5.2}$$

where H_i and H_n are the heights of level i and total height of the building, respectively. The characteristics of equivalent SDOF system, i.e., design displacement (Δ_d), effective mass (m_{eff}) and effective height (h_{eff}) are given in Equations 5.3, 5.4, and 5.5, respectively [SL12].

$$\Delta_d = \frac{\sum_{i=1}^{n} m_i \Delta_i^2}{\sum_{i=1}^{n} m_i \Delta_i} \tag{5.3}$$

$$m_e = \frac{\sum_{i=1}^{n} m_i \Delta_i}{\Delta_d} \tag{5.4}$$

$$h_e = \frac{\sum_{i=1}^{n} m_i \Delta_i h_i}{\sum_{i=1}^{n} m_i \Delta_i} \tag{5.5}$$

where n is the number of storeys and m_i and h_i are the mass and height of storey i, respectively. Representation of the energy dissipative capacity of the structures using equivalent viscous damping frame structures requires knowledge of structural ductility demand. The ductility of a structural system can be calculated from the geometry of the cross section of its members. The yield drift of frame structures given by [PCK07a] is:

$$\theta_y = C_2 \epsilon_y \frac{L_b}{H_b} \tag{5.6}$$

where C_2 is 0.5 and 0.65 for concrete and steel members, respectively; L_b and H_b are the beam span and depth, respectively; and ϵ_y is the flexural yielding strain for steel members. The yield displacement (Δ_y) and the associated ductility (μ) are given in Equations 5.7 and 5.8, respectively.

$$\Delta_y = h_e \times \theta_y \tag{5.7}$$

$$\mu = \frac{\Delta_d}{\Delta_y} \tag{5.8}$$

In DDBD the energy dissipative capacity of the structures is represented by EVD. Several authors derived the law of EVD ductility law for different structural systems (hysteretic laws) (details are given in Chapter 4). This EVD (ξ_{eq}) contains both the elastic and hysteretic components of damping. With the assumption of 5% elastic damping, Priestley [PCK07b] proposed the EVD-ductility law as follows:

$$\xi_{eq} = 0.05 + C\left(\frac{\mu - 1}{\mu\pi}\right) \tag{5.9}$$

where the coefficient C is in the range of 0.1 to 0.7 for various structural systems (hysteresis rules). Once the ductility demand is known it is possible to calculate the EVD using 5.9. Once, the design displacement (Δ_d) and EVD (ξ_{eq}) are established, the required effective period can be obtained from the displacement spectra (Figure 5.1d) for an appropriate EVD (ξ_{eq}) level. The average elastic displacement spectra can be scaled with the coefficient (η) to a highly damped spectra using Equation 5.10 [dN05].

$$\eta = \sqrt{\frac{10}{5 + \xi}} \tag{5.10}$$

The corresponding effective stiffness, K_e (Figure 5.1b), for the equivalent SDOF system can be obtained from Equation 5.11.

$$K_e = \frac{4\pi^2 m_e}{T_{eff}^2} \tag{5.11}$$

Finally, design base shear (V_b) can be calculated from the effective stiffness (K_e) and design displacement Δ_d as follows.

$$V_b = K_e \Delta_d \tag{5.12}$$

To select member sections with adequate strength, the structure should be analyzed under lateral forces distributed as shown Equation 5.13.

$$F_i = V_b \frac{m_i \triangle_i}{\sum_{i=1}^{n} m_i \triangle_i} \tag{5.13}$$

where F_i is the shear force at level i.

5.3 Proposed DDBD approach for CLT infilled SMRFs

The basics of DDBD method are discussed thoroughly in Chapter 2. The proposed framework to design CLT infilled SMRFs is outlined as shown in Figure 5.2. The proposed DDBD procedure is illustrated with a case study 3 storey - 3 bays (middle bay infilled steel moment resisting frame). The floor plan and elevation view of the case study building are given in Figures 5.3 and 5.4, respectively. The height of each storey of the building is 3.2 m. A constant bay width of 6 m is used for the entire building.

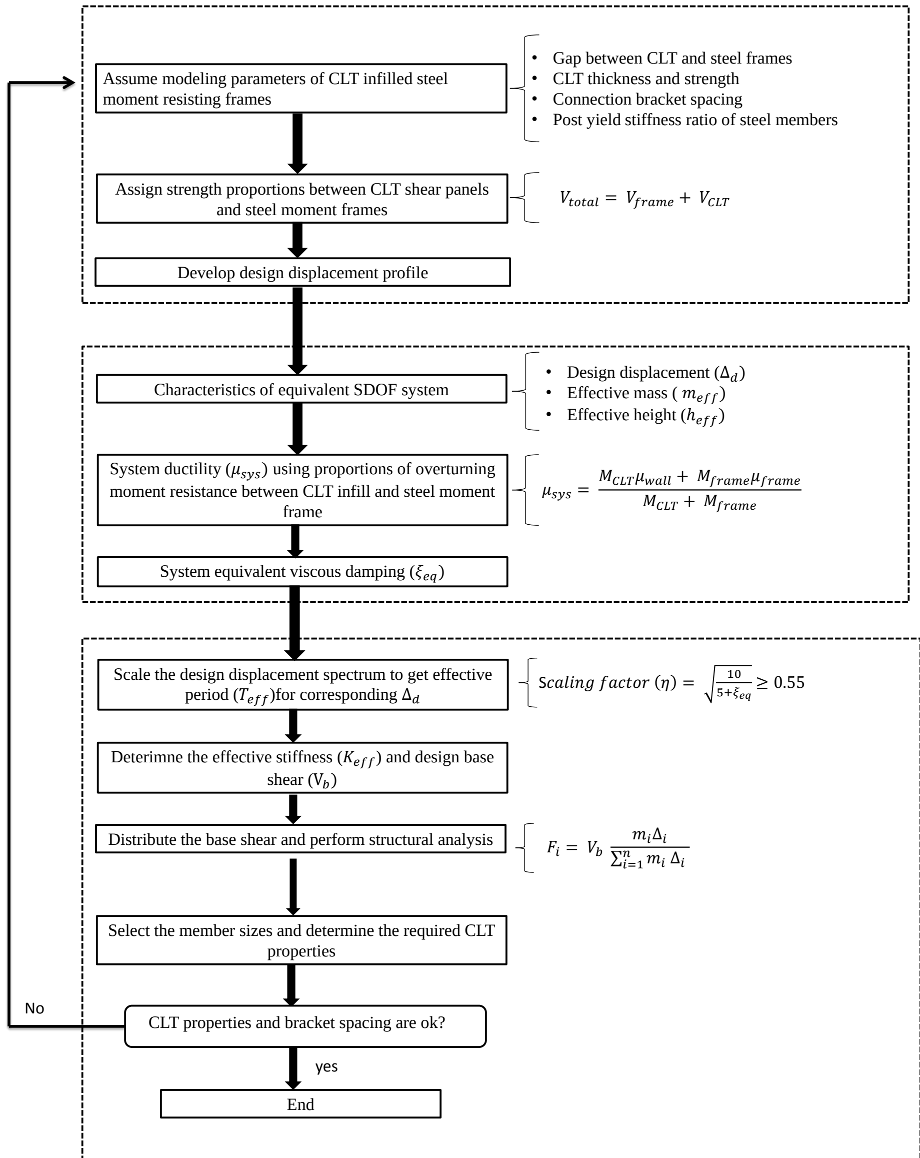

Figure 5.2: Framework of DDBD for CLT infilled SmRfs

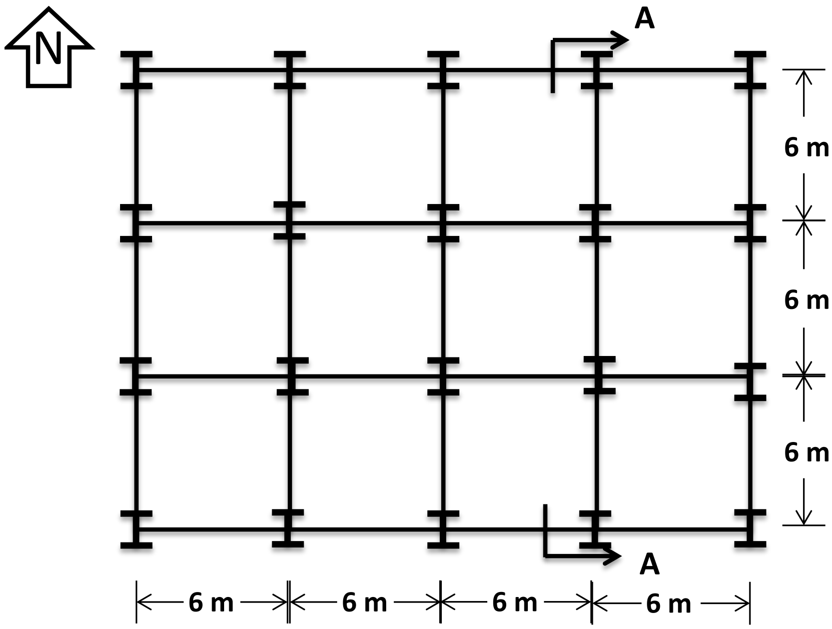

Figure 5.3: Building floor plan

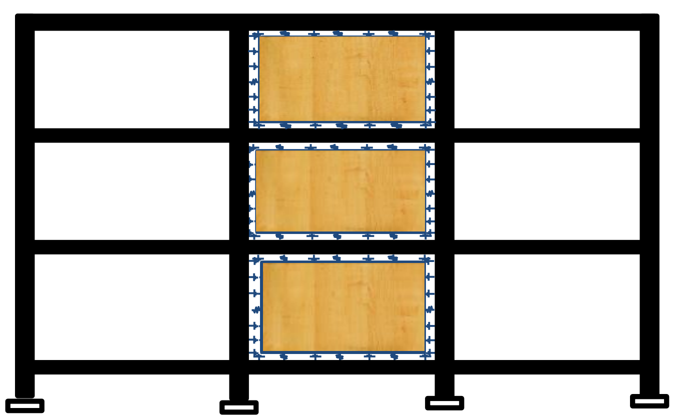

Figure 5.4: Elevation view of the 3 storey 2D frame

The building is assumed to be situated on a very dense soil and soft rock (site class C) with a peak ground acceleration 0.48g in Vancouver, Canada. The building is modeled as a two-dimensional structure and due to its symmetry in plan, accidental torsion is neglected both in the design and analysis phase. Both beam and column elements are detailed based on CSA G40.21 with a yielding strength of $F_y = 350$ MPa and modulus of elasticity (E_s) of 200 GPa. A constant floor seismic weight (including the CLT panels) of 253T was obtained by performing gravity load structural analysis using a commercial software SAP 2000 [HW05]. The proposed design methodology is comprised of 11 steps and presented in detail for the case study building.

Step 1: Assume modeling parameters of CLT infilled steel moment resisting frames

Results from multi-objective optimization of Chapter 3 are used to set the initial modeling parameters CLT infilled SMRFs. A bracket spacing 0.8 m, panel thickness and strength of 99 mm and 17.5 MPa, respectively, are used as a starting parameters for the current example. Steel members with a smaller post yield stiffness ratio dissipate a relatively large amount of energy. Therefore, based on the results of Chapter 4, the post yield stiffness ratio of 1% is used as an initial starting point.

Step 2: Assign strength proportions between CLT shear panels and steel moment frames

A concept of initial strength assignment to calculate the characteristics of an equivalent SDOF is adopted Sulliavn et al. [SPC06]. The CLT shear panels are not continuous (disconnected at the bottom and top of each storey) and deform in a pure shear behaviour. Therefore, it is reasonable to assign the shear strength proportion at the start of the process as their bending strength is not important. For the proposed hybrid system, Figure 5.5 shows the shear resistance proportions between the CLT shear panels and steel moment resisting frames. Since the steel frame shear resistance depends up on the beams strength, constant beam strength are used up to the roof level based on recommendation of Pauley [PP]. As depicted in Figure 5.6, 70% of the total shear is directly assigned to the frames. The shear resistance for the CLT wall is calculated by subtracting the frame shear from the total shear as given by Equation 5.14 [SPC06].

$$\frac{V_{i,CLT}}{V_b} = \frac{V_{i,total}}{V_b} - \frac{V_{i,frame}}{V_b} \tag{5.14}$$

where V_b is total design base shear, $V_{i,CLT}$ is the shear resisted by the CLT infill panels at story i, and $V_{i,total}$ is the total shear at story i. The total shear of the system is established as a function of design base shear, storey number (i) and total number of storeys (n) by [SPC06] as given in Equation 5.15.

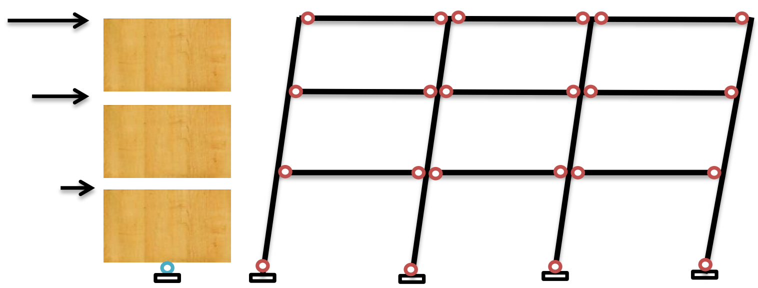

Figure 5.5: Shear distribution between CLT walls and steel frame

$$\frac{V_{i,total}}{V_b} = 1 - \frac{i(i-1)}{n(n+1)} \tag{5.15}$$

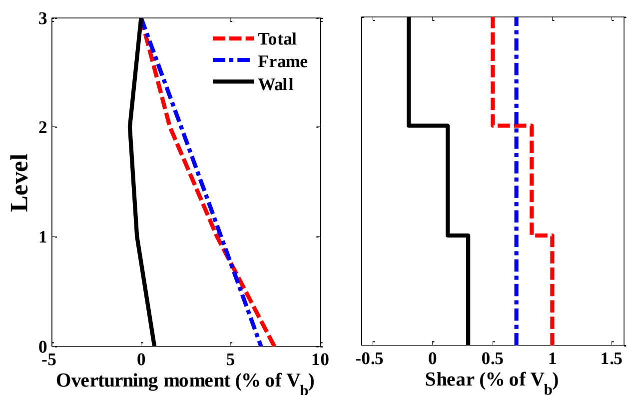

Figure 5.6: Moment and shear distribution of frame and CLT wall along the height of the building

The shear and overturning moment proportion distribution throughout the height of the building are shown in Figure 5.6. As shown in Figure 5.6, the inflection point for the wall starts above the first storey. At this point, the shear proportions can be tuned to effectively utilize the CLT panels that will give an optimum inflection height.

Step 3: Develop design displacement profile

The properties of an equivalent SDOF system are depends on the drift limit of the lower stories of moment frames and an assumed displacement profile. This displacement profile is corresponds to the inelastic first mode response of the structure under seismic excitation [PCK07b]. To ensure the satisfactory performance of the structures under seismic event, building codes specify limits on lateral storey drift values. The NBCC 2010 [NRC10] puts a 2.5% interstorey drift limit to represent extensive damage on the buildings. Previous studies [DST12, Dic13, DSBT14] on the CLT infilled SMRFs suggest that the CLT panel crushing can be an effective way of energy dissipation and easy for maintenance purposes. In their research, the authors showed that panel crushing occurs before the 2.5% interstorey drift limit of the system. Therefore, the drift limit θ_d of 2.5% corresponding to lower storey drift demand of the hybrid system is selected as a target drift limit. The displacement profile is established using Equation 5.16 [SPC10].

$$\Delta_i = \omega_\theta \theta_d h_i \left(\frac{4H_n - h_i}{4H_n - h_1} \right) \tag{5.16}$$

where Δ_i is the displacement at level i, h_i is the height of ith floor from the ground, H$_n$ is the total building height, ω_θ is the factor to account for the effects of higher modes and is given as:

$$\omega_\theta = 1.15 - 0.0034 H_n \leq 1 \tag{5.17}$$

Step 4: Characteristics of equivalent SDOF system

Equations 5.18, 5.19, and 5.20 [SL12] are used to calculate the design displacement ($\triangle_d$), effective mass (m_{eff}), and effective height (H_{eff}), receptively, for the substitute equivalent SDOF system from the masses lumped in each storey (m_i) and height of each storey from the base (h_i).

$$\Delta_d = \frac{\sum_{i=1}^{n} m_i \Delta_i^2}{\sum_{i=1}^{n} m_i \triangle_i} \tag{5.18}$$

$$m_{eff} = \frac{\sum_{i=1}^{n} m_i \Delta_i}{\Delta_d} \tag{5.19}$$

$$h_{eff} = \frac{\sum_{i=1}^{n} m_i \Delta_i h_i}{\sum_{i=1}^{n} m_i \Delta_i} \tag{5.20}$$

The summary of the equivalent SDOF system are summarized in Table 5.1.

Table 5.1: Characteristics of equivalent SDOF

Storey	h	Δ_i	θ_i	m_i	$m_i\Delta_i$	$m_i\Delta_i^2$	$m_i\Delta_i h_i$	Δ_d	m_{eff}	h_{eff}
3	9.6	0.196	1.59	253	49.68	9.75	476.92	0.156	680.9	7.28
2	6.4	0.145	2.04	253	36.8	5.35	235.52			
1	3.2	0.08	2.5	253	20.24	1.61	64.768			
0	0	0	0	0	0	0	0			

Step 5: System ductility (μ_{sys}) using proportions of overturning moment resistance between CLT infill and steel moment frame

As CLT panels crush at low drift values, the ductility associated with them is large. However, for the steel moment frames the inelastic response occurs at a relatively larger drift value. The displacement ductility value of CLT panels and frames is calculated as follows:

$$\mu_{CLT} = \frac{\Delta_d}{\Delta_{crush,CLT}} \tag{5.21}$$

The crushing displacement for the CLT wall ($\Delta_{crush,CLT}$) is calculated using the deflected shape of the CLT panel (Figure 5.7) as follows.

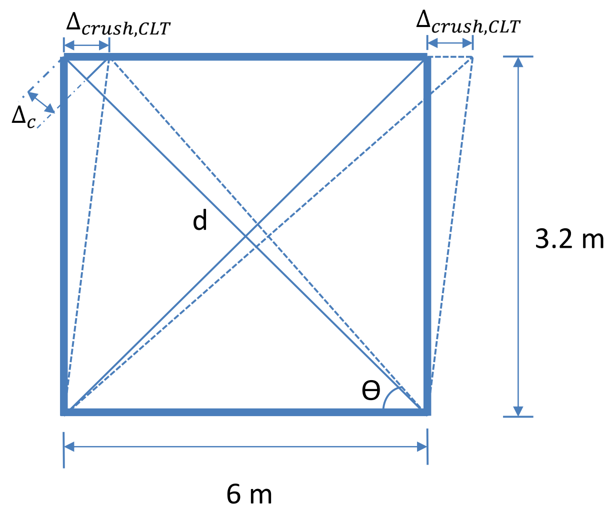

Figure 5.7: CLT panel representation with a compression strut

$$E_o = \frac{f_{CLT}}{\epsilon_{CLT}} = \frac{f_{CLT}}{\frac{\triangle_c}{d}} = \frac{d.f_{CLT}}{\triangle_c.cos\theta} \tag{5.22}$$

$$\triangle_{crush,CLT} = \frac{d.f_{CLT}}{E_o.cos\theta} \tag{5.23}$$

where E_o, f_{CLT}, and ϵ_{CLT} are the modulus of elasticity, crushing strength of CLT panel, and strain of the CLT panel, respectively. The displacement ductility of the steel moment resisting frame is calculated using Equation 5.24 [GSC10].

$$\mu_{frame,i} = \frac{\triangle_i - \triangle_{i-1}}{h_i - h_{i-1}}\left(\frac{1}{\theta_{y,steelframe}}\right) \tag{5.24}$$

where $\mu_{frame,i}$ is the ductility demand of i^{th} storey and $\theta_{y,steelframe}$ is the yield drift of the steel frame as given by Equation5.25 [PCK07b].

$$\theta_{y,steelframe} = 0.65\epsilon_y \frac{L_b}{h_b} \tag{5.25}$$

where L_b and h_b are the beam span length and depth, respectively. For this example, a trial beam depth of 500 mm based on initial gravity load analysis is used that gives $\theta_{y,steelframe}$ of 13.65 mm. As suggested by Pauley [PP], it is advantageous to use the constant beam sections throughout the height of the building. As such, it is possible to take the average frame ductility demand of each floor to get the overall frame ductility. Table 5.2 summarizes the ductility demands of each story and the average ductility ($\mu_{average}$).

Table 5.2: Average frame ductility

Storey	h	Δ_i	$\mu_{frame,i}$
0	0	0	0
1	3.2	0.08	1.83
2	6.4	0.145	1.49
3	9.6	0.196	1.16
		$\mu_{frame,average}$	1.12

Having both the CLT panel and frame ductility demands, it is now possible to determine the system ductility μ_{sys} that is weighted based on the respective overturning moment resistance using Equation 5.26 [GSC10]. For the case study building, the calculated system ductility (μ_{sys}) is 2.217.

$$\mu_{sys} = \frac{M_{CLT}\mu_{CLT} + M_{frame}\mu_{frame,average}}{M_{frame} + M_{CLT}} \tag{5.26}$$

Step 6: System equivalent viscous damping

An expression and plots of equivalent viscous damping of SDOF hybrid system are developed in Chapter 4. Figure 5.8 shows the damping ductility law corresponding to the assumed modeling variables of step 1. From the plot, the hysteretic component equivalent viscous damping (μ_{hyst}) corresponding to the system ductility of step 5 is 11.5%. The total equivalent damping of the system μ_{eq} is found by adding 3% elastic damping on μ_{hyst}.

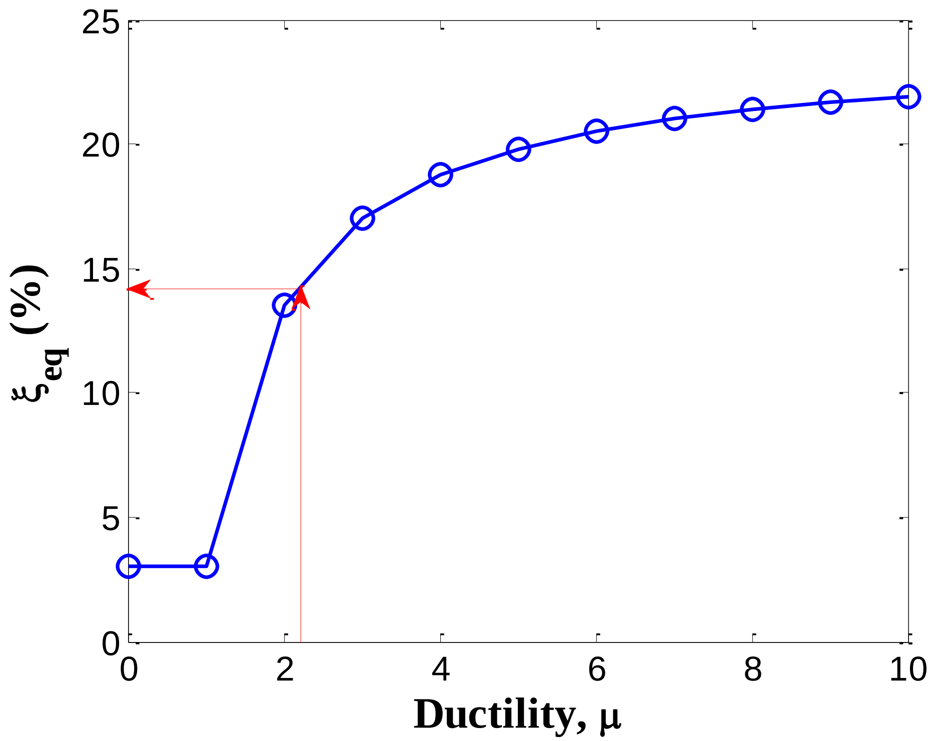

Figure 5.8: Equivalent viscous damping

Step 7: Effective period of the system

The effective period of the equivalent SDOF system is obtained from the highly damped displacement spectrum. The average elastic displacement spectrum of chapter 4 is used by scaling with an appropriate scaling factor. A scaling factor is calculated using Equation 5.27 [dN98] to obtain the highly damped displacement spectra corresponding to $\mu_{eq} = 14.5$ %. Figure 5.9 shows the damped spectrum used to calculate the system effective period (T_{eff}). An effective period of 2.26 sec is obtained from the plot.

$$\eta = \sqrt{\frac{10}{(5+\xi}} \tag{5.27}$$

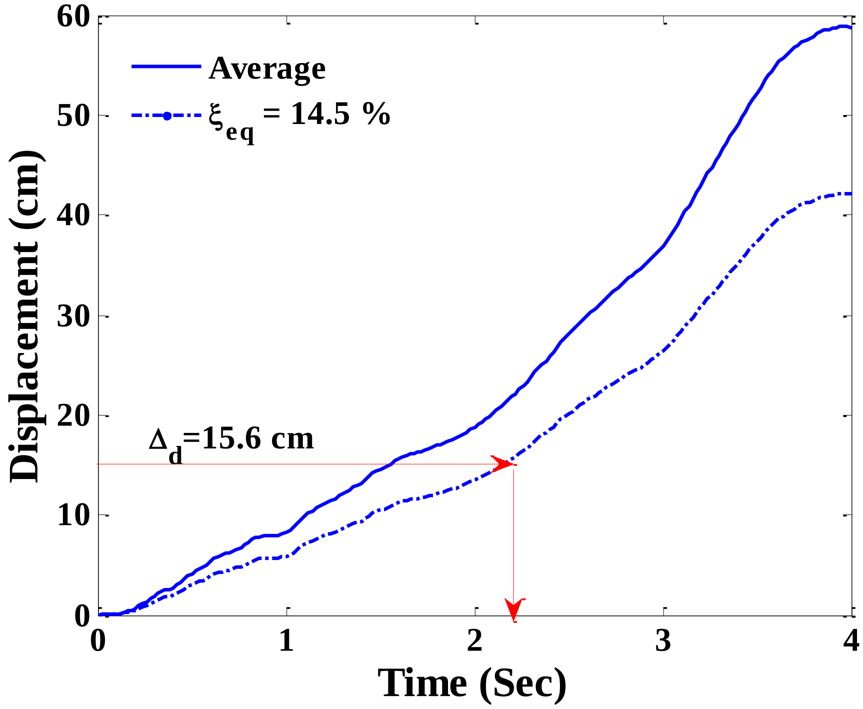

Figure 5.9: Effective period from damped displacement spectrum

Step 8: Effective stiffness and design base shear

The effective period and design base shear are calculated in Equations 5.28 and 5.29 as follows:

$$K_{eff} = 4\pi^2 \frac{m_{eff}}{T_{eff}^2} = 5257.4\ kN \tag{5.28}$$

$$V_b = K_{eff} \triangle_d = 824.04\ kN \tag{5.29}$$

Step 9: Distribute the base shear and perform a structural analysis

The above calculated design shear force is distributed to perform the structural analysis of the system. Equation 5.30 [SL12] is used to calculate the design shear forces at each level of the building (F_i).

$$F_i = KV_b \frac{m_i \triangle_i}{\sum_{i=1}^{n} m_i \triangle_i} \tag{5.30}$$

Table 5.3 summarizes the proportions of shear for frames (V_{frame}) and CLT wall V_{CLT} at each storey level of the building.

Table 5.3: Base shear proportions between frame and walls

Storey	$m_i\Delta_i$	$F_i(kN)$	$V_{i,total}(kN)$	$V_{frame}(kN)$	$V_{wall}(kN)$
3	49.68	383.60	383.60	268.52	115.08
2	36.8	284.15	667.75	467.42	200.32
1	20.24	156.28	824.03	576.82	247.21
0	0	0	0	0	0

The structural analysis is carried out using the approximate method. A portal method of analysis has been chosen to perform the analysis due to its simplicity and accuracy. As indicated in Figure 5.10, the inflection point for the bottom columns is taken to be at 60% of the storey height (h_s). This provision will avoid any soft storey mechanisms (formation of yielding point on the top of the lower story columns). However, for other columns of the frames, this inflection point is set at the mid height of the given storey. The method of structural analysis is illustrated in detail in Appendix:

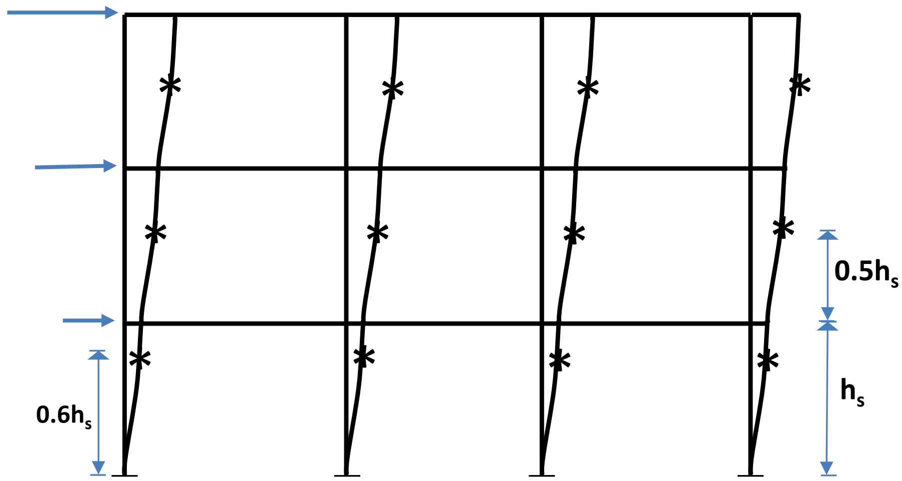

Figure 5.10: Inflection point on the deflected shape of the moment resisting frame

The final results for beams, columns, and joints of the frame are depicted in Figure 5.11.

Step 10: Beam and column strengths

The plastic moment strengths for the beams and columns are summarized and shown in Table 5.4. The detailed moment strengths for all beams and columns in the building are indicated in Figure 5.11. Subsequently, the plastic section modulus are calculated to choose an appropriate section that satisfies the demand.

Table 5.4: Beams and columns required moment strength

Storey	*Beam moment*	*Interior column moment*	*Exterior column moment*
3	71.6	143.13	71.6
2	196	249.28	124.64
1	247.7	369.13	184.5

It should be noted at this point that the selection of steel cross sections is accomplished with the following assumptions and provisions:

1. Gravity and seismic load actions (moment and shear) are not com-

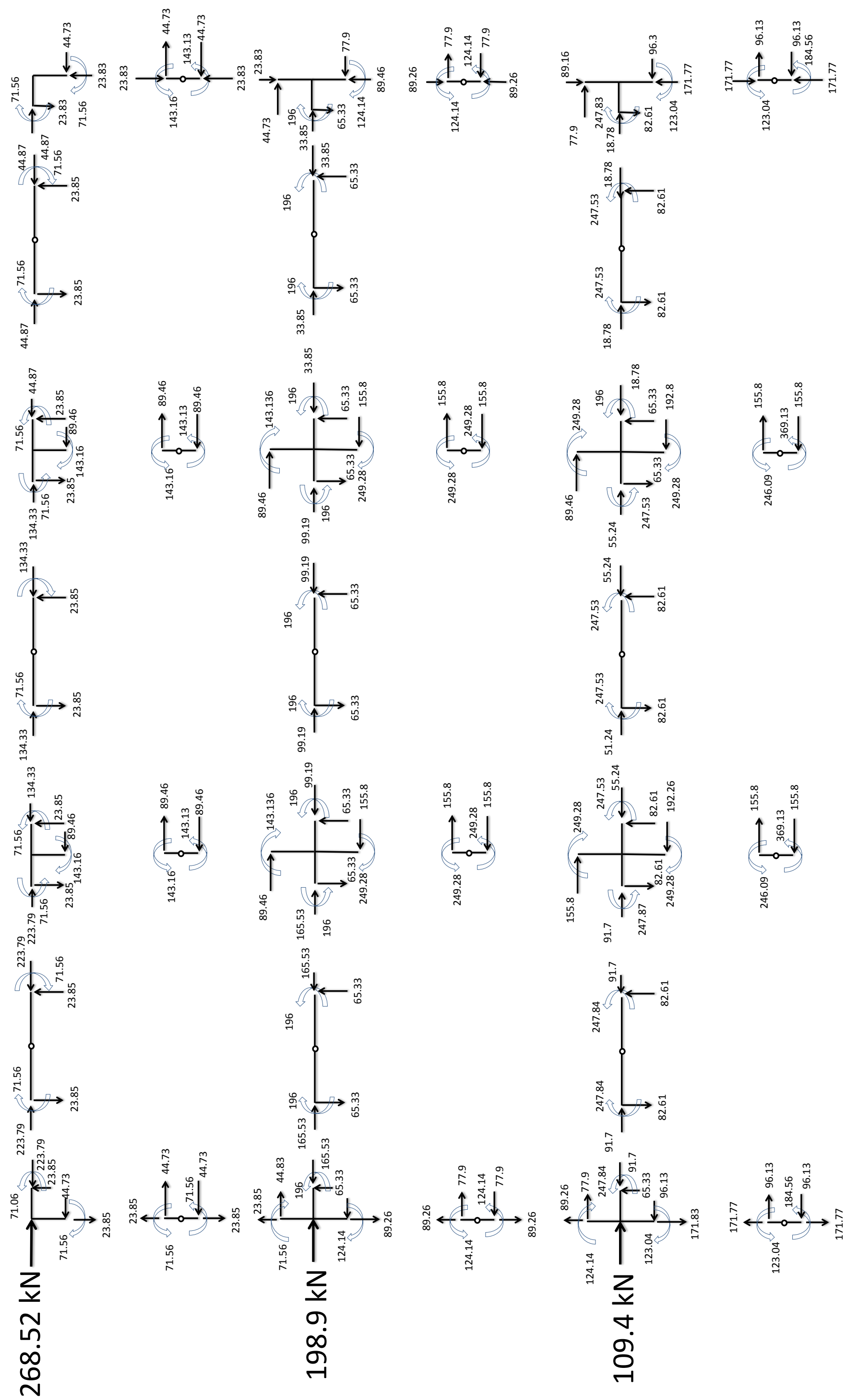

Figure 5.11: Detail results of approximate method of analysis

bined to select the element sections. Rather, the selection process is done with only the governing load (seismic actions). This assumption is correct for building designs in high seismic regions. Moreover, Pinto [Pin97], found negligible difference in seismic response of structures with or without gravity loads. Priestley [PCK07b] strongly argued the fallacy associated with combining DDBD seismic actions with gravity actions for the DDBD process. The addition of gravity moments with seismic moments, in DDBD, will result larger in sections. This will result a false sense of lower seismic response than the initial target displacement. In line with Priestley et al.[PCK07b], the element sections are selected for the higher of gravity and seismic moments. Since the buildings are designed for high seismic regions, for all buildings in this research the seismic loads governs the design.

2. As indicated in Chapter 4, the post yielding stiffness of the steel members is critical in the inelastic response and energy dissipation of the system. Garcia [GSC10], recommended a reduction factor on the design strength of members as seen in Equation 5.31. Since, at the start of the design process the post yielding stiffness is considered to be 1%, the reduction factor for the case study building is 1.002.

$$factor = 1 + r(\mu_{frame} - 1) \tag{5.31}$$

3. As required by CSA S16-09, both beams and columns are assumed to be constructed by considering bracing against lateral torsional buckling.

With the above assumptions, the member selection is carried out for beams and columns in the lower stories. Uniform cross sections of beams, exterior column, and interior columns are used through out the height of the building. The section modulus of beams and columns are used to select the sections from the CISC Handbook [CIS10]. Table 5.5 summarizes the selected sections for the case study building.

Table 5.5: Details of sections

Member	*Section*	$Z_{provided}(10^3 mm^3)$	$M_{r,provided}(kN.m)$
Beam	W310x52	841	261
Interior column	W360x79	1430	444
Exterior column	W310x45	708	220

The design checks for class of a selected section, overall member strength (OMS), and lateral buckling strength (LTBS) of members of the building is provided in Appendix. The design checks have been carried out based on CSA S16-09 regulations and conceptual suggestions from Filiatrault et al.[FRC+13].

Check for CLT properties

In this section, design checks have been carried out on initially assumed CLT panel properties. As discussed in Chapters 3 and 4, panel strength has a little effect on the dynamic behavior of the hybrid system. Numerical values from Structurlam manufacturing guideline [Strnd] are used to perform the design check. From the guideline, three layers CLT wall under pure shear can carry up to 304 kN load. However, the maximum shear demand on CLT walls for the case study building is 89.1 kN. Therefore, the CLT panel thickness (99 mm) that was considered at the start of the design process is acceptable. The steel connection brackets transfer the shear and axial loads from the steel frame to the CLT wall. The brackets in this hybrid system are under 3 different loads: shear, axial or their combination. Calibration of the Pinching4 model [LMA03] of OpenSees [MMS+06] by [SST+13] from the experimental tests performed by Schneider et al.[SST+12] on the bracket connections indicates that these connection type can carry up to 45 kN both in shear and axial directions. At the start of the design process, a total of 16 brackets are applied at the top and bottom of the panel. These brackets are under pure shear and combined axial-shear response. Therefore, these brackets transfer 16 $\times$ 45 kN shear and axial force with out failure. The maximum shear demand on the CLT wall is less than the bracket shear force transferring capability. Therefore, the initially assumed bracket spacing is is acceptable. However, the capability of the brackets under combined shear and axial loading needs further research and is not considered in the design check for this thesis.

For the detailed design of structures, a capacity design should be performed after this step. The application of this concept will vary member sections along the height of the building. Moreover, the column sizes will be expected to increase. Application of the capacity design is outside the scope of this thesis. More information on the application of capacity design principles in DDBD of hybrid structures can be found elsewhere [SPC06]. The above steps have been followed to design the middle bay CLT infilled six and nine storey 2D buildings of Figure 5.12. The floor plan for the buildings is shown in Figure 5.3.

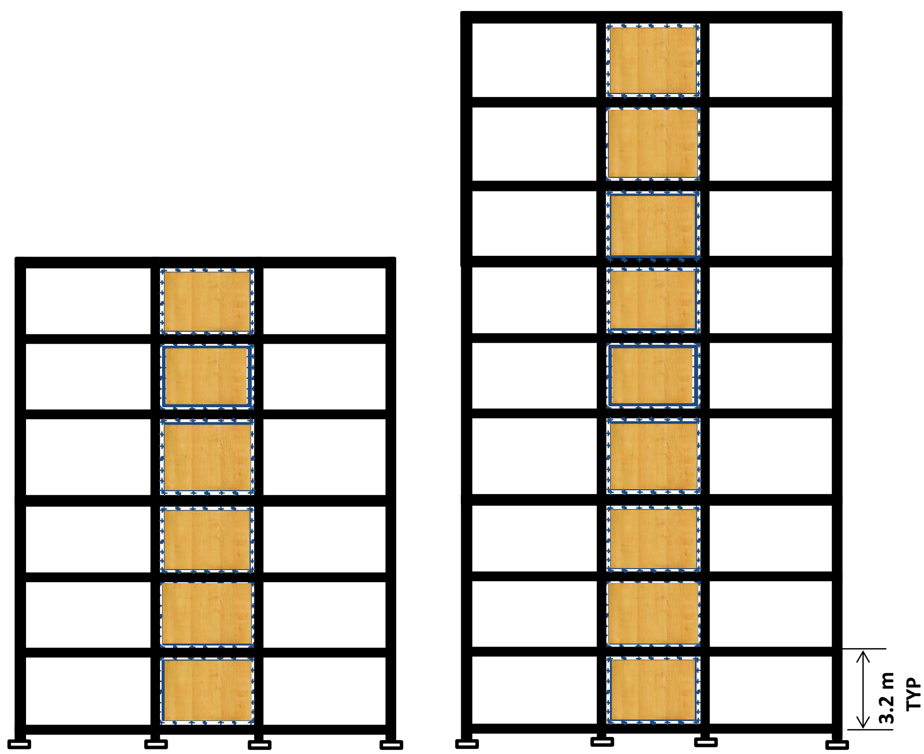

Figure 5.12: Elevation view of six and nine storey buildings

The final results of DDBD of 3, 6, and 9 storey buildings are summarized in Table 5.6. It should be noted at this point that all design checks were performed for the design of 6 and 9 storey buildings.

Table 5.6: Details of DDBD design

	3 storey	*6 storey*	*9 storey*
Proportion of Vb assigned to frames (%)	70	50	50
Design storey drift, thetad(%)	2.5	2.5	2.5
Design displacement (detald) (m)	0.156	0.28	0.409
Effective Height, heff (m)	7.28	13.5	19.73
Effective Mass, meff (T)	680.8	1287.3	1887.5
μ_{CLT}	12.05	21.7	31.4
$\mu_{frame,average}$	1.123	1.22	1.28
μ_{sys}	2.21	7.53	10.21
$\xi_{SDOF}(\%)$	14.5	20.5	21
Effective period, T_{eff} (sec)	2.26	3.2	4.2
K_{eff} (KN/m)	5257.4	4957.9	4219.9
V_b (kN)	824.04	1399.8	1726
Beam section	W310×52	W310×67	W360×79
Interior column section	W360×79	W360×91	W360×110
Exterior column section	W310×45	W310×52	W360×64
Beam strength, $M_{b,i}$ (KN.m)	261	326	444
Interior column strength, $M_{int.col,i}$ (KN.m)	444	552	640
Exterior column strength, $M_{ext.col,i}$ (KN.m)	220	261	354

5.4 Nonlinear Time History Analysis

In order to perform nonlinear time history analysis (NLTHA), OpenSees [MMS+06] finite element tool is used to model the designed hybrid structures. The details of the structural modeling are discussed in Chapter 3. Twenty earthquake ground motions that have been used to calibrate the EVD in Chapter 4 are used to perform NLTHA. Figure 3.5 shows the scaled spectra with the mean and target spectrum for considered hazard value. The average 5% damped displacement spectrum from all the ground motions is compared with Vancouver design spectrum as shown in Figure 16(b). The designed elements are modeled with their respective moment strength and 1% post yield stiffness ratio. Rigid floor systems are assumed for the building. Accidental torsion and P-Δ effects were not considered in the validation analysis. Seismic weight which is compromised of the self weight of the structure is applied at beam column connections. Since the structure is designed for high seismic region the structural elements are capable of carrying additional gravity loads. However, this assumption mat not work for the designs in moderate and low seismic regions.

5.4.1 Results of nonlinear time history analysis

The proposed DDBD method is validated by comparing its displacement responses with the initially assumed target displacement profile. In order to reduce the potential damage on the structures during the seismic event, maximum interstorey drift (MISD) of the building should be less than the target interstorey drift value (2.5%). In addition, according to Chapter 3, the residual interstorey drift (RISD) response should be checked as it can be high in the proposed hybrid structure. Sample seismic response of the 3 storey building in Northridge earthquake is given in Figure 5.13.

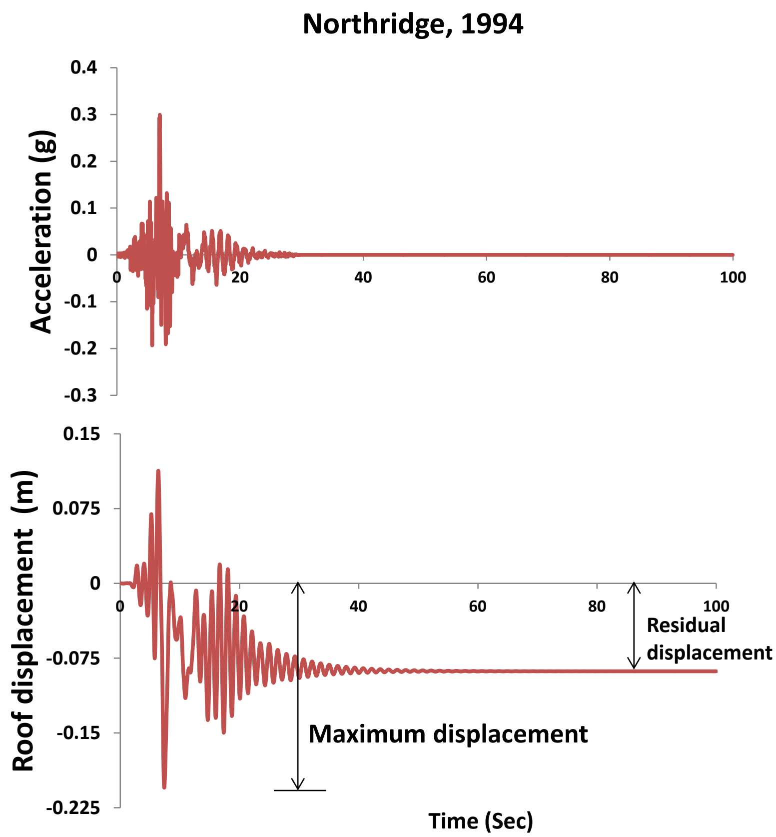

Figure 5.13: Response of 3 storey CLT infilled SMRF in Northridge 1994 earthquake

The storey displacement response of 3, 6, and 9 storey buildings are given in Figures 5.14, 5.15, and 5.16, respectively.

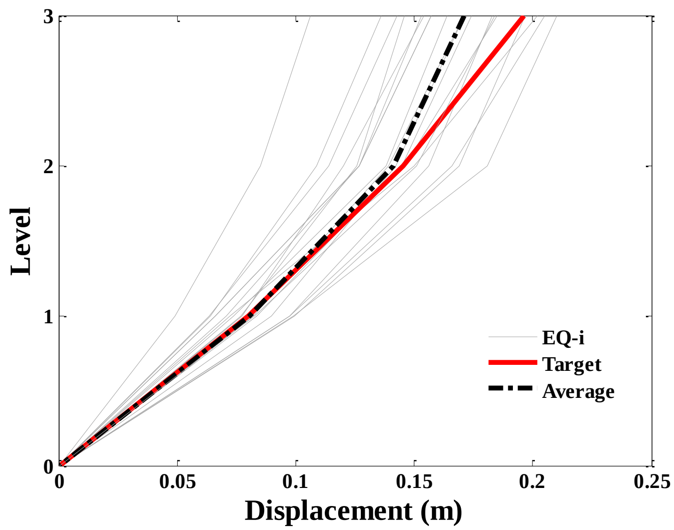

Figure 5.14: Maximum storey displacement of 3 storey hybrid building

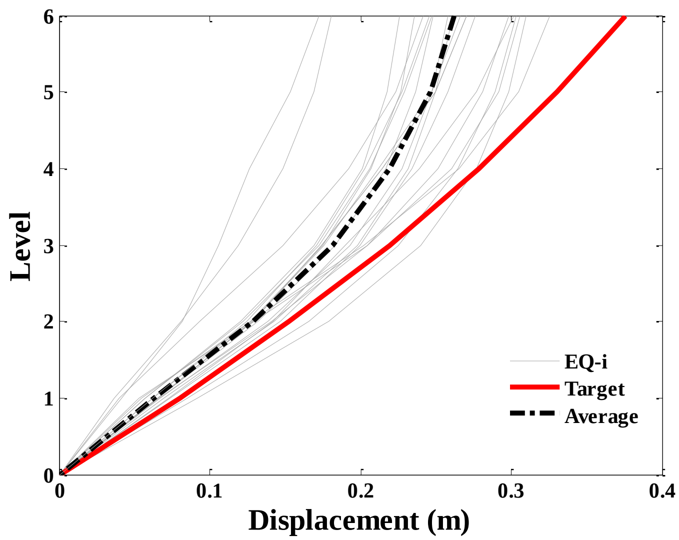

Figure 5.15: Maximum storey displacement of 6 storey hybrid building

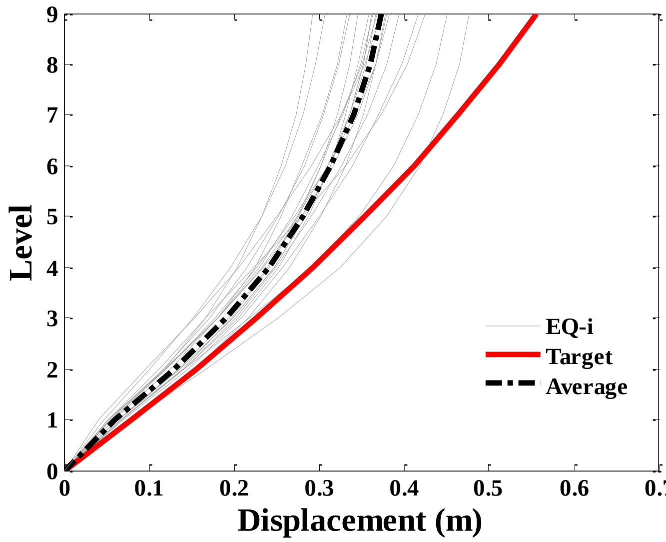

Figure 5.16: Maximum storey displacement of 9 storey hybrid building

The maximum intersorey drift response of 3, 6, and 9 storey buildings are given in Figures 5.17, 5.18, and 5.19, respectively.

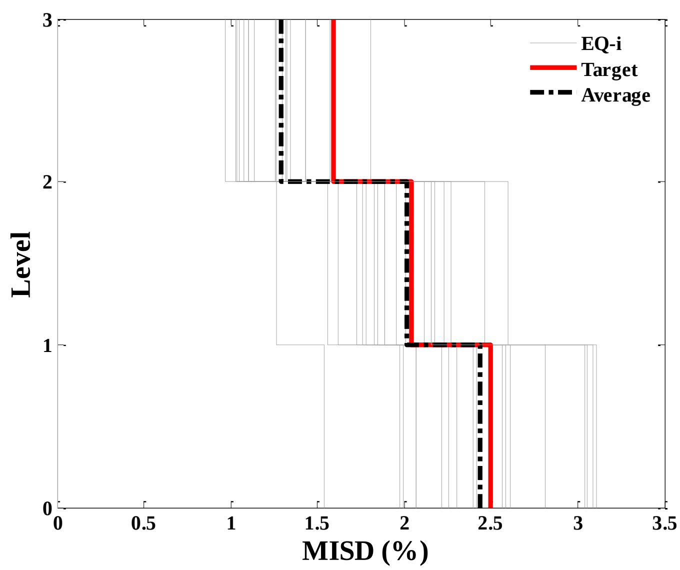

Figure 5.17: Maximum interstorey drift of 3 storey hybrid building

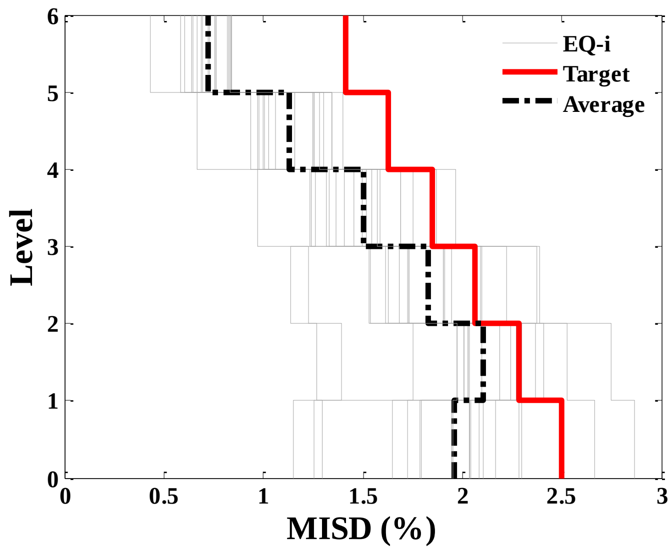

Figure 5.18: Maximum interstorey drift of 6 storey hybrid building

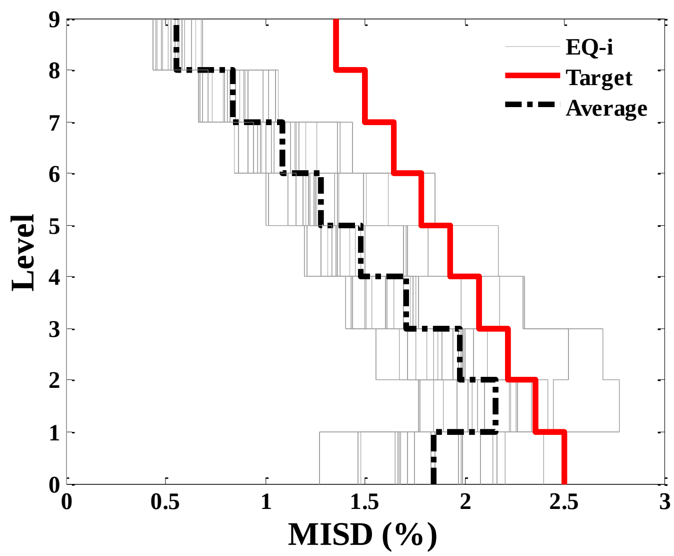

Figure 5.19: Maximum interstorey drift of 9 storey hybrid building

It is evident from Figures 5.14-C.5 that the target displacement and drift profiles are close to the average responses from the NLTHA. Irrespective of the height of the building, average displacement and intersorey drift demands are less than the initially assumed target values. This clearly indicates the capability of the proposed method in controlling the responses of structures under seismic excitation. However, the values of the design drift and displacement profiles for the top storeys of 6 and 9 storey buildings are not close enough to the average responses of NLTHA. This lower response is due to the application of uniform beam and column cross sections through out the height of the structure. This leads to lower drift values at the top of the buildings. The importance of residual interstorey drift is highlighted in Chapter 3. For brevity, the plots for the variation mean and individual RISD with the height of the building is given in Figures 5.20-5.22. The 3 storey building experienced RISD values of 0.01 - 0.3 %. A dispersed scatter plot is obtained for this building as shown in Figure 5.20. The RISD values for the six and nine storey buildings under each earthquake vary in the range of 0.01 - 1.35 % and 0.01 - 0.9 %, respectively. Values more than 0.5 % indicates extensive damage on the building. The mean RISD values are shown to increase linearly with the building height. However, large variability with ground motions is observed in the RISD responses.

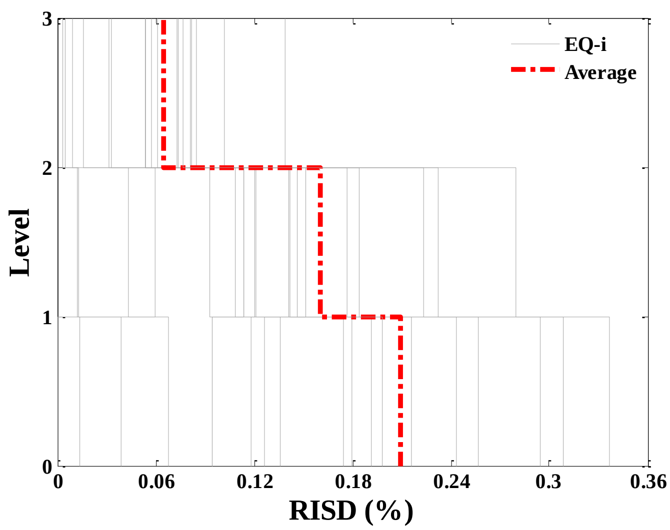

Figure 5.20: Residual interstorey drift of 3 storey hybrid building

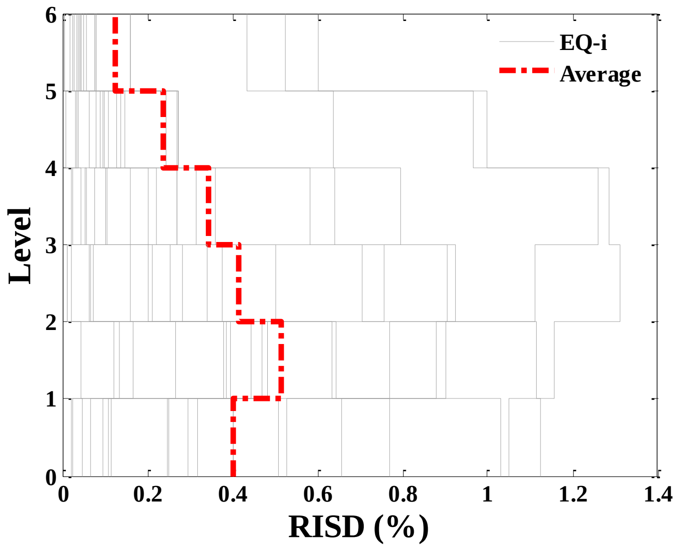

Figure 5.21: Residual interstorey drift of 6 storey hybrid building

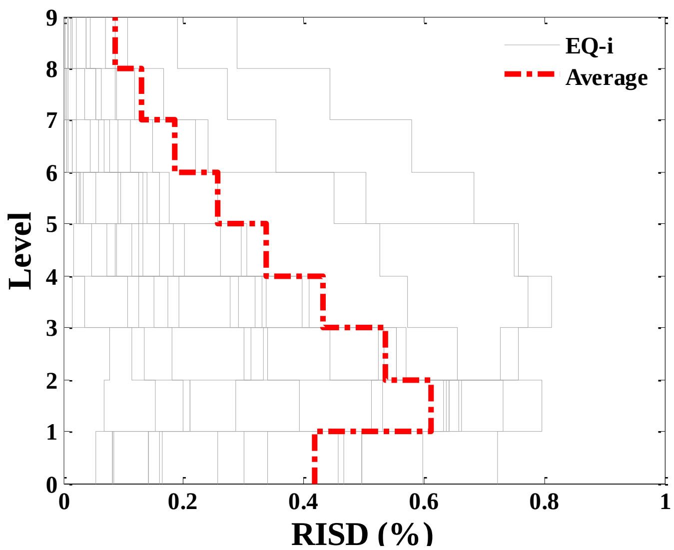

Figure 5.22: Residual interstorey drift of 9 storey hybrid building

5.5 Summary

A new iterative direct displacement based design method SMRFs with CLT infill walls has been developed and tested by designing 3-, 6-, and 9- storeys hybrid buildings. In summary, the developed method proved to effectively control seismic interstorey drifts and displacements. A robust finite element model of the hybrid structure that accounts for the CLT panel and frame interactions was used for the validation process. Initial shear proportions between the wall and frame are assigned at the start of the design process. The system ductility and equivalent viscous damping are explicitly accounted. Better control of storey drifts and displacement were achieved for low rise hybrid buildings.

Future research should aim at investigating the method to account for residual interstorey drift values (RISD). The RISD values that are obtained from NLTHA are between 0.2 - 0.6 %. RISD responses more than 0.5 % represent extensive damage on the buildings. Christopoulos [CPP04] indicated an effective way of controlling RISD in the DDBD method. Moreover, a further extension of the developed method is to couple it to the capacity design principles. This will make the method more rational for the designers.

6

Conclusions and future research perspectives

6.1 Summary and conclusions

This thesis has developed an iterative DDBD method for the Timber-Steel hybrid structure. The hybrid structure incorporates CLT shear panels as an infill in steel moment resisting frames (SMRFs). This structure has been developed at The University of British Columbia to overcome the height limitation of timber as a main structural element. The proposed hybrid system couples the ductile behaviour of steel moment resisting frames with thehigh stiffness to weight ratio of CLT shear panels.

The proposed hybrid structure is achieved by using L-shaped steel bracket connectors that are bolted to the steel frame and nailed to the CLT panel. These brackets are experimentally tested in axial and shear directions by Schneider et al. [SKP+13]. Analytical calibrations of the experimental tests on the brackets were performed by Shen et al. [SST+13]. A composite action is obtained by providing a gap between the frame and the CLT panel that allows the brackets to deform and disspiate energy. Preliminary overstrength and ductility factors were suggested for the system by Dickof et al. [DSBT14]. This hybrid system has proven to be efficient in decreasing the seismic vulnerability of steel moment resisting frames in high seismic regions Tesfamariam et al. [TSDB14]. The main motivation of this research was to develop a DDBD method for the proposed hybrid structure.

Initially, a polynomial predictive equation to quantify MISD was developed from corresponding RISD and significant modeling parameters by studying the seismic behaviours of 162 different hybrid buildings. The validation process confirmed that the equation can provide a good approximation of MISD for the proposed hybrid structures. Response surface methodology technique was successfully applied to develop the prediction equation. The developed equation does not need the dynamic characteristics of the structure in order to perform the post-seismic safety assessment of hybrid structures. Moreover, the dynamic analysis results were used to identify optimal modeling parameters of the hybrid structure. The optimization process adopts ANN based objective functions that are developed by using the Levenberg-Marquardt algorithm. A Pareto-front of optimal design solutions was obtained by applying a multi-objective optimization approach using the Genetic Algorithm. The obtained optimized values of modeling variables will result in the possible minimum RISD and MISD values under extreme seismic event. The following conclusions can be made based on the results of the parametric studies in Chapter 3:

- MISD can be estimated from the modeling parameters and RISD effectively. The validation process confirmed that the equation can provide good approximation of MISD for the proposed hybrid structures.

- Response surface methodology technique can be successfully applied to develop the prediction equation. D-Optimal deterministic experimental design technique was used for efficient sampling of design points without requiring additional dynamic analyses.

- The developed equation can be used for post-seismic safety assessment of hybrid structures without requiring the dynamic characteristics of the structure under consideration.

- MISD and RISD can be estimated from the modeling parameters by using ANN surrogate models.

- The proposed optimum values of modeling variables will result in the possible minimum RISD and MISD values under extreme seismic events.

- Adopting the proposed modeling parameters during the design process of the hybrid system will decrease the damages resulting from the earthquake events.

In Chapter 4, an EVD model was developed and calibrated for the hybrid structure under study. For this purpose, an analytical investigation was carried out for 243 single-storey single-bay CLT infilled SMRFs by varying the modeling parameters that can affect the hysteretic behaviour of the system. The equivalent viscous damping and ductility of each model were obtained from the hysteretic responses of semi-static cyclic analysis. Then an expression was developed for equivalent viscous damping as a function of ductility and various modeling parameters. Finally, an iterative non-linear time history analyses was conducted using 20 spectrum compatible earthquake ground motions to calibrate EVD from Jacobsen′s area based approach. The calibration process using NLTHA revealed that the Jacobsens area based approach overestimates the EVD ratio. The calibrated EVD-ductility law was found to be dependent on the gap between the frame and CLT panel, bracket spacing and the post yield stiffness ratio of the hybrid system. The following conclusions can be drawn based on the results of the research in Chapter 4

- The coefficient C of damping ductility law of Equation 4.1 is expressed as function of modeling variables of CLT infilled steel moment frames. This law can be used for the direct displacement based design method that allows simultaneous calibration and design procedure [MGD13].

- In general, the hysteretic damping is found to be higher for the hybrid system modeled with larger gap and bracket spacing. Hybrid systems with smaller gap between CLT and steel with larger post yield stiffness ratio experienced a higher degree of pinching. This pinching effect caused the systems to dissipate less amount of energy under cyclic loading.

- The effect of panel strength and thickness on damping is found to be minimal. This suggests that changing the thickness and crushing strength of panels will not influence the hysteretic behaviour of the system.

- Hybrid systems with larger post yielding stiffness ratio dissipate less amount of energy which results in a lower value of hysteretic damping.

- From the comparison graphs of Figure 4.16, it is concluded that for a given level of gap, post yield stiffness ratio, panel thickness and strength, and bracket spacing, the hysteretic damping is increased linearly up to ductility (μ) value of 2.

- The calibration process using NLTHA revealed that the Jacobsen′s area based approach overestimates the EVD ratio. The calibrated EVD-ductility law was found to be dependent on the bracket spacing and the post yield stiffness ratio of the hybrid system.

- The calibration process utilized NLTHA on SDOF hybrid systems and the effective period is in the range of (0.7 to 3.38 sec). Consistent with other researchers by [WNS11, PCK07b] the developed EVD-ductility laws in this paper can be applied to the direct displacement based design of MDOF of proposed hybrid structures.

Finally in Chapter 5, a new iterative direct displacement based design method for CLT infilled SMRFs has been developed and tested by designing 3-, 6-, and 9- storey hybrid buildings. A robust finite element model of the hybrid structure that accounts for CLT panel and frame interactions was used for the validation process. Initial shear proportions between the panels and frames were assigned at the start of the design process. The system ductility and equivalent viscous damping are explicitly accounted. Design checks have been carried out on a the class of section, lateral buckling strength, and overall member strength. In summary, the developed method effectively controls seismic interstorey drifts and displacements. There was greater control of storey drifts and displacements for low rise hybrid buildings. The following conclusions can be made based on the results of the research in Chapter 5:

- A new iterative direct displacement based design method for CLT infilled SMRFs has been successfully developed and tested by deigning 3-, 6-, and 9- storey hybrid buildings.
- The developed method proved to effectively control the seismic interstorey drifts and displacements of CLT infilled SMRFs.
- Better control of storey drifts and displacement were achieved for low rise hybrid buildings. .
- The developed method paves a path for designers to consider DDBD method as an alternative design approach for CLT infilled SMRFs.

perfomr

6.2 Future research perspectives

The following list includes some aspects of the proposed DDBD procedure that needs further study in order to increase its applicability and robustness.

1. Validate EVD-ductility law of Chapter 4 by using full scale Experimental tests. Moreover, important properties such as diagonal CLT panel crushing displacement and bracket behaviours in a combined axial and shear loads can be extracted from the tests.
2. Incorporate residual storey drift values as an input for the design process. The RISD values that are obtained from NLTHA of Chapter 5

are between 0.2 - 0.6 %. RISD responses more than 0.5 % represent extensive damage to the buildings. Christopoulos [CPP04] indicated an effective way of controlling RISD in the DDBD method.

3. Extend the proposed method to include torsion due to irregularity in building layout. Moreover, further investigation is needed to control higher mode effects.

4. A more comprehensive performance evaluation of the designed buildings can be done by using FEMA P695 [41] methodology.

5. Extend the method to consider different CLT panel configurations.

6. Investigation is needed towards the modified inelastic demand on SMRFs due to the presence of the infill panels.

Bibliography

[ASAH11] M.H. Al Shamisi, A.H. Assi, and H.A.N. Hejase. Using matlab to develop artificial neural network models for predicting global solar radiation in al ain city–uae. *Engineering education and research using MATLAB. Intech, New York*, pages 219–238, 2011. → pages 59

[ATC96] ATC. 40, seismic evaluation and retrofit of concrete buildings. *Applied Technology Council, report ATC-40. Redwood City*, 1996. → pages 20

[BBS07] G.T. Bitsuamlak, C Bedard, and T Stathopoulos. Modeling the effect of topography on wind flow using a combined numerical–neural network approach. *Journal of Computing in Civil Engineering*, 21(6):384–392, 2007. → pages 59

[BC94] P Bazzurro and C.A. Cornell. Seismic hazard analysis of nonlinear structures. i: Methodology. *Journal of Structural Engineering*, 120(11):3320–3344, 1994. → pages 44

[BCMM04] P Bazzurro, C.A. Cornell, C Menun, and M Motahari. Guidelines for seismic assessment of damaged buildings. In *Proceedings of the Thirteenth World Conference on Earthquake Engineering*, 2004. → pages 38

[Bla04] C.A. Blandon. *Equivalent viscous damping for DDBD*. PhD thesis, MSc Thesis, ROSE School, Pavia, Italy, 2004. → pages 29

[BP05] C.A. Blandon and M.J.N. Priestley. Equivalent viscous damping equations for direct displacement based design. *Journal of earthquake Engineering*, 9(sup2):257–278, 2005. → pages 67, 90

[C+07] ASCE/SEI Seismic Rehabilitation Standards Committee et al. Seismic rehabilitation of existing buildings (asce/sei 41-06). *American Society of Civil Engineers, Reston, VA*, 2007. → pages 42

[CDHB13] A.A. Christidis, E.G. Dimitroudi, G.D. Hatzigeorgiou, and D.E. Beskos. Maximum seismic displacements evaluation of steel frames from their post-earthquake residual deformation. *Bulletin of Earthquake Engineering*, 11(6):2233–2248, 2013. → pages 38

[CF06] A Ceccotti and M Follesa. Seismic behaviour of multi-storey x-lam buildings. In *COST E29 International Workshop on Earthquake Engineering on Timber Structures, Coimbra, Portugal*, pages 81–95, 2006. → pages 11

[CG01] A.K. Chopra and R.K. Goel. Direct displacement-based design: use of inelastic vs. elastic design spectra. *Earthquake Spectra*, 17(1):47–64, 2001. → pages 95

[CGA02] C.Z. Chrysostomou, P Gergely, and J.F. Abel. A six-strut model for nonlinear dynamic analysis of steel infilled frames. *International Journal of Structural Stability and Dynamics*, 2(03):335–353, 2002. → pages 3

[Cha05] Y.H. Chai. Incorporating low-cycle fatigue model into duration-dependent inelastic design spectra. *Earthquake engineering & structural dynamics*, 34(1):83–96, 2005. → pages 44

[CIS10] CISC. 2010. *Handbook of steel construction*. Canadian Inst of Steel construction, 2010. → pages 115

[CK95] G.M. Calvi and G.R. Kingsley. Displacement-based seismic design of multi-degree-of-freedom bridge structures. *Earthquake engineering & structural dynamics*, 24(9):1247–1266, 1995. → pages 95

[CKS03] Y Chen, G.A. Kopp, and D Surry. Prediction of pressure coefficients on roofs of low buildings using artificial neural networks. *Journal of wind engineering and industrial aerodynamics*, 91(3):423–441, 2003. → pages 59

[CNS06] H.El. Chabib, M Nehdi, and A Said. Predicting the effect of stirrups on shear strength of reinforced normal-strength concrete (nsc) and high-strength concrete (hsc) slender beams using artificial intelligence. *Canadian Journal of Civil Engineering*, 33(8):933–944, 2006. → pages 59

[Com95] SEAOC Vision 2000 Committee. Performance-based seismic engineering. *Structural Engineers Association of California, Sacramento, CA*, 1995. → pages 20

[CP04] C Christopoulos and S Pampanin. Towards performance-based design of mdof structures with explicit consideration of residual deformations. 2004. → pages 38

[CPP03] C Christopoulos, S Pampanin, and M.J.N. Priestley. Performance-based seismic response of frame structures including residual deformations. part i: Single-degree of freedom systems. *Journal of Earthquake Engineering*, 7(1):97–118, 2003. → pages 38

[CPP04] C Christopoulos, S Pampanin, and M.J.N. Priestley. Seismic design and response of buildings including residual deformations. *Proc. 13P th*, 2004. → pages 34, 95, 96, 126, 132

[CSA09] CSA. 2009. CSA-S16-09 design of steel structures. *Canadian Standards Association*, 2009. → pages 39, 160, 162, 163, 164, 165

[CSY10] A Ceccotti, C Sandhaas, and M Yasumura. Seismic behaviour of multistory cross-laminated timber buildings. In *International Convention of Society of Wood Science and Technology. Geneva, Switzerland*, 2010. → pages 11

[DAGT09] L Daniel A, Simon and B Girma T. Application of an artificial neural network model for boundary layer wind tunnel profile development. In *11th Americas Conference on Wind Engineering*, 2009. → pages 59

[DB93] H Demuth and M Beale. Neural network toolbox for use with matlab. 1993. → pages 151

[Deb01] K Deb. *Multi-objective optimization using evolutionary algorithms*, volume 2012. John Wiley & Sons Chichester, 2001. → pages 61

[Dic13] C Dickof. Clt infill panels in steel moment resisting frames as a hybrid seismic force resisting system. 2013. → pages 1, 12, 16, 18, 19, 38, 42, 66, 70, 84, 94, 106

[DK04] H.M. Dwairi and M.J. Kowalsky. Investigation of jacobsens equivalent viscous damping approach as applied to displacement-based seismic design. In *13th World Conference on Earthquake Engineering–13WCEE*, pages 1–6, 2004. → pages 67, 83

[DKN07] H.M. Dwairi, M.J. Kowalsky, and J.M. Nau. Equivalent damping in support of direct displacement-based design. *Journal of Earthquake Engineering*, 11(4):512–530, 2007. → pages 67

[DM01] A Dutta and J.B. Mander. Energy based methodology for ductile design of concrete columns. *Journal of Structural Engineering*, 127(12):1374–1381, 2001. → pages 44

[dN98] Comité Européen de Normalisation. Eurocode 8–design of structures for earthquake resistance–part 1: General rules, seismic actions and rules for buildings. *European Standard NF EN*, 1, 1998. → pages 89, 110

[dN05] Comité Européen de Normalisation. Eurocode 8–design of structures for earthquake resistance, part 3: Assessment and retrofitting of buildings. *European Standard NF EN*, 3, 2005. → pages 100

[DSBT14] C Dickof, S.F. Stiemer, M.A. Bezabeh, and S Tesfamariam. Clt-steel hybrid system: Ductility and overstrength values based on static pushover analysis. *Journal of Performance of Constructed Facilities*, 2014. → pages xi, 1, 12, 16, 17, 18, 38, 42, 66, 70, 84, 94, 106, 128

[DSS89] J.L. Dawe, A.B. Schriver, and C Sofocleous. Masonry infilled steel frames subjected to dynamic load. *Canadian Journal of Civil Engineering*, 16(6):877–885, 1989. → pages 3

[DST12] C Dickof, S.F. Stiemer, and S Tesfamariam. Wood-steel hybrid seismic force resisting systems: seismic ductility. *World Conference on Timber Engineering*, 15:19, 2012. → pages 1, 12, 16, 18, 38, 66, 94, 106

[ECTC10] J Erochko, C Christopoulos, R Tremblay, and H Choi. Residual drift response of smrfs and brb frames in steel buildings designed according to asce 7-05. *Journal of Structural Engineering*, 137(5):589–599, 2010. → pages 38

[ED02] W.W. El-Dakhakhni. *Experimental and analytical seismic evaluation of concrete masonry-infilled steel frames retrofitted using GFRP laminates.* PhD thesis, Drexel University, 2002. → pages 3

[EDEH03] W.W. El-Dakhakhni, M Elgaaly, and A.A. Hamid. Three-strut model for concrete masonry-infilled steel frames. *Journal of Structural Engineering*, 129(2):177–185, 2003. → pages 3

[EI64] R Emilio and H Ismael. On kind of hysteretic damping. In *Proceedings of the American Society of Civil Engineers*, 1964. → pages 67

[EY04] E Erduran and A Yakut. Drift based damage functions for reinforced concrete columns. *Computers & structures*, 82(2):121–130, 2004. → pages 37, 65, 94

[41] Federal Emergency Management Agency (FEMA). Quantification of building seismic performance factors, 2009. → pages 132

[Fed97] Federal Emergency Management Agency (FEMA). Nehrp commentary on the guidelines for the seismic rehabilitation of buildings. Technical report, Washington, DC, 1997. → pages 20, 21

[FF01] B Folz and A Filiatrault. Sawsversion 1.0: A computer program for seismic analysis of woodframe buildings.. *Rep. No. SSRP-2001*, 9, 2001. → pages 13

[FF02] A Filiatrault and B Folz. Performance-based seismic design of wood framed buildings. *Journal of Structural Engineering*, 128(1):39–47, 2002. → pages 95, 96

[FRC+13] A Filiatrault, T Robert, C Constantin, F Bryan, and P Didier. *Elements of earthquake engineering and structural dynamics*. Presses inter Polytechnique, 2013. → pages 116

[GA07] M Ghorbanie-Asl. *Performance-based seismic design of building structures*. ProQuest, 2007. → pages 30

[GAEB99] A Ghobarah, H Abou-Elfath, and A Biddah. Response-based damage assessment of structures. *Earthquake engineering & structural dynamics*, 28(1):79–104, 1999. → pages 37, 65, 94

[GEAA00] A Ghobarah, M El-Attar, and N.M. Aly. Evaluation of retrofit strategies for reinforced concrete columns:: a case study. *Engineering structures*, 22(5):490–501, 2000. → pages 22

[Gho01] A Ghobarah. Performance-based design in earthquake engineering: state of development. *Engineering structures*, 23(8):878–884, 2001. → pages ix, 20, 21

[GJT12] H Ghaffarzadeh, A Jafari, and N Talebian. Equivalent viscous damping in direct displacement-based design of steel braced reinforced concrete frames. *The Structural Design of Tall and Special Buildings*, 2012. → pages 67, 83

[GK99] A Gupta and H Krawinkler. *Seismic demands for the performance evaluation of steel moment resisting frame structures.* PhD thesis, Stanford University, 1999. → pages 38

[GP11] S Gagnon and C Pirvu. *CLT handbook: cross-laminated timber.* FPInnovations, 2011. → pages 72

[GS74] P Gulkan and M.A. Sozen. Inelastic responses of reinforced concrete structure to earthquake motions. In *ACI Journal Proceedings*, volume 71. ACI, 1974. → pages 94

[GSC10] R Garcia, T.J. Sullivan, and G.D. Corte. Development of a displacement-based design method for steel frame-rc wall buildings. *Journal of Earthquake Engineering*, 14(2):252–277, 2010. → pages xi, 26, 27, 95, 108, 109, 115, 162

[HW05] A Habibullah and E Wilson. Sap 2000" static and dynamic finite element analysis of structures. *Computers and Structures Inc. Berkeley, California*, 2005. → pages 104

[ISK06] Y Iwata, H Sugimoto, and H Kuguamura. Reparability limit of steel structural buildings based on the actual data of the hyogoken-nanbu earthquake. *Proceedings of the 38 th Joint*

Panel. Wind and Seismic effects. NIST Special Publication, 1057:23–32, 2006. → pages 38

[Jac60] L.S. Jacobsen. Damping in composite structures. In *Proceedings of the 2nd world conference on earthquake engineering*, 1960. → pages 66

[KA02] M.J. Kowalsky and J.P. Ayers. Investigation of equivalent viscous damping for direct displacement-based design. In *PEER-2002/02, The Third US-Japan Workshop on Performance-Based Earthquake Engineering Methodology for Reinforced Concrete Building Structures, 1618 August 2001, Seattle, Washington, Berkeley: Pacific Earthquake Engineering Research Center, University of California.*, pages 173–185, 2002. → pages 67

[KC04] H.S. Kim and Y.S. Chun. Structural damage assessment of building structures using dynamic experimental data. *The Structural Design of Tall and Special Buildings*, 13(1):1–8, 2004. → pages 37, 65, 94

[KM10] A.I. Khuri and S Mukhopadhyay. Response surface methodology. *Wiley Interdisciplinary Reviews: Computational Statistics*, 2(2):128–149, 2010. → pages 50

[KMA03] H Krawinkler, R Medina, and B Alavi. Seismic drift and ductility demands and their dependence on ground motions. *Engineering structures*, 25(5):637–653, 2003. → pages 37, 65, 94

[KMHN98] K Kawashima, GA MacRae, J Hoshikuma, and K Nagaya. Residual displacement response spectrum. *Journal of Structural Engineering*, 124(5):523–530, 1998. → pages 35

[KPI+01] H Krawinkler, F Parisi, L Ibarra, A Ayoub, and R Medina. *Development of a testing protocol for woodframe structures*, volume 102. CUREE Richmond, CA, 2001. → pages 75

[KPM95] M.J. Kowalsky, M.J.N. Priestley, and G.A. Macrae. Displacement-based design of rc bridge columns in seismic regions. *Earthquake engineering & structural dynamics*, 24(12):1623–1643, 1995. → pages 95

[LBC04] N Luco, P Bazzurro, and C.A. Cornell. Dynamic versus static computation of the residual capacity of a mainshock-damaged building to withstand an aftershock. In *Proceedings of the 13th World Conference on Earthquake Engineering*, 2004. → pages 38

[LDT] L Landi, P.P. Diotallevi, and A Tardini. Equivalent viscous damping for the displacement-based seismic assessment of infilled rc frames. → pages 83

[LK10] D.G. Lignos and H Krawinkler. Deterioration modeling of steel components in support of collapse prediction of steel moment frames under earthquake loading. *Journal of Structural Engineering*, 137(11):1291–1302, 2010. → pages 42

[LMA03] L.N. Lowes, N Mitra, and A Altoontash. *A beam-column joint model for simulating the earthquake response of reinforced concrete frames*. Pacific Earthquake Engineering Research Center, College of Engineering, University of California, 2003. → pages 13, 116

[LS06] B Lu and P.F. Silva. Estimating equivalent viscous damping ratio for rc members under seismic and blast loadings. *Mechanics Research Communications*, 33(6):787–795, 2006. → pages 67

[MAIN08] J McCormick, H Aburano, M Ikenaga, and M Nakashima. Permissible residual deformation levels for building structures considering both safety and human elements. *14th WCEE, Beijing, China*, 2008. → pages 38

[MASR] S.A. Moayed Alaee, TJ Sullivan, and C.A. Rogers. Towards a direct displacement-based design procedure for cold-formed steel frame/wood panel shear walls. → pages 36, 95, 96

[MAT13] MATLAB. *version 8.2.0.701 (R2013b)*. The MathWorks Inc., Natick, Massachusetts, 2013. → pages 62, 151

[MDLZ04] M.Y. Mansour, M Dicleli, J.Y. Lee, and J Zhang. Predicting the shear strength of reinforced concrete beams using artificial neural networks. *Engineering Structures*, 26(6):781–799, 2004. → pages 59

[MGD13] S Malekpour, H Ghaffarzadeh, and F Dashti. Direct displacement-based design of steel-braced reinforced concrete frames. *The Structural Design of Tall and Special Buildings*, 22(18):1422–1438, 2013. → pages xi, 29, 31, 95, 96, 129

[MK00a] M.S. Medhekar and D.J.L. Kennedy. Displacement−based seismic design of buildings−application. *Engineering structures*, 22(3):210−−221, 2000. → pages 23, 95

[MK00b] M.S. Medhekar and D.J.L. Kennedy. Displacement−based seismic design of buildings−theory. *Engineering structures*, 22(3):201−−209, 2000. → pages 19, 22, 23

[MK05] R.A. Medina and H Krawinkler. Evaluation of drift demands for the seismic performance assessment of frames. *Journal of Structural Engineering*, 131(7):1003–1013, 2005. → pages 37, 65, 94

[MMS+06] S Mazzoni, F McKenna, M.H. Scott, G.L. Fenves, and B Jeremic. Open system for earthquake engineering simulation (opensees). *Berkeley, California*, 2006. → pages 4, 13, 38, 42, 87, 116, 118

[Moe92] J.P. Moehle. Displacement-based design of rc structures subjected to earthquakes. *Earthquake spectra*, 8(3):403–428, 1992. → pages 95

[Mog04] H.A. Moghaddam. Lateral load behavior of masonry infilled steel frames with repair and retrofit. *Journal of structural engineering*, 130(1):56–63, 2004. → pages 3

[Mon97] D.C. Montgomery. *Design and analysis of experiments*, volume 7. Wiley New York, 1997. → pages 50

[MP97] G Manfredi and M Pecce. Low cycle fatigue of rc beams in nsc and hsc. *Engineering structures*, 19(3):217–223, 1997. → pages 44

[MRG02] E Miranda and J Ruiz-García. Evaluation of approximate methods to estimate maximum inelastic displacement demands. *Earthquake engineering & structural dynamics*, 31(3):539–560, 2002. → pages 67

[MTM08] A Mohebkhah, A.A. Tasnimi, and H.A. Moghadam. Nonlinear analysis of masonry-infilled steel frames with openings using discrete element method. *Journal of Constructional Steel Research*, 64(12):1463–1472, 2008. → pages 3

[NRC95] NRCC. 1995. National building code of canada, associate committee on the national building code, national research council of canada, 1995. → pages 22

[NRC05] NRCC. 2005. National building code of canada, associate committee on the national building code, national research council of canada, 2005. → pages 10

[NRC10] NRCC. 2010. National building code of canada, associate committee on the national building code, national research council of canada, 2010. → pages 18, 19, 20, 39, 43, 44, 87, 106

[PCK07a] M.J.N. Priestley, G.M. Calvi, and M.J. Kowalsky. Direct displacement-based seismic design of structures. In *5 th NZSEE Conference*, 2007. → pages 66, 98, 99

[PCK07b] M.J.N. Priestley, G.M. Calvi, and M.J. Kowalsky. *Displacement-based seismic design of structures.* Pavia, Italy : IUSS Press : Distributed by Fondazione EUCENTRE, c2007, 2007. → pages 19, 24, 34, 35, 65, 66, 97, 100, 106, 108, 115, 130

[PCP03] S Pampanin, C Christopoulos, and M.J.N. Priestley. Performance-based seismic response of frame structures including residual deformations. part ii: Multi-degree of freedom systems. *Journal of Earthquake Engineering*, 7(1):119–147, 2003. → pages 38

[PEE05] NGA PEER. Database. pacific earthquake engineering research center: Nga database, 2005. → pages 43, 87

[Pin97] P.E. Pinto. *Seismic design of reinforced concrete structures for controlled inelastic response: recent advances in design concepts and codes.* Comité Euro-Internat. du Béton, 1997. → pages 115

[PK00] M.J.N. Priestley and M.J. Kowalsky. Direct displacement-based seismic design of concrete buildings. *Bulletin of the New Zealand National Society for Earthquake Engineering*, 33(4):421–444, 2000. → pages 95

[PKC11] M Popovski, E Karacabeyli, and A Ceccotti. Seismic performance of cross-laminated timber buildings-chapter 4. *CLT Handbook-Cross-Laminated Timber, FPInnovations Special Publication SP-528E, Canadian Edition*, 2011. → pages 8

[PP] T Paulay and M.J.N. Priestley. Seismic design of reinforced concrete and masonry buildings. 1992. → pages 104, 109, 162

[PR07] W.C. Pang and D.V. Rosowsky. Direct displacement procedure for performance−based seismic design of multistory woodframe structures. *NEESWood Report NW*, 2, 2007. → pages 95, 96

[PR09] W.C. Pang and D.V. Rosowsky. Direct displacement procedure for performance−based seismic design of mid−rise wood-framed structures. *Earthquake spectra*, 25(3):583−−605, 2009. → pages 95, 96

[Pri93] M.J.N. Priestley. Myths and fallacies in earthquake engineeringconflicts between design and reality. *Bulletin of the New Zealand National Society for Earthquake Engineering*, 26(3):329–341, 1993. → pages 22, 67, 95

[Pri99] M.J.N. Priestley. Displacement-based approaches to rational limit states design of new structures. In *Proc. 11th Eur. Conf. Earthquake Eng.: Invited Lectures*, pages 317–335, 1999. → pages 96

[Pri00] M.J.N. Priestley. Performance based seismic design. *Bulletin of the New Zealand Society for Earthquake Engineering*, 33(3):325−−346, 2000. → pages 19

[Pri03] M.J.N. Priestley. *Myths and fallacies in earthquake engineering, revisited*. IUSS press, 2003. → pages 83

[PvdLP12] S Pei, J.W. van de Lindt, and M Popovski. Approximate r-factor for cross-laminated timber walls in multistory buildings. *Journal of Architectural Engineering*, 19(4):245–255, 2012. → pages 95

[RHA13] A.B.M. Rafiqul H and M.S. Alam. Direct displacement-based design of industrial rack clad buildings. *Earthquake Spectra*, 29(4):1311–1334, 2013. → pages 95

[RM86] E Rosenblueth and R Meli. *The 1985 earthquake: causes and effects in Mexico City*. 1986. → pages 37

[SCBC98] N Shome, C.A. Cornell, P Bazzurro, and J.E. Carballo. Earthquakes, records, and nonlinear responses. *Earthquake Spectra*, 14(3):469–500, 1998. → pages 44

[Sch09] J Schneider. Connections in cross-laminated-timber shear walls considering the behaviour under monotonic and cyclic lateral loading. Master's thesis, 2009. → pages 13, 15, 16

[SDT12] S.F. Stiemer, C Dickof, and S Tesfamariam. Timber-steel hybrid systems: seimic overstrength and ductility factors. *Advances in Steel Concrete Composite and Hybrid Structures*, 2012. → pages 1, 12, 16, 18, 38, 66, 94

[SE10] I Stat-Ease. Design expert version 8, 2010. → pages 51

[Sel12] A.A. Seleemah. A multilayer perceptron for predicting the ultimate shear strength of reinforced concrete beams. *Journal of Civil Engineering and Construction Technology*, 3(2):64–79, 2012. → pages 59

[SHE10] R Stürzenbecher, K Hofstetter, and J Eberhardsteiner. Structural design of cross laminated timber (clt) by advanced plate theories. *Composites Science and Technology*, 70(9):1368–1379, 2010. → pages x, 8

[SKP+13] J Schneider, E Karacabeyli, M Popovski, S.F. Stiemer, and S Tesfamariam. Damage assessment of connections used in cross laminated timber subject to cyclic loads. *Journal of Performance of Constructed Facilities*, 2013. → pages 2, 12, 13, 127

[SL12] T.J. Sullivan and A Lago. Towards a simplified direct dbd procedure for the seismic design of moment resisting frames with viscous dampers. *Engineering Structures*, 35:140–148, 2012. → pages 99, 107, 111

[SPC06] T.J. Sullivan, M.J.N. Priestley, and G.M. Calvi. Direct displacement-based design of frame-wall structures. *Journal of earthquake engineering*, 10(S1):91–124, 2006. → pages 26, 29, 31, 95, 96, 104, 105, 117

[SPC10] T.J. Sullivan, M.J.N. Priestley, and G.M. Calvi. Introduction to a model code for displacement-based seismic design. In *Advances in Performance-Based Earthquake Engineering*, pages 137–148. Springer, 2010. → pages 106

[SPKA97] T.W. Simpson, J Peplinski, P.N. Koch, and J.K. Allen. On the use of statistics in design and the implications for deterministic computer experiments. *Design Theory and Methodology-DTM'97*, pages 14–17, 1997. → pages 55

[SR78] S.B. Stafford and JR Riddington. The design of masonry infilled steel frames for bracing structures. *The Structural Engineer*, 56(1):1–7, 1978. → pages 3

[SS74] A Shibata and M.A. Sozen. The substitute-structure method for earthquake-resistant design of reinforced concrete frames. Technical report, University of Illinois Engineering Experiment Station. College of Engineering. University of Illinois at Urbana-Champaign., 1974. → pages 94

[SST+12] J Schneider, S.F. Stiemer, S Tesfamariam, E Karacabeyli, and M Popovski. Damage assessment of cross laminated timber connections subjected to simulated earthquake loads. *World*, 15:19, 2012. → pages 13, 16, 116

[SST+13] Y Shen, J Schneider, S Tesfamariam, S.F. Stiemer, and Z Mu. Hysteresis behavior of bracket connection in cross-laminated-timber shear walls. *Construction and Building Materials*, 48:980–991, 2013. → pages x, 12, 13, 14, 15, 42, 116, 128

[Sta67] S.B Stafford. Methods for predicting the lateral stiffness and strength of multi-storey infilled frames. *Building Science*, 2(3):247–257, 1967. → pages 73

[STKP12] S.F. Stiemer, S Tesfamariam, E Karacabeyli, and M Propovski. Development of steel-wood hybrid systems for buildings under dynamic loads. *STESSA 2012, Behaviour of Steel Structures in Seismic Areas*, 2012. → pages 1, 12, 16, 18, 38, 66, 94

[Strnd] Structurlam. Cross laminated timber design guide, nd. → pages 116

[Sul09] T.J. Sullivan. Direct displacement-based design of a rc wall-steel ebf dual system with added dampers. *Bulletin of the New Zealand Society for Earthquake Engineering*, 42(3):167, 2009. → pages xi, 32, 95

[TB75] M.D. Trifunac and A.G. Brady. A study on the duration of strong earthquake ground motion. *Bulletin of the Seismological Society of America*, 65(3):581–626, 1975. → pages xii, 43, 45

[TBS14] S Tesfamariam, M.A. Bezabeh, and S.F. Stiemer. Drift demands of clt infilled steel moment frames multiobjective optimization using genetic algorithm. In *7th European conference of Steel and Composite Structures (EUROSTEEL 2014)*. University of Napoli Federico II, 2014. → pages 61

[TSDB14] S Tesfamariam, S.F. Stiemer, C Dickof, and M.A. Bezabeh. Seismic vulnerability assessment of hybrid steel-timber structure: Steel moment resisting frames with clt infill. *Journal of Earthquake Engineering*, (just-accepted), 2014. → pages x, 1, 2, 12, 18, 38, 42, 70, 128

[UC97] Building Seismic Safety Council (US) and Applied Technology Council. *NEHRP guidelines for the seismic rehabilitation of* *buildings*, volume 1. Federal Emergency Management Agency, 1997. → pages 20, 21

[vdLRPP12] J.W. van de Lindt, D.V. Rosowsky, W Pang, and S Pei. Performance-based seismic design of midrise woodframe buildings. *Journal of Structural Engineering*, 139(8):1294–1302, 2012. → pages 95, 96

[WLYL04] C.L. Wu, C Loh, Y Yang, and C.H. Lin. Consideration of collapse and residual deformation in reliability-based performance evaluation of buildings. In *Proc. of the 13th World Conference on Earthquake Engineering*, pages 1–6, 2004. → pages 38

[WNS11] K.K. Wijesundara, R Nascimbene, and T.J. Sullivan. Equivalent viscous damping for steel concentrically braced frame structures. *Bulletin of Earthquake Engineering*, 9(5):1535–1558, 2011. → pages 23, 67, 83, 85, 130

[WR] K.K. Wijesundara and P Rajeev. Direct displacement based design of steel concentric braced frame structures. In *Proceedings of the SAITM Research Symposium on Engineering Advances SAITM-RSEA 2012*, pages 11–14. → pages xi, 23, 24, 25, 95, 96

[YA13] K Young and H Adeli. Fundamental period of irregular moment-resisting steel frame structures. *The Structural Design of Tall and Special Buildings*, 2013. → pages 19

[YD08] U Yazgan and A Dazio. Utilization of residual displacements in the post-earthquake assessment. In *14th. world conference on earthquake engineering*, 2008. → pages 38

Appendix

A

Surrogate models of MISD and RISD using Artificial Neural Network

A.1 Designing the ANN network

The design of network topology is carried out after obtaining data for objective functions (MISD and RISD) from nonlinear time history analysis. From Figure 3.15, it is shown that the input layer consists of 6 members and the output layer is comprised of 2 members. The design of topology is then literally means determining the number of hidden layers, which was obtained by trial and error approach. The selection of network topology was based the regression coefficient (R) for the training and validation as a target objective. The network design and analysis was carried out by using Neural Network toolbox [DB93] in MATLAB numerical computing program [MAT13]. The Neural Network Toolbox was used to design, implement, test and validate the proposed network. Later, for optimization process, the code from tool box was exported for further manipulation.

A.2 Training the ANN network

The training process is adjusting the weights for each of the iterations in order to create the largest possible regression coefficient (R). For this thesis, a Levenberg-Marquardt back propagation (trainlm) back propagation (trainbr) algorithm is used. A network topology of 6-9-9-1 for both RISD and MISD is obtained to be good by trial and error approach and is shown in Figure A.1. After implementing the proposed topology, the regression outputs are shown in Figure A.2 and A.3 for MISD and RISD, respectively.

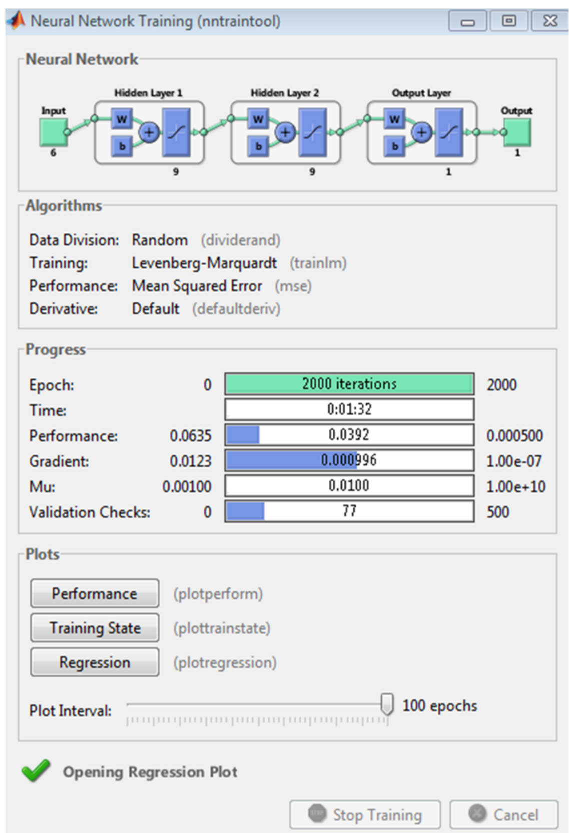

Figure A.1: MATLAB toolbox window for MLP training

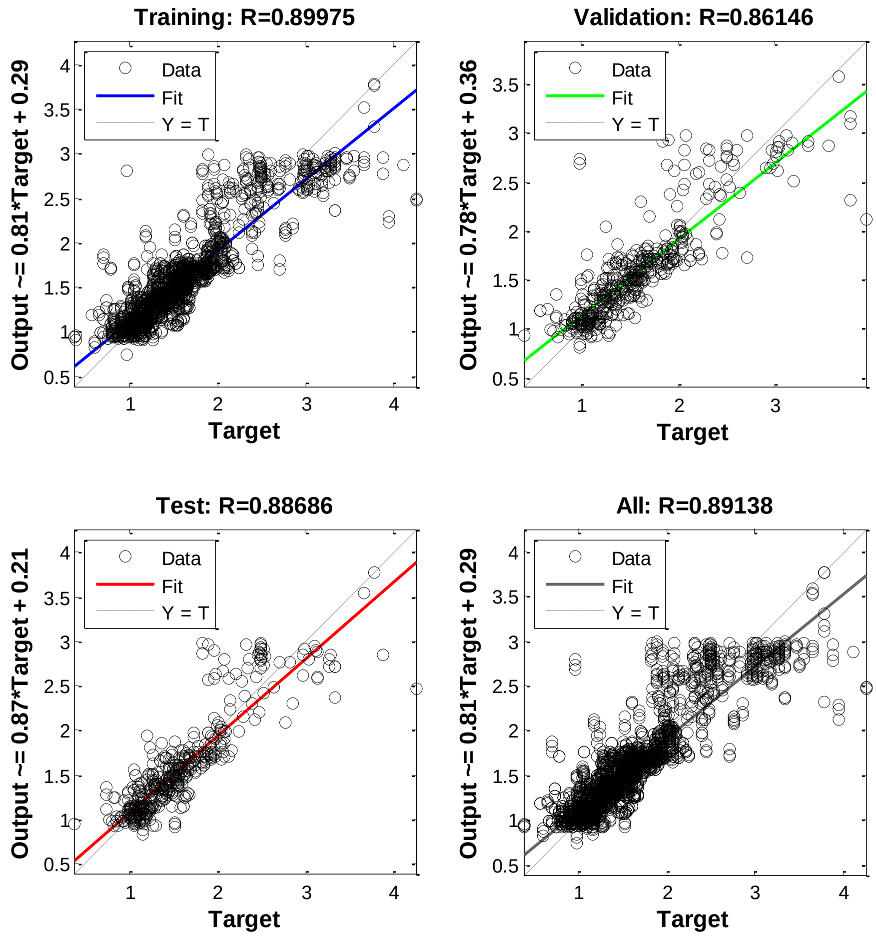

Figure A.2: Regression outputs for MISD

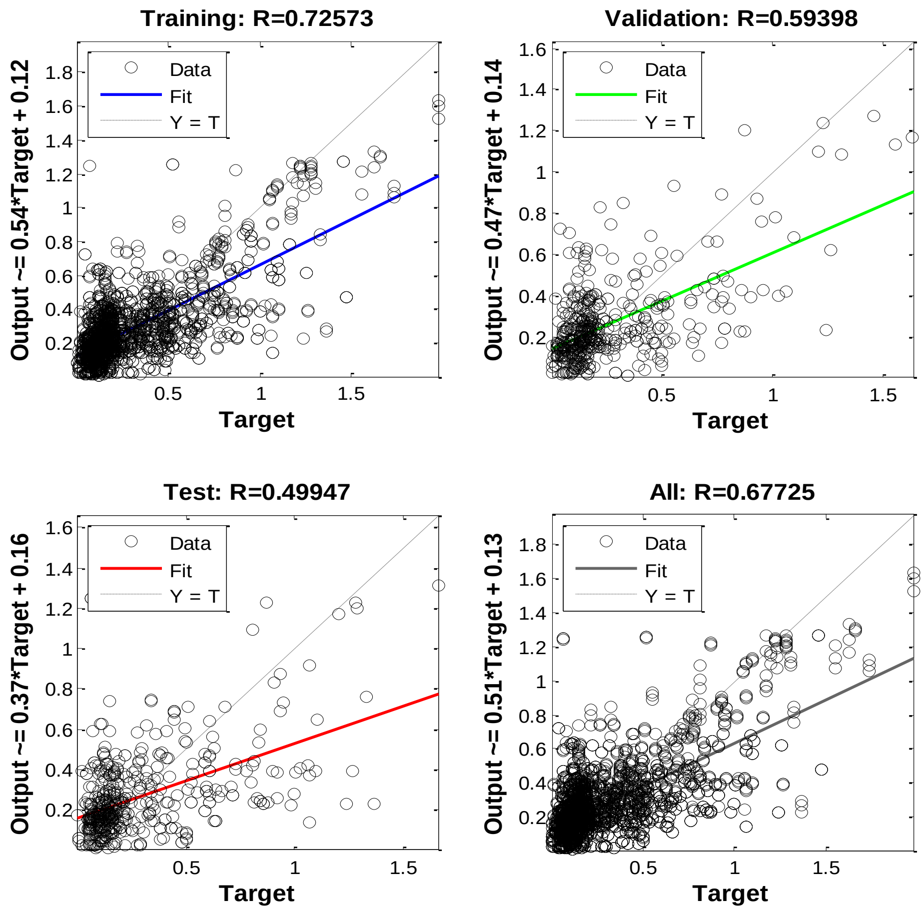

Figure A.3: Regression outputs for RISD

As can be shown in Figures A.2 and A.3, the regression coefficient for the RISD is smaller than MISD. This is due to the fact the RISD values of the system are highly nonlinear that makes it difficult to develop statistical relationship between inputs and outputs.

B

Approximate method of structural analysis

The inflection point for the frame structures occurs at a point where the curvature of the member changes its sign. Figure 5.10 shows the approximate inflection point locations and deflected shape of the structure under distributed horizontal shear forces. The internal columns of the structure carry two times larger shear than the exterior columns. It should be noted at this point that the structure is considered as it is made from different single storey single bay elements as shown in Figure B.1 to support the above assumption.

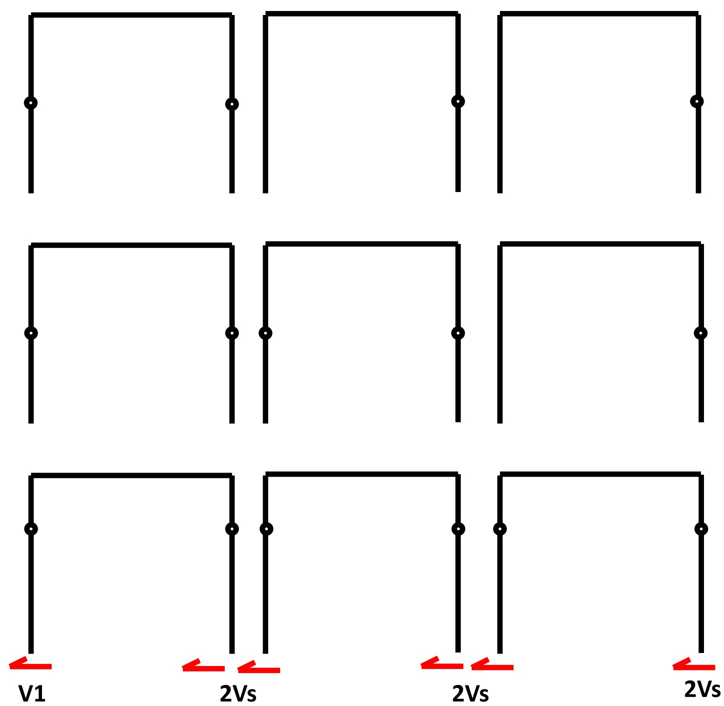

Figure B.1: Shear proportion between interior and exterior columns

In each storey, based on the assumption it is possible to express the shears in either of the columns in terms of the other column. From this assumption a total of 9 equations can be obtained.

Column shear

The column shears are calculated by passing an imaginary horizontal lines (a-a, b-b, and c-c) at the bottom of each storey as depicted in Figure B.2

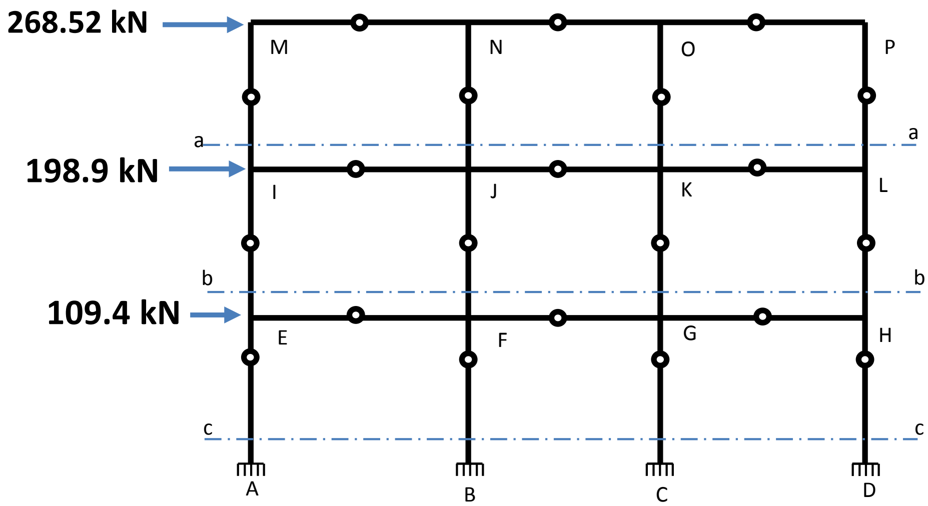

Figure B.2: Simplified steel moment frames with assumed hinges

Considering portion of frame above the imaginary cutting line, the free body diagram that is shown in Figure B.3 is obtained. Based on the previous discussions, the shear carried by internal columns is taken as twice of the exterior columns. Equilibrium of forces in horizontal direction is used to calculate shear force carried by each column as indicated in Figure B.3.

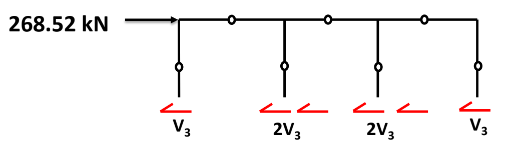	$\sum F(x) = 0$ $268.52\ kN = V_3 - 2V_3 - 2V_3 - V_3$ $S_3 = 44.75\ kN$
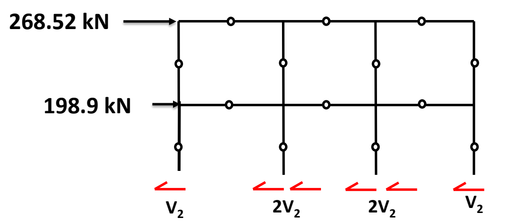	$\sum F(x) = 0$ $268.52\ kN + 198.9\ kN = V_2 - 2V_2 -$ $2V_2 - V_2$ $V_2 = 77.9\ kN$
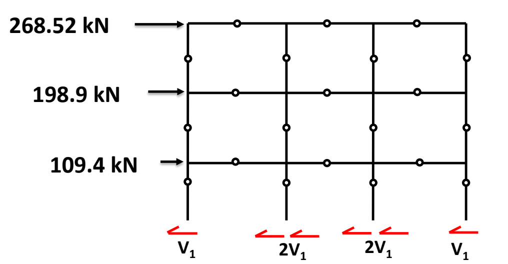	$\sum F(x) = 0$ $268.5kN + 198.9\ kN + 109.4\ kN =$ $V_1 - 2V_1 - 2V_1 - V_1$ $V_1 = 96.136\ kN$

Figure B.3: Column shear

Column moments, beam moments, and axial forces

The moments in columns are obtained by applying moment equilibrium condition at inflection points. For clarity, the detail analysis of the column MI, beam MN and joint M will be discussed as shown in Figure B.4.

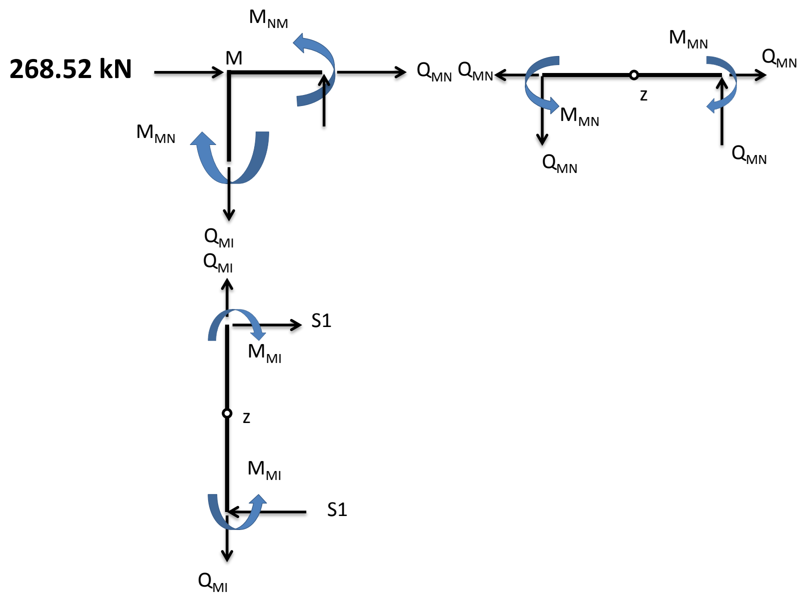

Figure B.4: Details of joint M, beam MN, and column MI

Since the shear on column MI is known it is advantageous to start the analysis from the left top corner side of the frame. The column moment (M_{MI}) of Figure B.4 is determined by applying equilibrium condition of $\sum M_z = 0$ at the inflection point of the column. The column axial forces (Q_{MN}) are found by applying equilibrium equation $\sum M_y = 0$ at the inflection point of the beam (MN). Using the same approach all the shear, axial and moment of beam and column have been quantified.

C

Design checks

Exterior beam in first story

In this section, the exterior beam on the left side of the lower storey is checked. The details of the beam are shown in Figure C.1. For ductile design of frames, the beam section should meet a width-thickness ratio of class 1 of CSA S16-09 [CSA09].The limiting requirement from CSA S16-09 [CSA09] for flange and web are indicated below in Equations C.1 and C.2, respectively.

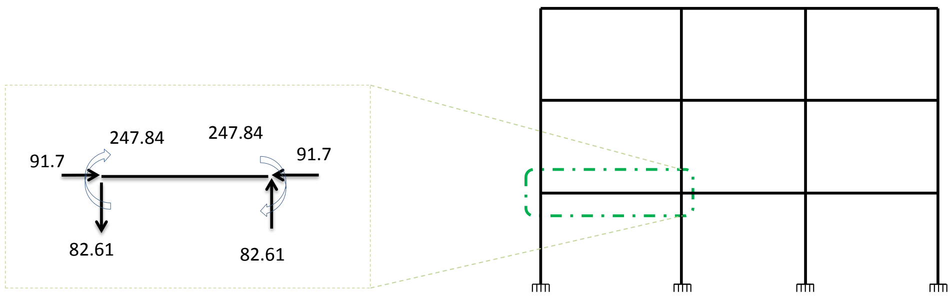

Figure C.1: Detail results of approximate method of analysis

$$Flange = \frac{b}{2t} < \frac{145}{\sqrt{f_y}} = 7.75 \tag{C.1}$$

$$Web = \frac{h}{w} < \frac{1100}{\sqrt{f_y}} = 58.79 \tag{C.2}$$

where b, t, h, and w are flange width, flange thickness, web depth, and web thickness, respectively. The cross-sectional properties of the selected beam section are given below. The calculated requirements and checks are given.

A $= 6670\ mm^2$	d = 318 mm
$I_x = 119\ E6\ mm^4$	b = 167 mm
$Z_x = 841\ E3\ mm^3$	t = 13.2 mm
$r_y = 39.2$ mm	w = 7.6 mm

$$Flange = \frac{b}{2t} = 6.32 \tag{C.3}$$

$$Web = \frac{h}{w} = \frac{d-2t}{w} = 38.36 \tag{C.4}$$

As shown in Equations C.3 and C.4, the web and flange slenderness requirements are with in the limit. Therefore the section used for the beam is Class 1. Moreover, the shear resistance of the beams is 495 kN. The beam section considered here satisfies both shear and moment requirement.

Other beams

As suggested by Pauley [PP] and Garcia [GSC10], beams of equal strength are used for the entire height of the structure. This recommendation is based on the idea of facilitating the construction time. However, this recommendation is not valid for buildings designed with non-uniform gravity load distrbution among floor levels [GSC10].

Exterior column in first story before yielding due to seismic forces

The first storey columns, as discussed in section 5.3 are allowed to yield at their bottom. Due to this ductile behavior, according to CSA S16-09 [CSA09] the section should be Class 1. The formation of the plastic hinges in the upper parts of the bottom storey columns is avoided by providing appropriate corrections for the inflection points. Therefore, the base columns should remain elastic up to the point of yielding to satisfy the requirements against premature failures. Even though the columns are assumed to be braced, design checks against overall member strength and (OMS) and lateral buckling strength (LTBS) are carried out. The verification against the class of the section, OMS and LTBS are calculated as follows.

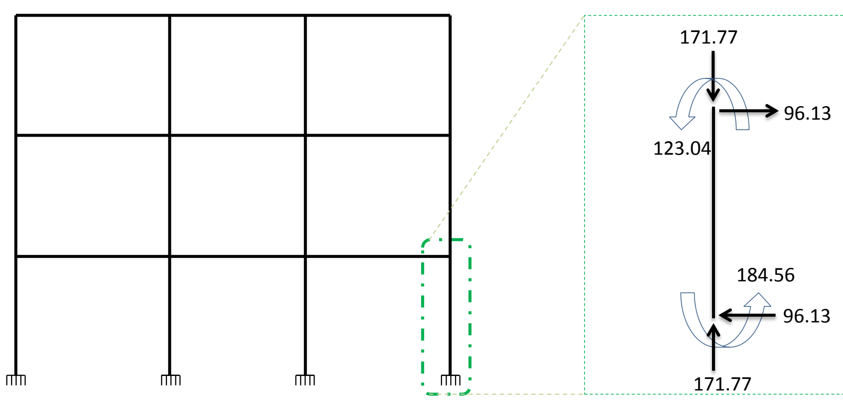

Figure C.2: Details of exterior column

The cross-sectional properties of the selected beam section are given below. The calculated requirements and checks are shown below.

A = 5690 mm^2	d = 318 mm
I_x = 99.2 $E6\ mm^4$	b = 166 mm
Z_x = 708 $E3\ mm^3$	t = 11.2 mm
r_y = 38.8 mm	w = 6.6 mm

$$Flange = \frac{b}{2t} = 7.41 \tag{C.5}$$

$$Web = \frac{h}{w} = \frac{d-2t}{w} = 44.78 \tag{C.6}$$

As shown in Equations C.5 and C.6, the web and flange slenderness requirements are with in the limit. Therefore, the section used for the exterior columns is Class 1.

Overall member strength (OMS)

The overall member strength for columns that are under combined axial and bending loadings is checked using Equation C.7 of CSA S16-09[CSA09] section 13.8.2.

$$OMS: \qquad \frac{C_f}{C_w} + \frac{0.85U_{1x}M_{1x}}{M_{rx}} \leq 1 \tag{C.7}$$

where C_f and C_{rx} are the applied axial load and factored axial compressive resistance for column, respectively. In addition, M_f and M_{rx} are the applied bending moment and factored moment resistance for column, respectively. M_{rx} is calculated without considering lateral torsional buckling. U_{1x} is the factor to account for the second order effect due to deformation of a member in its end and taken here as 1.0. The axial compressive resistance is calculated using Equation C.8.

$$C_r = \phi A f_y (1+\lambda^{2n})^{\frac{-1}{2n}} \tag{C.8}$$

where ϕ is compression resistance factor and is given as 0.9. A is cross sectional area and n is a factor associated with residual stress patterns for groups of W shape sections. For cold formed non-stress relived sections n is 1.34. The non-dimensional slenderness parameter (λ) is calculated by Equation C.9.

$$\lambda = \frac{KL}{r}\sqrt{\frac{F_y}{\pi^2 E}} \tag{C.9}$$

For the exterior column understudy, K (effective length factor), is taken as 1.0. Then the slenderness ratio KL/r in both direction x and y axis are 24.4 and 82.47, respectively. The axial compressive resistance C_{rx} and C_{ry} are 1731.72 and 975.71 KN, respectively. Therefore, the OMS check is:

$$\frac{C_f}{C_{rx}} + \frac{0.85U_{1x}M_{1x}}{M_{rx}} = \frac{171.77}{1731.72} + \frac{0.85.1.123.04}{220} = 0.57 < 1.0 \tag{C.10}$$

From the above calculation, it can be concluded that the exterior columns will remain elastic prior to yielding.

Lateral buckling strength (LTBS)

The lateral buckling strength for columns that are under combined axial and bending loadings is checked using Equation C.11 of CSA S16-09 section 13.8.2 [CSA09].

$$LTBS: \qquad \frac{C_f}{C_{ry}} + \frac{0.85U_{1x}M_{1x}}{M_{rx}} \leq 1 \tag{C.11}$$

$$\frac{C_f}{C_{ry}} + \frac{0.85U_{1x}M_{1x}}{M_{rx}} = \frac{171.77}{975.1} + \frac{0.85 \times 1 \times 123.04}{220} = 0.65 < 1.0 \tag{C.12}$$

From the above calculation, it can be inferred that the exterior columns are safe against lateral torsional buckling and will remain elastic prior to yielding.

Check for axial bending and tension

CSA S16-09 [CSA09] requires the following design checks of Equation (C.13) for member under combined axial tension and bending. As can be inferred from Figure 5.11, the lower storey exterior column in the right side is subjected to both axial tension and bending.

$$\frac{T_f}{T_r} + \frac{M_f}{M_r} \leq 1.0 \tag{C.13}$$

where T_f and T_r are the axial applied load and resistance of the column. From the analysis, it is verified that the column can handle the uplift force with the applied bending moment. To shorten construction time, the same cross-sections of interior and exterior columns used throughout the height of the building. Therefore, the design checks for the upper storeys columns are omitted.